INTERFACIAL TOUGHENING OF CARBON FIBER REINFORCED POLYMER (CFRP) MATRIX COMPOSITES USING GRAPHENE OXIDE CONTAINING NANOFIBERS

A THESIS SUBMITTED TO
THE GRADUATE SCHOOL OF NATURAL AND APPLIED SCIENCES
OF
MIDDLE EAST TECHNICAL UNIVERSITY

BY

CANSU ÇAYLAN

IN PARTIAL FULFILLMENT OF THE REQUIREMENTS
FOR
THE DEGREE OF MASTER OF SCIENCE
IN
CHEMICAL ENGINEERING

SEPTEMBER 2019

Approval of the thesis:

INTERFACIAL TOUGHENING OF CARBON FIBER REINFORCED POLYMER (CFRP) MATRIX COMPOSITES USING GRAPHENE OXIDE CONTAINING NANOFIBERS

submitted by **CANSU ÇAYLAN** in partial fulfillment of the requirements for the degree of **Master of Science in Chemical Engineering Department, Middle East Technical University** by,

Prof. Dr. Halil Kalıpçılar
Dean, Graduate School of **Natural and Applied Sciences** _____

Prof. Dr. Pınar Çalık
Head of Department, **Chemical Engineering** _____

Assoc. Prof. Dr. Erhan Bat
Supervisor, **Chemical Engineering, METU** _____

Prof. Dr. Bora Maviş
Co-Supervisor, **Mechanical Engineering, Hacettepe Uni.** _____

Examining Committee Members:

Prof. Dr. Göknur Bayram
Chemical Engineering, METU _____

Assoc. Prof. Dr. Erhan Bat
Chemical Engineering, METU _____

Prof. Dr. Görkem Külah
Chemical Engineering, METU _____

Prof. Dr. Bora Maviş
Mechanical Engineering, Hacettepe Uni. _____

Assoc. Prof. Dr. Seha Tirkeş
Chemical Engineering and Applied Chemistry, Atılım Uni. _____

Date: 02.09.2019

I hereby declare that all information in this document has been obtained and presented in accordance with academic rules and ethical conduct. I also declare that, as required by these rules and conduct, I have fully cited and referenced all material and results that are not original to this work.

Name, Surname: Cansu Çaylan

Signature:

ABSTRACT

INTERFACIAL TOUGHENING OF CARBON FIBER REINFORCED POLYMER (CFRP) MATRIX COMPOSITES USING GRAPHENE OXIDE CONTAINING NANOFIBERS

Çaylan, Cansu
Master of Science, Chemical Engineering
Supervisor: Assoc. Prof. Dr. Erhan Bat
Co-Supervisor: Prof. Dr. Bora Maviş

September 2019, 132 pages

The importance of carbon fiber reinforced polymer (CFRP) composites is increasing day by day in everyday life. While they have great importance owing to their high strength- and stiffness-to-weight ratios, these new materials still have some weak aspects which need to be improved. One of these aspects is 'delamination'. To increase the delamination resistance, the most promising technique is the one that includes the use of nanofibers because of ease of process and no increase in total weight of composites. Recently, hybrid systems which combine the properties of two or more monolithic materials have attracted considerable attentions.

This work focuses on the enhancement of interfacial toughness of CFRP composites using hybrid nanofibers which are graphene oxide containing electrospun nanofibers by using nylon 6 (N6)/polycaprolactone (PCL) polymers with different N6 mass ratios (60, 80, 100 wt %). With this aim, firstly, GO has been synthesized and after that homogeneous distribution of containing different size of GO (GO1: 466 nm, GO2: 230 nm, GO3: 165 nm) along the fiber have been studied. The results showed that N6 containing 2 wt % of GO2 provides the increase of $G_{1c\text{-}in}$ and $G_{1c\text{-}prop}$ values about 21% and 13% according to reference. Composites containing N6/PCL-60/40 with varying

quantities of GO3 nanofibers, G_{1c} values could not be increased because of the deterioration of the synergistic relationship between ‘debonding/fiber bridging’ mechanisms. Highest G_{1c} value was obtained with N6/PCL-80/20 containing 0.5 wt % of GO2 composite with a 26% improvement on the $G_{1c\text{-}in}$ and 42% on that of $G_{1c\text{-}prop}$.

Keywords: Carbon Fiber Reinforced Polymer Matrix Composites (CFRP), Graphene Oxide (GO), Electrospinning, Interlaminar Fracture Toughness (G1c), Double Cantilever Beam (DCB) Test

ÖZ

GRAFEN OKSİT İÇEREN NANOFİBERLERİN KULLANILARAK KARBON FİBER TAKVİYELİ POLİMER MATRİS KOMPOZİTLERİNİN (KFTP) ARAYÜZ TOKLAŞTIRILMASI

Çaylan, Cansu
Yüksek Lisans, Kimya Mühendisliği
Tez Danışmanı: Doç. Dr. Erhan Bat
Ortak Tez Danışmanı: Prof. Dr. Bora Maviş

Eylül 2019, 132 sayfa

Karbon fiber takviyeli polimer matrisli (KFTP) kompozitlerin önemi günlük yaşamda gün geçtikçe artmaktadır. Yüksek mukavemet/ağırlık ve sertlik/ağırlık oranlı bu malzemeler büyük öneme sahip olmalarına rağmen, bu yeni malzemeler hala geliştirilmesi gereken bazı zayıf yönlere sahiptir. Bu yönlerden biri 'delaminasyon'dur. Delaminasyon direncini arttırmak için en umut veren teknik, işlem kolaylığı ve kompozitlerin toplam ağırlığında bir artışa neden olmayan nanofiberlerin kullanımını içeren tekniktir. Son zamanlarda, iki ya da daha fazla malzemenin özelliklerinin birleşmesi ile oluşan melez sistemler büyük dikkat çekmiştir.

Bu çalışma, grafen oksit (GO) içeren farklı N6 kütle oranlarına (ağırlıkça % 60, 80, 100) sahip naylon 6 (N6)/polikaprolakton (PCL) polimerleri kullanılarak elektroeğirilen hibrid nanofiberler kullanılarak KFTP kompozitlerinin arayüzey sağlamlığının arttırılmasına odaklanmıştır. Bu amaçla ilk önce GO sentezlenmiş ve bundan sonra farklı boyutlarda GO'in (GO1: 466 nm, GO2: 230 nm, GO3: 165 nm) fiber boyunca homojen dağılımı incelenmiştir. Sonuçlar, ağırlıkça %2 oranında GO2 içeren N6 nanofiberinin referansa göre $G_{ıc\text{-}başlangıç}$ ve $G_{ıc\text{-}ilerleme}$ değerlerinde yaklaşık

%21 ve %13 oranlarında artış sağladığını göstermiştir. Farklı miktarlarda GO3 içeren N6/PCL-60/40 kompoziterinde, ‘bağaçınım/fiber köprüleme’ mekanizmaları arasında sinerjik ilişkinin bozulmasından dolayı G_{1c} değeri arttırılamamıştır. En yüksek G_{1c} değeri, referansa göre $G_{ıc\text{-}başlangıç}$ değerinde %26 ve $G_{ıc\text{-}ilerleme}$ değerinde %42 bir iyileşmeyle ağırlıkça % 0.5 GO2 içeren N6/PCL-80/20 kompoziti ile sağlanmıştır.

Anahtar Kelimeler: Karbon Fiber Takviyeli Polimer Matrisli (KFTP) Kompozitler, Grafen Oksit (GO), Elektroeğirme, Tabakalar arası kırılma tokluğu (G1C), Çift Konsol Kiriş Testi

To my precious family…

ACKNOWLEDGEMENTS

I would like to express my sincere gratitude to my supervisor Dr. Erhan Bat for providing his comments and suggestions throughout my master thesis study. I would specially thank to my co-supervisor Dr. Bora Maviş for constantly motivating me to work harder and valuable advice at all levels of my study.

Also, I would like to thank Dr. Güngör Gündüz for his endless guidance and valuable advices about not only my thesis study.

I would like to thank my project colleague Melike Kılıçoğlu, who carried out some of my experiments together and for her help and friendship. I am thankful to Nur Merve Kazaroğlu Sönmez and Naci Örnek for their help and supports.

I would especially like to thank amazing friends Zeynep Cansu Özçınar and Cemre Avşar for being an important part of my happiest memories and comments those will never forget through the rest of my life. Special thanks laboratory mates Gözde Şahin, Seda Sivri, Hatice Özyetiş, Elif Kıratlı and Öznur Doğan for their support.

There is one person I owe my special thanks to Volkan Baydar for his excellent motivation, understanding, endless patience and invaluable love. Without his love and support everything would have been more difficult, thank you very much for perfect friendship and true love.

Lastly, nobody has been more important to me in the pursuit of this master study than the members of my family. I would like to thank my parents; whose love and support are with me in whatever I pursue. I wish to thank my lovely family my mother, Gönül, and my father, Sami, my twin, Tansu and my brother-in-love Ahmet who provide unending inspiration and love in my life. I am so lucky to have them.

Lastly, I would like to thank TUBİTAK for its financial contribution to project number 214M110.

TABLE OF CONTENTS

LIST OF TABLES

TABLES

LIST OF FIGURES

FIGURES

LIST OF ABBREVIATIONS

ABBREVIATIONS

CFRP	Carbon Fiber Reinforced Polymer
N6/PA6	Nylon 6/ Polyamide 6
PCL	Polycaprolactone
PET	polyethylene terephthalate
PBI	Polybenzimidazole
PAN	Polyacrylonitrile
PSF	Polysulfone
PEK-C	Polyetherketon-cardo
PVDF	Polyvinylidene difluoride
PAI	Polyamide-imide
PVB	Polyvinyl butyral
GO	Graphene oxide
GNPs	Graphene nano-platelets
CNT	Carbon Nanotubes
H_2SO_4	Sulfuric acid
H_3PO_4	Orthophosphoric acid
HCl	Hydrochloric acid
H_2O_2	Hydrogen peroxide
$KClO_3$	Potassium chlorate

$KMnO_4$	Potassium permanganate
$NaNO_3$	Sodium nitrate
HNO_3	Nitric acid
Mn_2O_7	Dimanganese heptoxide
DCM	Dichloromethane
DMF	Dimethylformamide
TFE	Trifluoroethanol
THF	Tetrahydrofuran
HFIP	Hexafluoro-2-propanol
DCB	Double Cantilever Beam
DSC	Differential Scanning Calorimeter
SEM	Scanning Electron Microscope
TEM	Transmission Electron Microscope
SEM	Scanning Electron Microscope
EDX	Energy Dispersive X-ray
St. Dev./STD	Standard deviation
IPN	Interpenetrating network
R1	Reference 1
R2	Reference 2
ASTM	American Society for Testing and Materials
G_{1c}	Mode I- Interfacial Fracture Toughness
$G_{1c\text{-}in}$	Mode I- Interfacial Fracture Toughness in crack initiation

$G_{1c\text{-}prop}$	Mode I- Interfacial Fracture Toughness in crack propagation
Tg	Glass transition temperature

CHAPTER 1

INTRODUCTION

Composites are produced by combination of two or more materials and after this combination, the properties of composite materials have better properties than the individual components used in composite materials. In last decade, composites have replaced metals and other materials in industry due to their low weight and superior properties such as corrosion resistance, higher strength and stiffness, wear resistance and hardness by comparison with conventional materials [1]. However, there are some obstacles against use of composites. Besides production costs, test-based production and production techniques difficult to standardize, the failure mechanisms of laminated composite structures caused by the structure of composites are still present problems. The most commonly observed failure in composites is delamination. Delamination is the separation of layers due to weakness of layer between them. Delamination may originate from low velocity impact, strangeness in structural load paths that cause out-of-plane loads, or from heterogeneous and stacked nature, which create local out-of-plane loads [2]. Fibers in laminate do not supply reinforcement, and therefore the composite is based on matrix which is relatively weak for carrying loads in this direction [3]. As a result of this, a crack occurs between the layers and this problem occurs when the starting crack moves along the surface of the sheet. Various methods have been evolved for years to enhance the delamination resistance of composite laminates, such as laminate stitching [4], [5], matrix-toughening [6-10], modification of fiber [11], ply termination [12], [1]. However, these methods cause some problems such as reduction in in-plane mechanical properties and processability of matrix due to high viscosity, fiber breakage at stitch hole, misalignment of fibers and stitch failures. Also, these methods involve extra machining and so have high manufacturing cost [12]. In addition to these methods, interfacial toughening by

placing films [13], [14], particles [15], resins [9] and microfibers [16] between the layers of composite laminates before curing is more effective method to solve this problem. However, interleaved particles, films, microfiber and resins increase the weight and volume and can cause decrease in some mechanical properties such as elastic modulus and stiffness [17]. Nanofibers, added to composite interlayer, produced using electrospinning process (Figure 1.1) have attractive features such as high surface area to volume rate, no considerable thickening of cross-sectional area of composite, without exceeding the 2% weight increase of composite, perfect mechanical performance, easy processability and flexibility in surface functionalities, compared to microfibers of the same material [18].

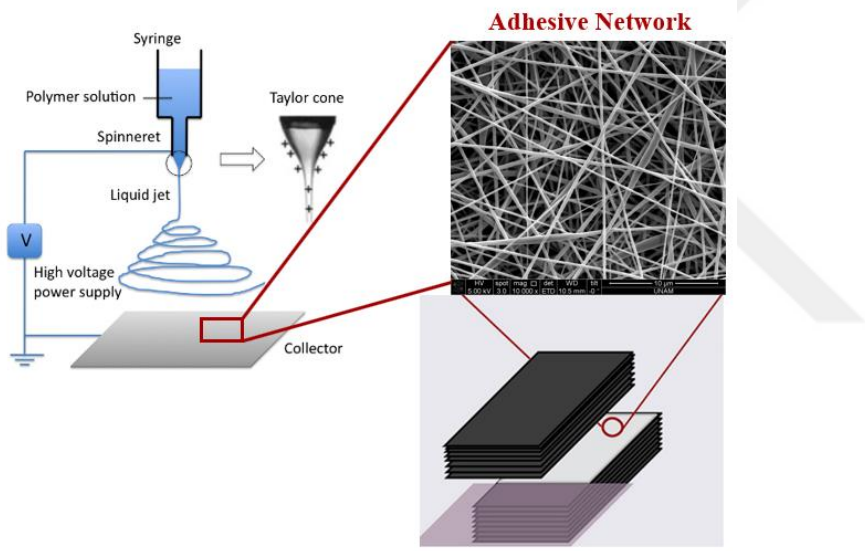

Figure 1.1. A schematic illustration of nanofibers between the layers of composite laminates [19]

It has been shown by some studies that nanofibers added between the layers produce some toughening mechanisms during delamination and hardens or delays the progression of the crack. This increase fracture toughness during propagation may be related to the hardening mechanism of ‘nanofiber bridge’: nanofibers will bridge the

crack regions and absorb energy by breaking, straining and creeping [20]. There are three basic mechanisms that are effective in nanofiber bridging regions; 1- elongation (straining) of the nanofibers without debonding, 2- straining of the nanofiber with little debonding, 3- totally peeling of nanofibers and schematic view of bridging nanofibers are shown Figure 1.2. The images shown in the Figure 1.2 can be seen in the following scenarios. If a strong interface between the epoxy and the nanofiber is established, there is no debonding, and the fibers can be sponged or can be seen to be broken or tapering at the intermediate side (Figure 1.2-b). If there is a weak interface interaction between the epoxy and the nanofiber, slotted images appear on the separated surfaces showing the traces of fiber morphologies and nanofibers strain partially debonding (Figure 1.2-c). If the bonding between epoxy and nanofibers are too low, void growth and imprints form in the epoxy surface after debonding (peeling) [20].

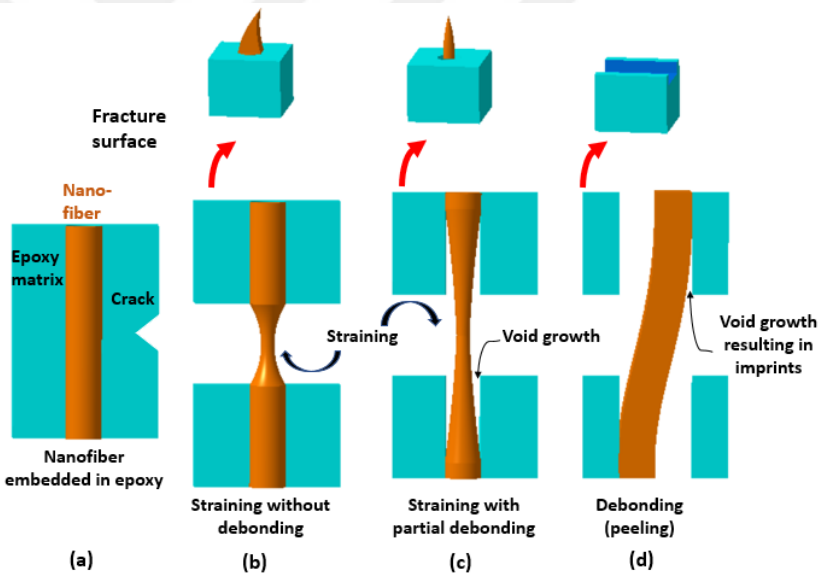

Figure 1.2. Bridge interaction with crack front nanofibers (a) nanofiber embedded with the crack front, that can cause (b) elongation of nanofibers without debonding, (c) straining of the nanofiber with little debonding, or (d) totally peeling of nanofibers [20]

In studies conducted so far, homopolymers, mixed polymers system such as spinning of two or more polymers at the same time, co-electrospinning of varied polymers and core-shell nanofibers systems have been used in composite systems to develop delamination resistance and interfacial fracture toughness. Instead of single component nanofiber systems, it is possible to diversify the toughening mechanisms with a synergistic effect as a result of the use of polymer mixtures or hybrid systems to be formed by the additions some inserts having nanoparticle level to the fibers. In a study in literature, polyvinyl butyral (PVB) and solutions containing CNTs were electrospun onto carbon fiber prepreg layers and the effect of CNTs on Mode I and Mode II fracture toughness (G_C) was researched. The results show that CNTs interlayered composites withstand higher deformation and showed notable development in G_C [19]. In studies where more than one polymer is used by mixing; polymers were electrospun in two different forms as layers and as core shells [21], from different syringes [22] and two different forms as layers and as core shells [21].

In addition to these systems, hybrids are systems produced by the addition of particles that have the potential to elicit different toughening mechanisms into the polymers. The use of carbon based materials is quite high attention because of their superior properties which are high modulus, specific strength, ultra-light and damping capacity in recent years [23]. Among carbon based materials, graphene and graphene based materials have attracted numerous investigations to improve interface properties of fiber reinforced polymer (CFRP) composites because of its unique chemical, physical and mechanical features [24]. GO contains much abundance of oxygen functional groups such as carboxyl, hydroxyl, carbonyl and epoxide groups, that provide high processability and interface interaction between these groups and matrices. In a study with GO, a 53 % increase in interfacial bonding strength of carbon/epoxy composites was recorded by adding silane-functionalized graphene oxides (sGOs) in epoxy resin [25]. Bortz *et al.* report enhancement of Mode I fracture toughness about 28-111 % with by addition of GO in a weight ratio 1% to an epoxy [26]. Ning *et al.* referred that the fracture toughness (in Mode I) and resistance of the CFRP specimens increase by

170.8% and 108.0%, respectively with epoxy containing 2 g/m^2 adding of GO into the interface of CFRP laminates [27]. Among studies about GO, there is no works about usage of nanofibers containing GO for increase of interfacial toughening by using electrospinning in carbon fiber/epoxy composite systems.

The main purpose in this study is to develop the interfacial fracture toughness of carbon fiber reinforced polymer (CFRP) composites with the use of minimum amount of nanofillers in the interfaces of laminates. To succeed the aim of incorporating nanofillers into the laminates, GO containing nylon 6 (N6)/polycaprolactone (PCL) nanohybrid nanofibers are proposed as a interleave for the nanofibers. N6 and PCL have been determined as ideal mixture components with their compatibility with epoxy matrix and with higher toughness values compared to epoxy.

According to the proposed hypothesis, addition of graphene oxide into the nanofibers will result in multi-functional interleaves with exceptional interlaminar toughness and strength because of GO's extraordinary mechanical properties. Also, GO sheets which are overflowing out of nanofibers could have three important roles in this system. The first task of GO is to act as a deflector by changing the direction of the crack propagating at the interface and so, crack surface area may increase and interfacial fracture in Mode I improved. The second role is that graphene oxide enhances interfacial bonding with epoxy resin because of the abundance of oxygen functional groups on its surface and therefore this developed debonding mechanisms and made it difficult to peel of nanofibers easily. Lastly, with the addition of graphene oxide into the fibers, there will be a change in the crystal structure of the fibers, which will lead to the formation of different mechanisms and synergistic effects. As a result of the studies, it is also discussed why samples that do not increase the interface toughness do not show the expected performance.

CHAPTER 2

BACKGROUND AND LITERATURE SURVEY

2.1. Graphene Oxide

The carbon element in the periodic table is one of the most important elements that form the basis of life on Earth. It is also essential for many technological applications such as drugs, optics, aerospace, composites and so on [28]. Figure 2.1 shows different carbon structures.

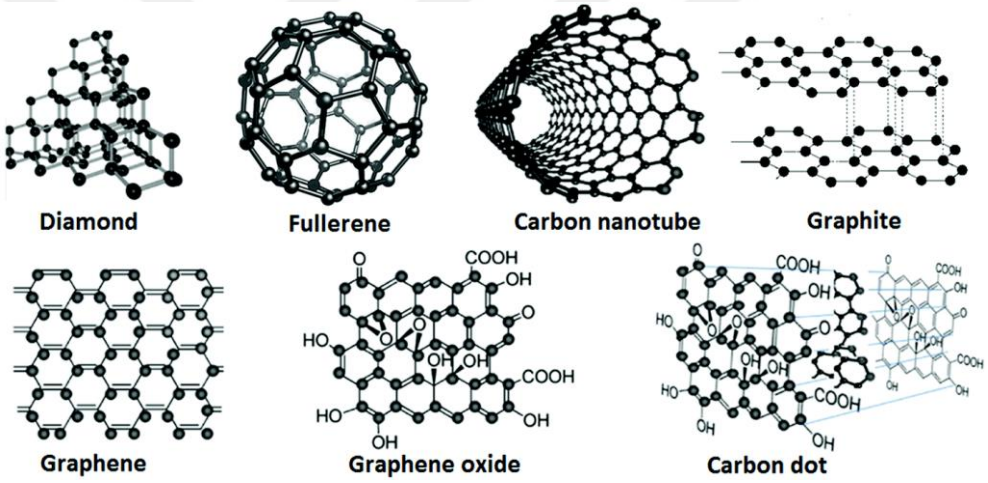

Figure 2.1. Different forms of carbon element [29]

When carbon based nano materials are examined, graphite is a three-dimensional carbon-based material consisting of millions of layers of graphene. Through oxidation of graphite using strong oxidizing agents, oxygenated functional groups are introduced into the graphite structure not only to extend the layer separation, but also make the material hydrophilic. This feature provides the exfoliation of graphite oxide (GtO) in water or other organic solvents using sonication, resulting in monolayer or

few layer graphene, known as graphene oxide (GO) [30]. GtO is seen as a highly oxidized form of graphite, which has multilayer structure with a higher interlayer spacing due to the presence of oxygen functionalities. The basal plane of GtO is highly filled with hydroxyls and epoxides while the edge-plane mainly contains of carboxyl and carbonyl groups. Reduction of oxygen-containing functional groups on the GO results in reduced graphene oxide (RGO) formation. The reduction of GO under physical (high temperature) or chemical (reducing agents) reduction conditions causes in the production of RGO [31]. Chemical structures of graphene derivatives are shown in the Figure 2.2.

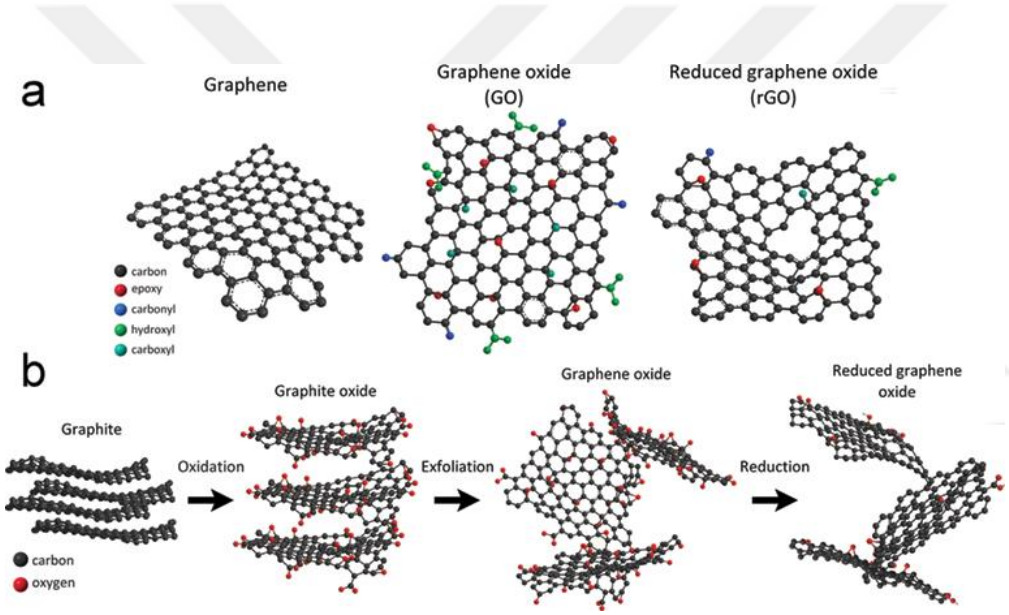

Figure 2.2. Schematic chemical structures of graphene, graphene oxide and reduced graphene oxide, (b) graphite to graphene oxide conversion

GO is usually obtained by mechanical stirring or ultrasonication methods in an organic polar solvents or aqueous media. The ultrasonication method allows for more efficient and faster exfoliation of stacked GtO sheets. However, sometimes this method causes structural damage and causes the GO layers to be divided into smaller sheets [33].

The conversion of GO to graphene is demonstrated by experimental observations, usually by a color change of the reaction mixture from brown (graphene oxide) to black (graphene) and consequently increased hydrophobicity/aggregation of the material, which are shown in Figure 2.3. Also, when most of the oxygen groups are removed from the graphene oxide, the resulting reduced graphene oxide (RGO) is more difficult to disperse due to the tendency to agglomerate [34].

Therefore, the main difference between graphite oxide and GO is the number of layers. There are several layers of flakes and one layer of flakes in a GO dispersion [34]. Also, GtO is an extremely stacked structure with oxide functionality, whereas GO has a wide gap between layers due to water intercalation.

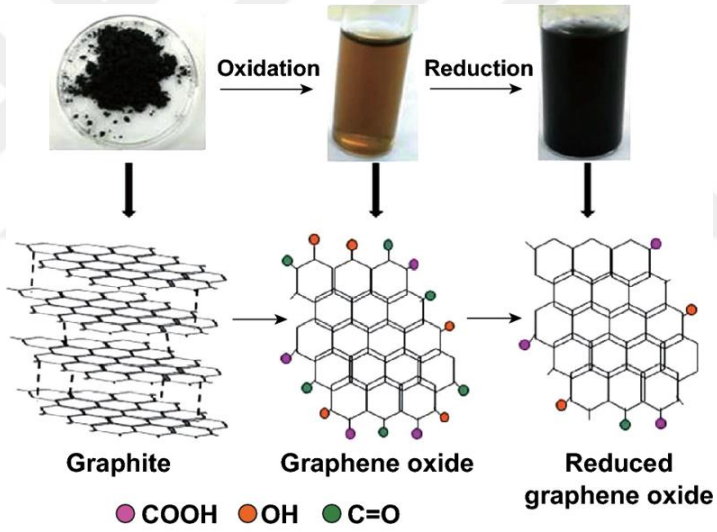

Figure 2.3. Dispersed images of graphene oxide and reduced graphene oxide [31]

In recent years, graphene, new member of carbon nanomaterial with a two-dimensional structure has attracted the attention of many researchers because this material has high specific surface area, perfect mechanical and thermal properties [35]. Several fields have started using the composite materials because of achieving multi-

functional characteristics in polymers by reinforcing with graphene. This growth was investigated in a study and published studies were recorded graphically, shown in Figure 2.4 [36].

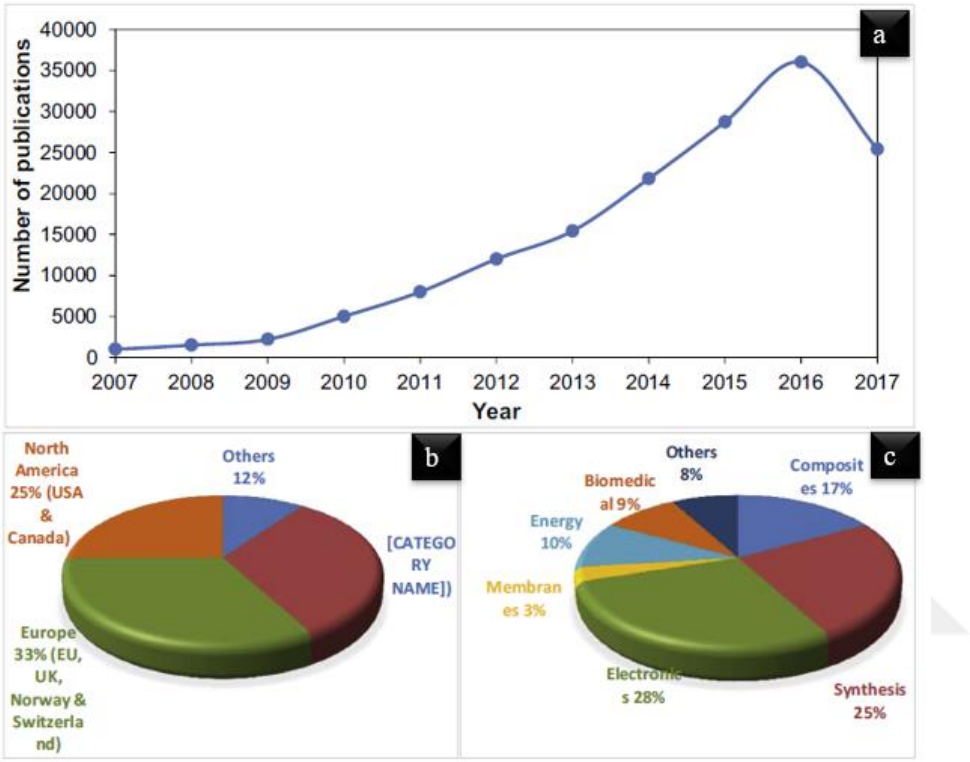

Figure 2.4. (a) Publications of graphene published from 2007 to 2017 [Source- Web of Science], (b) publications as a percentage by country and (c) publications as a percentage by sectors

However, since graphene is not compatible with organic polymers, it does not form a homogeneous composite structure. Just the opposite, GO sheets are oxygenated graphene that can be dispersed in most solvents such as aqueous or polar organic chemicals [37]. Also, GO shows excellent promise as nanofiller in polymeric

composites because GO possesses high aspect ratio, broad specific surface area and excellent mechanical properties [38].

GO, the oxidized form of single-layer graphene nanosheets, is formed by chemical treatment of graphite by oxidation process. Regarding the structure, there have been various models suggested over the years. These models argue that there are oxygen-containing functional groups on the graphene oxide. The chemical structure of graphene oxide has not been concluded over the years and has been the subject of considerable controversy, and even to this day there is no definite model. This is due to the uncertainty arising from both the nature and distribution of the functional groups containing oxygen and the lack of precise analytical techniques to characterize the GO structure [39]. However, there are some structural models (Figure 2.5) proposed for the structure of GO.

When the structure of Hofmann and Holst was examined, it consisted of epoxy groups, spread over the basal planes of graphite. In 1946, Ruess hybridized the basal plane structure from sp2 to sp3 and proposed a model containing hydroxyl groups in the basal plane. Scholz and Boehm suggested a new structure that completely removed the ether and epoxide groups, substituting corrugated carbon layers in the GO structure in 1969. Nakajima and Matsuo proposed the new model that depends on the assumption of a framework like poly(dicarbon monofluoride) which produces a stage two graphite intercalation complex material. The last and well-known model which have refused the lattice-based model is one by Lerf and Klinowski. According to this model, the basal plane includes epoxy and hydroxyl groups, whereas edges have carboxyl groups [40].

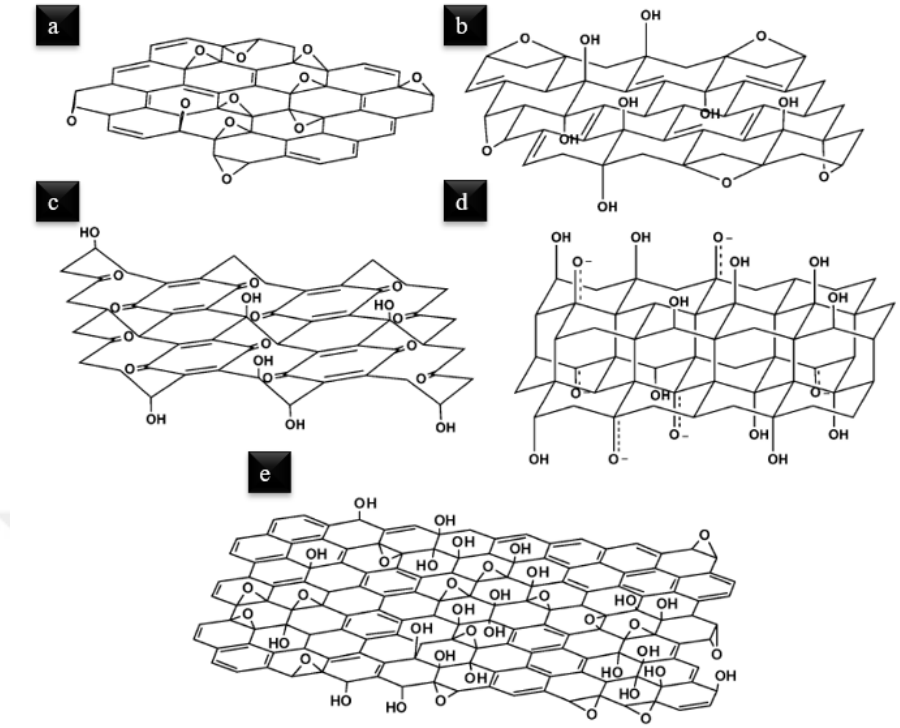

Figure 2.5. Different structural models of graphene oxide (a) Hofmann, (b) Ruess, (c) Scholz-Boehm, (d) Nakajima-Matsuo and (e) Lerf-Klinowski [40]

2.1.1. Graphene Oxide Synthesis Methods

GO is produced from the oxidation of graphite powder in concentric strong acid and with strong oxidizing agents. There are different methods for graphite oxidation in the literature studies. Among these studies, some of them use concentrated sulfuric acid with fumic HNO_3 and $KClO_3$ (Staudenmaier's method), HNO_3 and $KClO_3$ (Hoffman's method), H_3PO_4 and $KMnO_4$ (Tour's method) or $NaNO_3$ and $KMnO_4$ (Hummers' method) [30].

In 1859, a pioneering study on the synthesis of GO was reported by British Chemist B. C. Brodie. In his method, nitric acid (HNO_3) is used as acidic media and potassium chloride ($KClO_3$) is used as oxidizing agent. Brodie found that the product was made

up of carbon, hydrogen and oxygen, and found that this resulted in an increase in the total mass of flake graphite [40].

After nearly 40 years, L. Staudenmaier developed a new method by adding potassium chlorate in multiple aliquots at a time. He succeeded high yield of C: O atomic ratio (~2) in a single step [35]. The methods used by Brodie, Staudenmaier and Hofmann carry a risk of explosion due to the release of materials such as NO_x and chlorine dioxide, and the reactions take several days [30].

Almost 60 years later, Hummers and Offeman developed an alternative method by reacting graffiti with a mixture of potassium permanganate ($KMnO_4$) and concentrated sulfuric acid (H_2SO_4). This change allowed to shorten the reaction time and increase the C/O atomic ratio, but not to prevent the formation of toxic NO_x gases. Nowadays, the Hummers' method is the most preferred method for simplicity and safety and this method were modified by changing ratio of graphite to oxidizing agent, oxidation time and condition.

In 2010, a new method, Hummer's method (Tour method) was improved by using sulfuric acid and phosphoric acid mixture. The advantages of this method are higher yield, no toxic gas formation during synthesis and no time consuming [41]. Therefore, Tour method can be the best choice for the synthesis of GO since well-regulated experimental conditions remove the risks of self-ignition or explosion.

2.2. Electrospinning

Electrospinning is a method used to produce polymeric, ceramic and carbon fibers having diameters from ten to several hundred nanometers. These nanofibers produced by electrospinning is commonly termed as 'electrospun nanofibers' [42].

Nanofibers with a large surface area/volume ratio have the potential to greatly improve the current technology and to be used in new areas of application. Furthermore, electrospun nanofibers are preferred because they are easy, continuous and inexpensive in terms of producibility. Although there are many more methods for

producing nanofibers, for example melt fibrillation, nanolithography and gas jet, the applicability of these methods is limited due to material constraints, cost and production difficulties [42]. In last decade, studies with nanofibers have increased and attract attention in many areas especially in the composite sector. Patents and annual publication list in this field are shown in Figure 2.6. When this figure is examined, this research area has attracted the attention of academicians and industrialists and the studies in this field have increased day by day. The increasing amount of research on electrospinning is promising for electrospun materials [43].

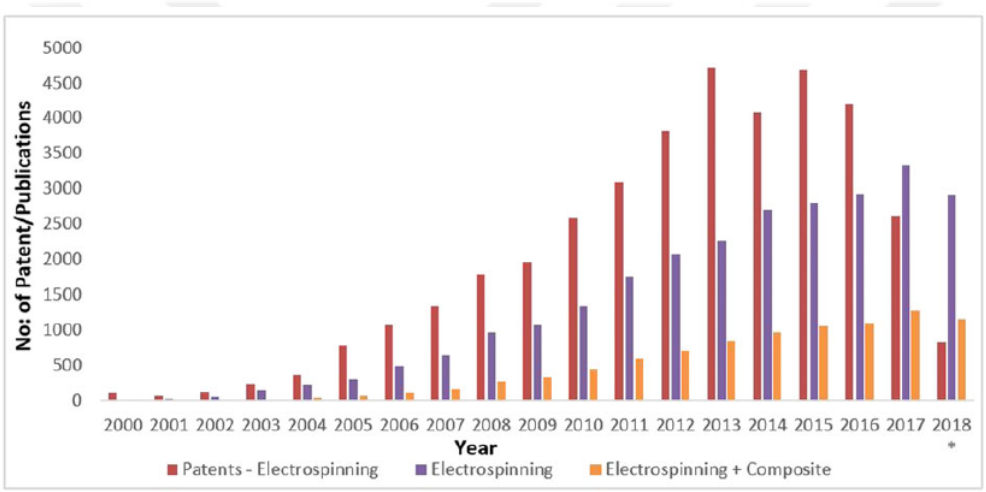

Figure 2.6. Number of annual publications and patents in the field of "electrospinning" and "combination of electrospinning and composite," [43]

Electrospinning setup consists of four main components: (1) a syringe system, (2) voltage power supply, (3) a flat tip needle and (4) a collecting plate, shown in Figure 2.7. During the process, by applying voltage to the system, the polymer solution at the needle tip turns into a conical structure called 'Taylor Cone' under electrostatic force. The polymer solution jets out of the tip of the Taylor cone and when the applied electrical force exceeds the force on the conic, the electrospinning process begins.

After that, the formed jet starts to accumulate in the collector by thinning and winding in 3D. When fibers collected in the collector, solvent evaporation occurs. At the end of the electrospinning process, thin-film fibers are produced onto collecting plate [44].

Some properties of the polymeric solution affect the factors in electrospinning as shown in Figure 2.7. These factors are environment, solution and electrospinning variables. These factors affect the morphologies of nanofibers such as diameter, length and presence of bead structures [44].

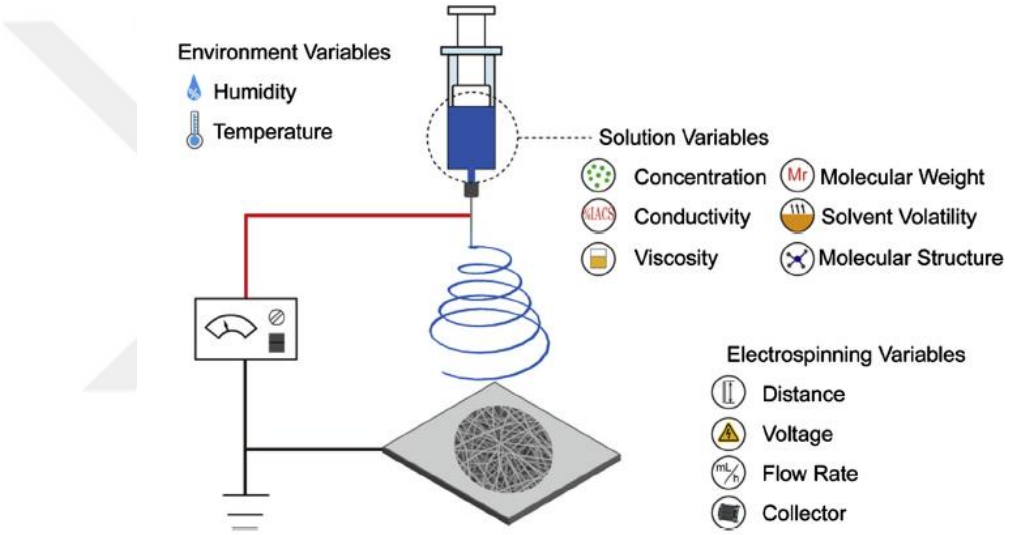

Figure 2.7. Schematic diagram of the factors affecting the electrospinning [44]

2.3. Composite Materials

Composites have long been used and have an important history. Although their exact onset is unknown, studies have been recorded for some types of composites. The Egyptians and Mesopotamians used a mixture of mud and straw to build durable settlements, and this mixture was recorded as the first composite material used in 1500s B.C. Later, in 1990s, vinyl, polystyrene, phenolic and polyesters plastics were

developed but plastics alone could not provide enough strength and so reinforcement was needed to provide rigidity and strength. In 1935, Owens Corning has developed a very strong and lightweight material by combining fiberglass and plastic polymer. In the 1970s, composites industry started to develop and continued to advance. Plastic resins and better fibers such as carbon fibers, aramid fibers were advanced around this time [45].

A composite material which is shortened to '*composite*' is formed by two or more combined constituents which are remarkably various physical or chemical properties that, when, produce a useful third material. One continuous constituent is called **'*the matrix*'.** This constituent binds the composite and transmits loads from the matrix to the fibers. The other more discontinuous phase is **'*the reinforcement*'**, which is typically harder, stronger, stiffer and more stable than the matrix phase [46].

Materials can be classified as either isotropic or anisotropic. Commonly used engineering materials such as metals and polymers are usually considered to be homogeneous and isotropic materials which mean that they have the same material properties in all directions. In contrast, anisotropic (anisotropic means without isotropy) materials have different material properties in all directions at a point in the body [1]. Unlike metals and polymers, composite materials show heterogeneous (anisotropic) properties therefore they have properties that vary with direction within the material [47].

In composites, polymers, metals or ceramics are used as matrix, while fibers, flakes, particles and/or fillers are used as reinforcement which is embedded in a matrix phase [48]. Composites are commonly classified by their matrix/fiber phase and this classification is shown in Figure 2.8.

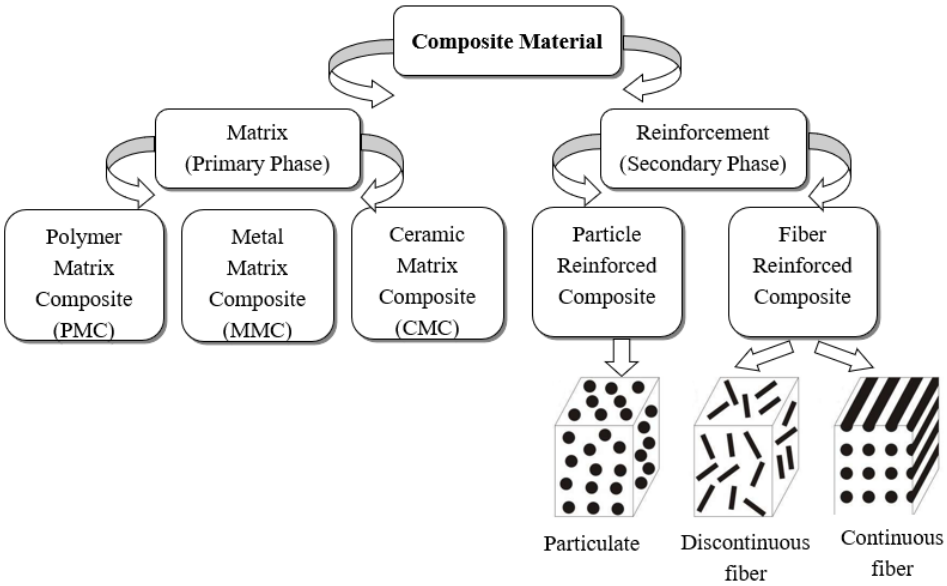

Figure 2.8. Classification of composites

The reinforcements are generally present in fiber and particulate form but may also be of regular or irregular geometry. Particle reinforced composites are weaker and less rigid than fiber reinforced composites. Composites containing continuous reinforcements are shown in Figure 2.9.

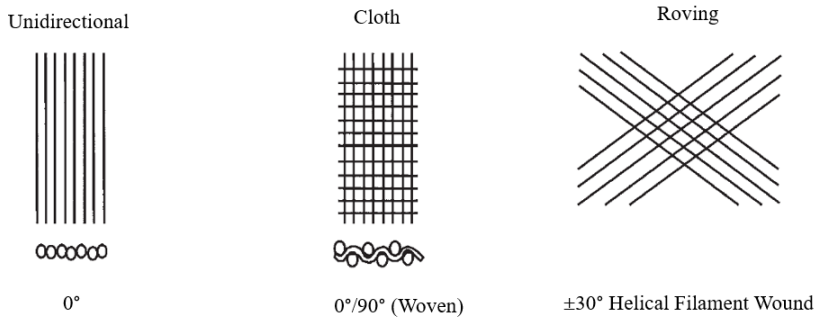

Figure 2.9. Typical continuous fiber reinforcement types

Fibers form composites which have high-strength owing to their nano scale diameter; they include less defects than the material manufactured in bulk form [48]. Typical fibers typically used in composites include carbon, glass, and aramid, which may be continuous or discontinuous.

Continuous fiber composites are produced by stacking layers in different directions to produce the desired strength and stiffness properties and so continuous fibers are generally preferred in composite industry. Because the orientation of fibers without delay affects mechanical properties of composites, it appears logical to orient as many of the layers as viable in the fundamental load-carrying direction. While this approach might also work for some structures, it is important to stabilize load bearing capability in a range of various directions [48]. The plies stacked at various (defined as laminate) and same orientation (lamina) are shown in Figure 2.10.

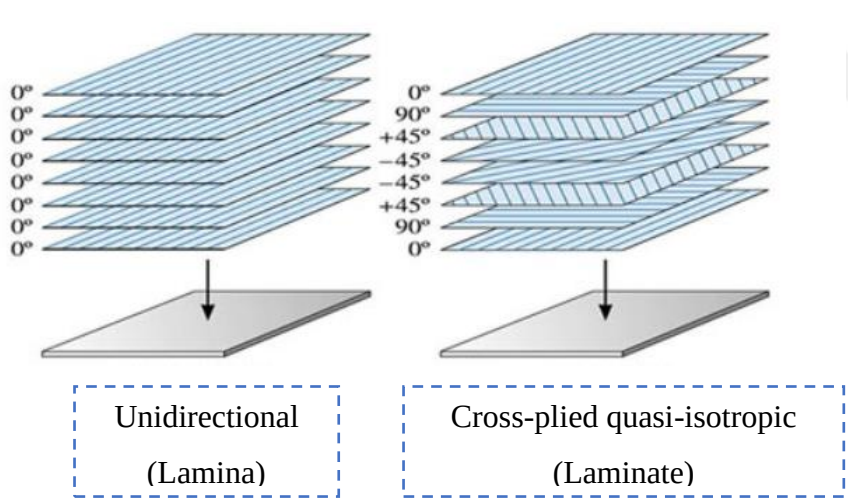

Figure 2.10. Laminate stacking and ply orientation in composites [16]

2.3.1. Applications and Advantages of Composite Materials

Composite materials have been formed as preferred structural materials for many applications due to their outstanding properties compared with other materials such as metals, alloys, plastics, glasses and ceramics. First developed for military aircraft applications in the early 1970's, composites, especially carbon fiber reinforced composites (CFRCs) now play important role in broad range of some systems such as transportation, construction, defense, automotive, medical and more recently infrastructure [49], as shown in Figure 2.11. Fiber reinforced epoxy composite laminates are known to have high in-plane stiffness, strength and fatigue resistance under tensile loadings. The fibers possess the fundamental work to carry the load enforced on the laminate and particularly carbon fibers have an extraordinary tensile strength [50].

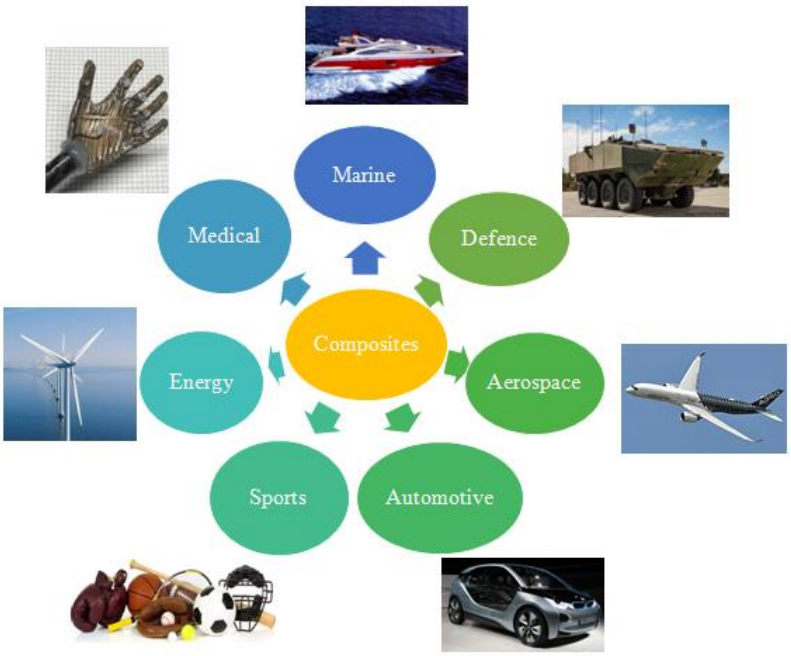

Figure 2.11. Some applications of composites

When the materials forming the composites are brought together, the poor properties of each material are combined in a manner that minimizes and produces better properties. The diagram in Figure 2.12 summarizes the relationship between the classes of materials used in engineering and the development of composite materials [47]. “Composite” simple means offers little mark of the individual combination range which included a variety of materials in this class.

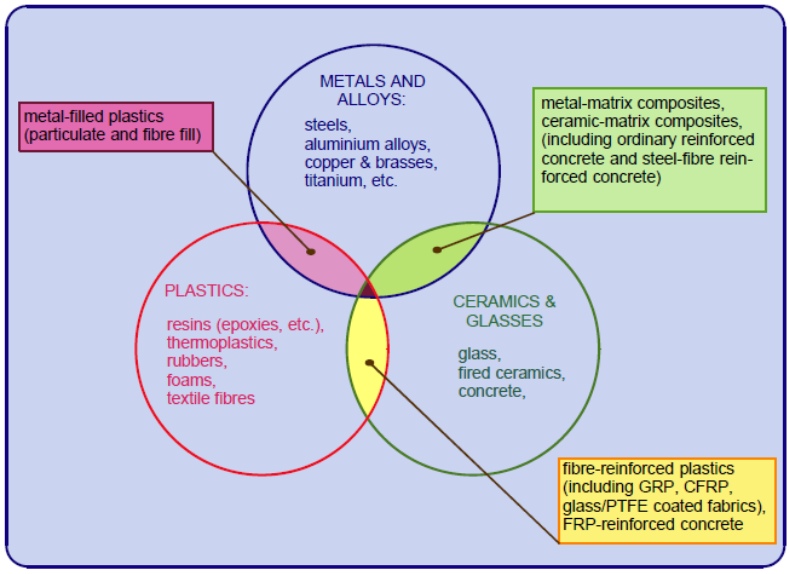

Figure 2.12. Relationships between classes of engineering materials, showing the evolution of composites [47]

Composite materials have many advantages involving lighter weight, the capability to tailor the layup for ideal strength and stiffness, corrosion resistance, improved fatigue life, and, with good design application, less installation costs. The specific strength and modulus of high strength fibers such as carbon are higher than those of other comparable metallic alloys, especially aerospace applications [46].

Higher weight savings give the system higher performance and thus offer advantages in terms of greater payload, longer range and gas savings. Composites used in

aerospace applications provide weight savings generally from 15 to 25 percent range [48].

In addition to the advantages of composite materials, there are some disadvantages such as high raw material costs and usually high fabrication and assembly costs [48]. In addition, unlike metals, composites are not isotropic structure, that is their properties are not same in all directions and therefore, there is poor strength in out of plane direction. Due to their complex nature and anisotropy of the structure, composite materials exhibit different modes of failure and damage with respect to metals or other conventional materials [51].

2.3.2. Failure and Damage Modes for Carbon Fiber Reinforced Polymer (CFRP) Composites

Unlike metals or other conventional materials, CFRP composites exhibit various modes of failure and damage due to their non-homogeneity and the anisotropy of the structure of composites. As a result, the stress-strain field and resulting failure process in laminated CFRP composites are exceedingly nonuniform. The randomness of the strength-toughness and the inhomogeneity of the stress-strain field cause the typical micro-structural mechanisms of damage accumulation such as cracking of matrix, rupture of fiber, matrix/fiber debonding and delamination [47]. In Figure 2.13 laminates modes of failure are presented.

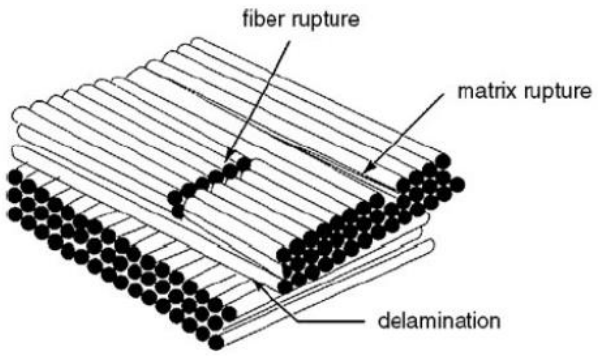

Figure 2.13. Some damages modes in composites [51]

The failure mode is severely affected by the matrix as well as its compatibility with the fibers. Matrix is the first element to fail when the load is carried by the matrix and not by the fibers. When external load or deformation occurs stronger and fibers cannot withstand the load, even the fibers can break. The fiber/matrix debonding damage mode depends on the strength of the bond between the matrix and the fiber, which affects the load transfer mechanism from the matrix to the fiber. '*Delamination*', the separation of two adjacent plies in composite laminates, is a critical and common failure mechanism in laminated carbon fiber reinforced polymer matrix composites. This failure is one of the major factors limiting the service life of polymer composites in engineering structure [12]. Delamination can be arising from many elements shown in Figure 2.14 that causes reduction of the material stiffness.

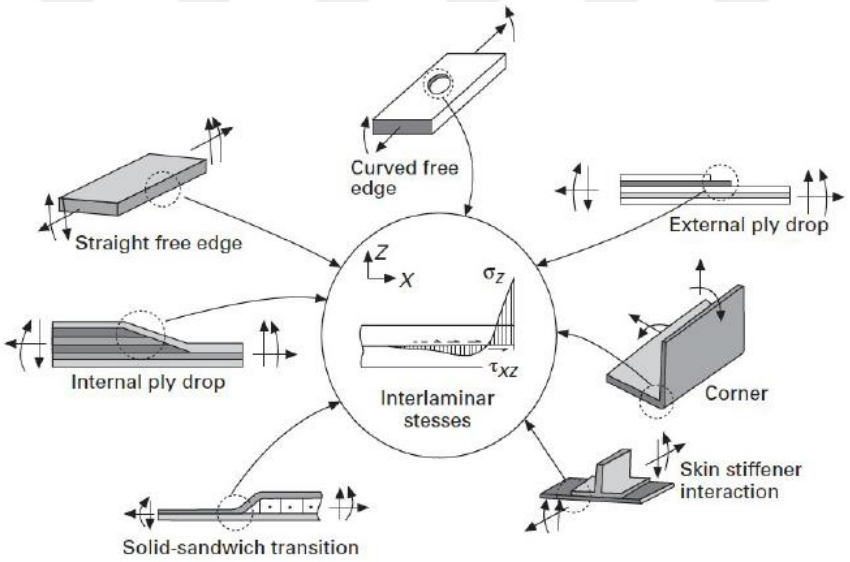

Figure 2.14. Causes of delamination [48]

The basic failure modes for delamination mechanisms in composites can be classified based on the direction of the applied load. They are opening mode ''Mode I'', the sliding shear mode ''Mode II'' and the tearing shear mode ''Mode III'' [52]. They are shown in Figure 2.15. The fact that laminated composites are anisotropic and non-

homogeneous means that all three modes can be effective in propagating delamination [53].

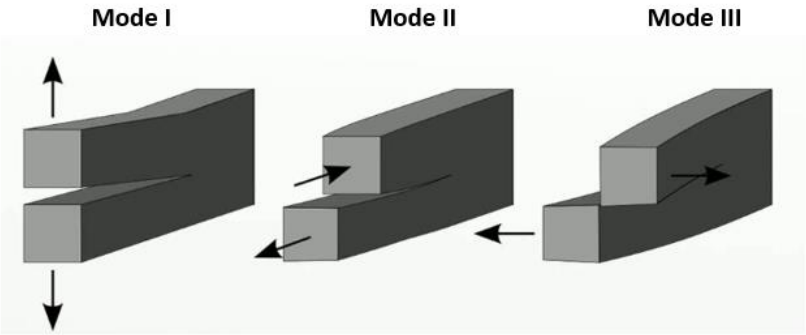

Figure 2.15. Typical modes of fracture in composites

The resistance of CFRP composite material against the initiation and propagation of crack in these modes is called the '*Interfacial Fracture Toughness in Mode I (G_{1C})*'. Various interlaminar fracture test methods and specimen geometries have been introduced to measure the delamination toughness under different mode loadings [53]. In this study, the Mode I fracture toughness of composites was measured according to the ASTM D-5528 ''Standard Test Method for Mode I Interlaminar Fracture Toughness of Unidirectional Fiber-Reinforced Polymer Matrix Composites'' [54]. Mode I delamination properties of continuous fiber-reinforced polymer composites are investigated using the well-known double cantilever beam (DCM) specimen geometry in this standard.

The DCB specimen shown in Figure 2.16 consists of a rectangular, uniform thickness, unidirectional laminated composite specimen including a non-adhesive insert (Teflon band) on the midplane that provides a delamination initiator. Opening forces are implemented to the DCB specimen by means of loading block (end block) bonded onto the two sides of the specimen end having the pre-crack. The ends of the DCB open at a certain speed in a controlled manner by applying a certain amount of load.

The load and delamination length applied during the test are recorded and these values are used to calculate the G_{1C} [54].

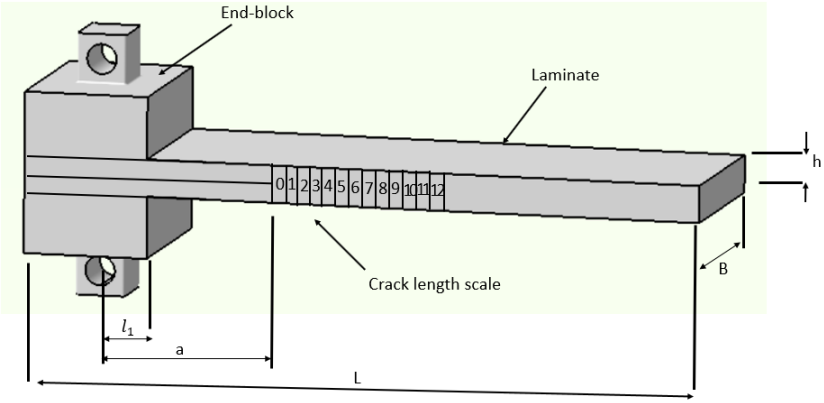

Figure 2.16. The DCB specimen

The samples to be tested before starting the test should be prepared as follows;

- DCB specimens were cut from laminates, approximately 250 mm x 25 mm x 3.4 mm with pre-crack length of approximately 60 mm. At least 5 coupons for each test should be tested.
- Both side edge of the specimen was marked with white paint every 1 mm for the first 5 mm from the insert, and then, mark the remaining 45 mm with thin vertical lines every 5 mm in order to facilitate the measurement of crack length.
- After the preparation of test specimen, load blocks were mounted on the specimen and the specimen is placed the grips of the loading machine. As the load is applied, the sample starts to separate from the interface placed on the non-adhesive insert. When the crack followed by the camera on the machine reaches the drawn areas marked on the sample, the load and displacement are recorded. The example showing the load-displacement graph after DCB test is shown in Figure 2.17.

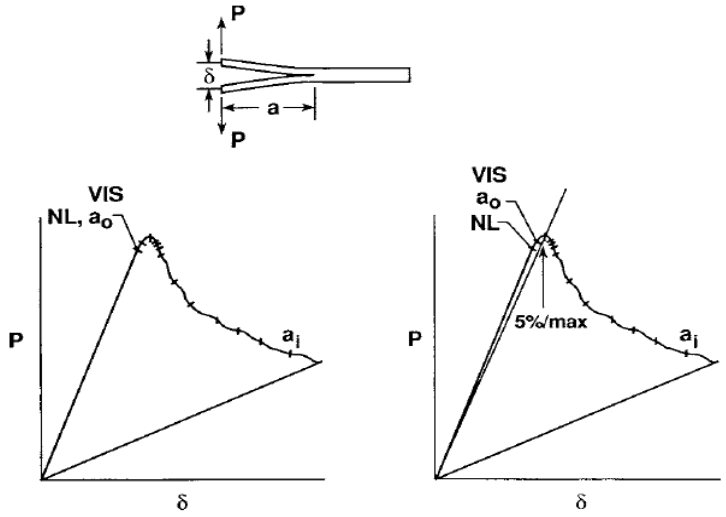

Figure 2.17. Load-Displacement curve from DCB test[1] [54]

The corrected beam theory described in standard was used to calculate G_{1C} values using the equation 1 [21]:

$$G_I = \frac{3P\delta}{2b(a + |\Delta|)} \qquad Equation\ 1$$

Where G_I is the Mode I interlaminar fracture toughness, P is the applied load, δ is the opening displacement, b is specimen width, a is the delamination length (crack length) and Δ is a crack length correction factor which is found experimentally by plotting the cube root of the compliance ($C^{1/3}$), as a function of delamination length (a) (Figure 2.18). The compliance, C, is the ratio of the load point displacement to the applied load, δ/P [21].

[1]*NL point*: The point of deviation from linearity, *VIS point*: The point at which delamination onset is visually detected and *5% max point*: The point at which the compliance has increased by 5%.

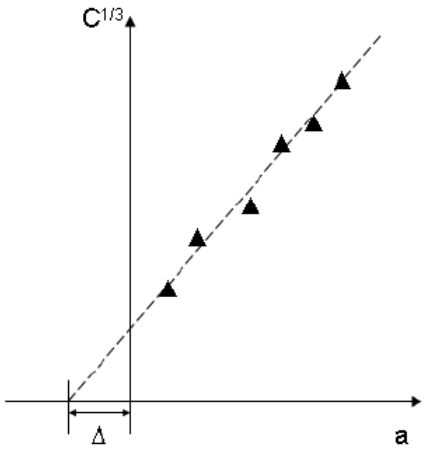

Figure 2.18. Correction factor graph for the modified beam theory [55]

2.4. Methods to improve delamination resistance

There have been several methods to solve delamination problem and improve the interfacial fracture toughness of CFRP composites. The methods can be classified as laminate design, edge design, modification of matrix and interleafing [1].

Laminated polymer composites are highly anisotropic materials, thus loading stress distribution in a laminate are not homogeneous. This stress distribution can be modified by altering laminate stacking order. Interlaminar stresses can be considerably reduced with a proper stacking-sequence while keeping the same global properties of the laminate composites. For example, the delamination stress σ_z in a symmetric laminate with a [15°/45°/-45°/-15°]s layup is much lower than that in a similar laminate with a [15°/-15°/45°/-45°]s layup under constant in-plane tension [56].

2.4.1. Laminate Design

'*Laminate design'* using hybrids and discontinuous plies is other method. These laminates structure can decrease the mismatch across the interface, also increase the fracture toughness. However, they may also reduce the laminate global strength and

tailored properties. Additionally, 3D weaving and braiding are other method to suppress delamination, but the limitation of 3D woven and braided structures is their high manufacturing cost [57].

2.4.2. Edge Design

The other delamination resistance method is modification of '*edge design'* by changing the nature of the free edge that does not contain any reinforcement. Edge reinforcement is strengthening of the free edge by using various methods such as laminate stitching [4], [5], laminate stitching [1] and ply termination [12], [1] shown in Figure 2.19. These free edge delamination-suppression methods can improve the delamination strength; however, they contain extra machining so have high manufacturing cost. Stitching method may cause fiber breakage at stitch hole, misalignment of fibers in laminate composites. Also, these methods may be unsuitable in multi-layered laminated systems [12].

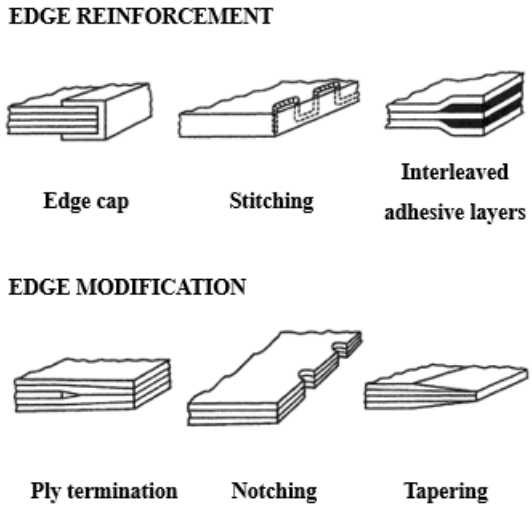

Figure 2.19. Free-edge delamination-suppression concepts [1]

2.4.3. Modification of Matrix

'Modification of matrix' is another method to improve delamination resistance in CFRP composites. The fracture toughness of thermosetting resins is relatively low, thus the interlaminar toughness in composites can be directly enhanced by developing the fracture toughness of resins. In the case of polymer matrix composites (PMCs), the polymer matrices are reinforced with the high-strength, high-modulus fillers or fibers [14]. Much research was done on toughened epoxy resins with rubbery materials [58], [14], [59], [60], polymeric nanofiber [17], thermoplastics films/particles [61], [62], some particulates [63], [64], [65].

In addition to these systems, by combining with more than one material, '*hybrid*' resin systems for composites with outstanding properties can be developed. Tomohiro and his work mate have studied the mechanical properties of CFRP laminates by using cup-stacked carbon nanotubes (CSCNTs) hybrid system as reinforcement. CSCNTs are composed of stacked several layers of truncated conical graphene sheets and they are placed in relation to each other like metal bellows. CSCNT-dispersed epoxy was only performed between the middle layers where crack propagates. It was reported that cup-stacked carbon nanotubes (CSCNT) used in both epoxy matrix and the interface of CFRP sub-laminates increased the fracture toughness by threefold [66]. Sprenger *et al.* researched that the performance of CFRP composites by effect of epoxy toughened by rubber-toughening with silica nanoparticles. The addition of rubber in epoxy increases the measured fracture toughness of CFRP composites but reduces the modulus and T_g of the bulk material whereas silica nanoparticles toughen an epoxy polymer and increase the modulus and fracture toughness of composite system. The use of silica nanoparticles and micron-sized rubbery particles to form hybrid toughened epoxy polymers show a significant increase in the toughness, interlaminar fracture energy, and fatigue/impact performance simultaneously. Hence, this hybrid system shows the best balance of properties with the synergistic effect [67].

Recently, more research on high-performance '*graphene-based epoxy system*' has been carried out and attracted attention. Han *et al.* prepared CFRP composites using epoxy resin with well dispersed GO nanosheets as matrix [35]. GO was dispersed into the epoxy resin and then was brushed onto plies of carbon fiber fabrics. It was reported that the incorporation of 0.10 wt % GO into the epoxy resin achieved the largest interlaminar shear strength (ILSS) of 96.14 MPa for laminates, 8.05% higher than that without GO. Also, the glass transition temperature of the composite was increased by approximately 5 °C [35]. Tang *et al.* reported that the poorly and highly dispersed reduced graphene oxide (RGO) at 0.2 wt % loading resulted in about 24% and 52% improvement in fracture toughness (K_{1C}) of cured epoxy thermosets, respectively [68]. Du *et al.* worked on improvement of toughness of CFRP composites by using graphene/epoxy resin [69]. With the incorporation of 1.0 wt % of graphene into epoxy, they achieved ~150% and 140% improvement in matrix fracture energy and mode I interlaminar fracture energy of composites, respectively [69].

However, matrix modification may cause some problems such as decrease in in-plane properties such as elastic modulus, reduce the processing ability of matrix resin due to high viscosity and the difficulties in obtaining a homogeneous dispersion of particles in matrix resin [12]. In addition, these additions cause the glass transition temperature (T_g) of the matrix to decrease [15].

2.4.4. Interleafing (interleaving)

'*Interleaving'* seems to be a more useful and remarkable approach to improve the interfacial mechanical properties of composites [70]. This method includes the insertion of toughening films [71], particles [72], solid resins, micro/nanofibers [16] or hybrid systems between the layers of laminates. Jiang *et al.* studied both Mode I and Mode II fracture toughness development through incorporating polyethylene terephthalate (PET) films between the composite layers. Mode I fracture toughness decreased whereas Mode II fracture toughness increased [13].

Hojo *et al.* studied fracture toughness improvement of CFRP composites through incorporating two kinds of interlayer/interleaf which are polyamide particles and interleaf of ionomer resin. It was found that polyamide particles interleaving resulted in a four time the fracture toughness (G_{1C}) increase compared to the reference, however the propagation value, G_{IR}, was almost identical for both laminates. Also, G_{1C} and G_{1R} values of ionomer laminates were 3.2 times and 3.5 times higher than those of the base laminates [73]. Wong *et al.* prepared the dissolvable phenoxy fiber, which are placed at the interlaminar region in a carbon fiber/epoxy composite. It was found that the average Mode-I fracture toughness value, G_{1C} increased tenfold with only 10 wt. % phenoxy fiber added [74]. White and Sue prepared the CFRCs containing epoxy/polyamide (PA) interlayers and epoxy/PA/multi-walled carbon nanotubes (MWCNTs) thin film at the laminate mid-plane. Composites interlayered with epoxy/PA/MWCNT hybrid system exhibits nearly 2.5 and 1.5 times higher fracture toughness than composites containing neat epoxy and epoxy/PA interlayers, respectively [15]. Borowski *et al.* studied Mode I interlaminar fracture toughness of CFRP composites with the addition of carboxyl functionalized multi-walled carbon nanotubes (COOH-MWCNTs). The experimental results show a 25% increase in the maximum interlaminar fracture toughness of the CFRP composites with the addition of 0.5 wt % MWCNTs [75].

Addition of studies about epoxy matrix modified with GO to strengthen the interface of CFRP composites, as well as the use of the studies about addition of GO to the interface region have recently attracts attention. Seshasai studied the fracture toughness and flexural strength of carbon fiber reinforced epoxy resins modified with polyvinylpyrrolidone (PVP) dispersed graphene oxide (GO) in the interface region. These samples were prepared that sixteen layers of prepregs were cut according to the planned dimensions and exfoliated GO in PVP solution was painted on the surface. A 100% improvement in the fracture toughness with as little as 5 wt % of GO in the interface has been achieved [52]. Ning *et al.* reported 170.8% increase of Mode I fracture toughness for GO reinforced epoxy interleaf (GO-epoxy paste) into the

interface of CFRP laminates at the GO loading of 2 g/m^2 [27]. Zanjani *et al.* developed three different designs which are deposition of graphene sheets onto the surface of carbon fabric mats with electrospraying methods (first arrangement), graphene sheets dispersed into the epoxy matrix (second arrangement) and the combination of the first and second arrangements to enhance carbon fiber epoxy matrix composite systems. In the hybrid composite structure in which graphene sheets are used as both interface modifier and matrix reinforcing agent, remarkable developments are observed in the work of fracture by about 55% and the flexural strength by about 51% [6]. Du *et al*. investigated the graphene/epoxy (G/E) and graphene/epoxy interleaves effects for delamination toughening of carbon fiber/epoxy composite laminates. The results show that; the incorporation of 1.0 wt % of graphene into epoxy was found to considerably improve the matrix fracture energy by ~150% and lower the thermal expansion coefficient by ~30%. When these partially cured G/E composites were used as interleaves in carbon fiber/epoxy (CF/E) composites and co-cured, a remarkable 140% increase in Mode I interlaminar fracture energy was succeeded [69].

In all these applications, the impact of increment the fracture toughness is observed but the amount of material placed between the layers must increase to a certain level to improve interfacial mechanical properties of composites and this causes some disadvantages. It is said that in the literatures, the main disadvantage of interleafing is its thickness and weight penalties [76]. As a result of studies conducted up to now, it is emphasized that in an attempt to overcome the drawbacks of interleafing and other toughening methods, one possible solution may be in the use of nanotechnology [12]. With the development of nanotechnology, researchers are beginning to use nano scaled materials such as nanoparticles, nanotubes, nanorods and nanofibers to reinforce the CFRP composites. In recent years, polymer nanofibers have attracted much attention because of the mechanical properties such as ultimate tensile strength, young modulus (Figure 2.20), flexibility, excellent porous characteristics, and extremely large surface-to-volume ratio [77]. In addition, due to nanofibers' thin and light weight, they do not influence the thickness of layer and weight of the composites

to which they are added to interlayer of the composites [12]. The most commonly used method for producing polymer nanofibers is '*electrospinning*'.

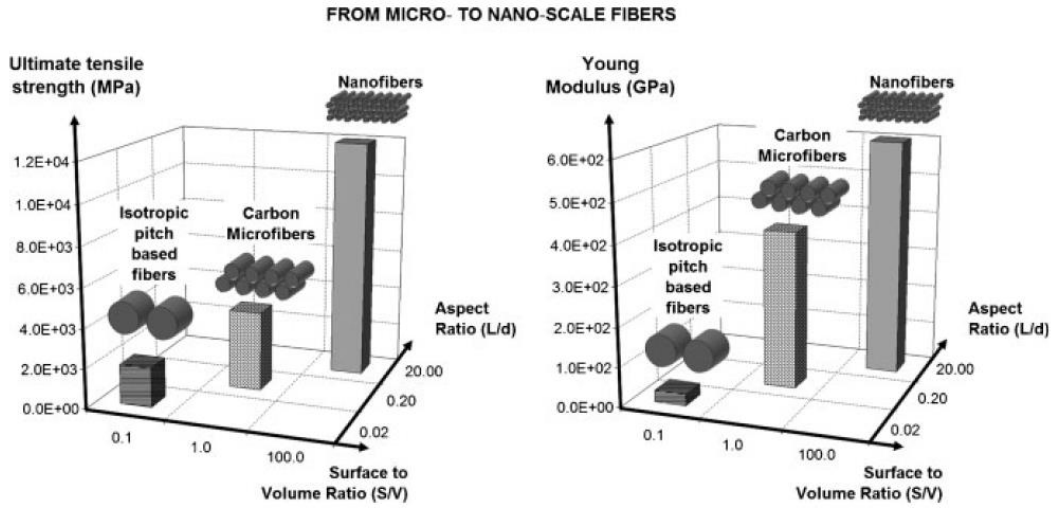

Figure 2.20. Ultimate tensile strength and young modulus properties of micro to nano-scale fibers as reinforcement of bulk composites [78]

The interface hardening can be divided into three groups by using the nanofiber insertion method between the layers in the literatures. These are (i) single polymer (homopolymers) nanofibers, (ii) multiple polymer nanofibers and (iii) hybrid systems obtained by mixing another component in the polymer nanofiber. In these studies, the preparation of the laminated composites, curing cycles, and the method of transferring the nanofiber layer into the interface can be changed.

The first of these groups are homopolymers produced using a single type of polymer. Some researchers use homopolymers like Polymenzimidazole (PBI) [79], polyacrylonitrile (PAN) [12], polysulfone (PSF) [80], polyetherketon-cardo (PEK-C) [76], polyvinylidene difluoride (PVDF) [81], polyamide-imide (PAI), polyamide (PA66), polycaprolactone (PCL) [21] and survey the influence of these polymers G_{1C} of composites have been used in the literature as a single polymer. The studies and results of the toughening of the interface using the homopolymers are shown in Table

2.1. When Table 2.1 is examined, some polymers increase the $G_{1c\text{-initiation}}$ ($G_{1C\text{-in}}$) value, while simultaneously causing sudden decreases in $G_{1c\text{-propagation}}$ ($G_{1C\text{-prop}}$) [21].

Table 2.1. Interfacial toughening studies with nanofibers using homopolymers

Polymer	**G_{1C}**	**Other Test Results**	**References**
Polymenzimidazole (PBI)	G_{1C} + 144%	K_{1C} + 76% Elastic Modulus +27%	[18]
Polyacrylonitrile (PAN)	G_{1C} + 75% G_{IIC} + 15%		[12]
Polysulfone (PSF)	G_{1C} + 180%		[80]
Polyetherketon-cardo (PEK-C)	G_{1C} + 80%		[76]
Polyvinylidene difluoride (PVDF)	G_{1C} - 20% G_{IIC} + 53%		[82]
Poly (Hydroxyether of Bisphenol A	G_{1C} initiation + 97,5% G_{1C} propagation + 118 % G_{1C} maximum + 106 % G_{IIC} + 21%	Interlaminar shear strength (ILSS) does not change.	[83]
Polycaprolactone (PCL)	G_{1C} + 92%	Elastic Modulus + 11%	[81]
Polyacrylonitrile (PAN)	G_{1C} decrease		
Polyvinylidene difluoride (PVDF)	G_{1C} decrease		
Nylon 6,6 (PA66)	G_{1C} + 5%	Elastic Modulus + 0,9% Flexural strength +6%	[84]
Polyamide 66 (PA66)	G_{1C} initiation (insert) +173% G_{1C} initiation (front crack) +11% G_{1C} propagation - 6%		[21]
Polycaprolactone (PCL)	G_{IC} initiation (insert) + 14% G_{1C} initiation (front crack) +4% G_{1C} propagation + 12%		
Polysulfone (PSF)	G_{1C} initiation (insert) - 4% G_{1C} initiation (front crack) - 52% G_{1C} propagation - 52%		
Polyamide-imide (PAI)	G_{1C} initiation (insert) - 36% G_{1C} initiation (front crack) -58% G_{1C} propagation - 68%		

* In the graph '+' refers to the increase, '-' indicates the decrease.

Beside of homopolymers, some multi polymer system such as alternating layers of two different polymers [85], electrospinning of various polymers at the same time from different needles [22], or core- shell structure [21] are used for developing the interfacial fracture toughness of composites. Studies using nanofibers using more than one polymer for interfacial toughening are shown in Table 2.2.

Table 2.2. Interfacial toughening studies with nanofibers using more than one polymer

Polymers	**G_{1C}**	**References**
PCL and PA66 (fiber layers)	G_{1C} + 21% G_{IIC} + 56%	[85]
PCL and PA66 (fiber mixing)	G_{1C} initiation + 64% G_{1C} propagation + 16% G_{1C} maximum + 10%	[22]
PA66 and PVB (fiber layers)	G_{1C} initiation (insert) - 33% G_{1C} initiation (front crack) - 48% G_{1C} propagation - 63%	[21]
PA66 and PVB (core-shell)	G_{1C} initiation (insert) - 26% G_{1C} initiation (front crack) - 48% G_{1C} propagation - 64%	

In the system where PCL and PA66 are used together in singular and layers, $G_{1C\text{-}in}$ and $G_{1C\text{-}prop}$ are increased [85]. In another study in which PA66 and PCL were used, polymers were also electrospun from different syringes and PA66 was effective in the crack initiation stage, PCL was effective in the crack propagation stage, and as a result, both $G_{1C\text{-}in}$ and $G_{1C\text{-}prop}$ are increased [22]. In another study, PA66 and polyvinylbutyral (PVB) polymers were electrospun in two different forms as layers and as core shells, and a decrease in G_{1C} values was observed in both methods [21].

Hybrid systems are systems formed by the addition of particles that have the potential to elicit different toughening mechanisms into the polymers. Eşizeybek *et al.* used carbon nanotubes (CNTs) reinforced polyacrylonitrile (PAN) electrospun hybrid mats as interleaving in the carbon/epoxy composite laminates. The Mode I interlaminar fracture toughness values were enhanced up to 77% by introducing CNTPAN nanofibrous interleaves. Their experiments showed that the nano-scale toughening mechanisms such as CNTs bridging, CNTs pull-out, and sword-sheath increased the Mode I fracture toughness by 45% with respect to neat PAN nanofibrous interleaves [73]. Hamer *et al.* studied both Mode I and II fracture toughness development through incorporating pristine and MWCNT reinforced electrospun nylon 66 interleaves. The MWCNT reinforced nanofibril mat interleaving resulted in a 1.33 time the Mode I fracture energy increase compared to the pristine nanofibril mats interleaving [86]. Goodarz *et al.* studied the development of hybrid multi-scale aramid/epoxy composites interleaved with electrospun graphene nano-platelets/Nylon 66 (GNPs/PA66) mats. The experimental results revealed that; at 0.5 wt % GNPs, toughness went up by 25% while it pronouncedly increased by 68% at 1 wt % loading, which was maximum for other samples [87]. Li *et al.* prepared the MWCNTs-EP/PSF (polysulfone) nanofibers which are electrospun onto carbon fiber/epoxy prepregs attached on a rotating drum collector and then the hybrid nanofibers reinforced and toughened CFRP were prepared and the mechanical properties of the composites were investigated. At the interface layer of CFRP composites, the curing reaction of epoxy matrix and in-situ phase separation of hybrid nanofibers resulted in the formation of network structures, which contained four phases: MWNTs-EP, PSF sphere, carbon fiber and epoxy matrix. The proposed network structure of the correlative four phases contributed to synchronous reinforcing and toughening effects by crack pinning, cold drawing deformation, crack bridging and effective load transfer mechanisms, which led to improvement of strength and toughness of composites [88].

Among studies about CFRP composites, there is no works about usage of more than one polymer nanofibers containing GO for increase of interfacial toughening (G_{1C}) by

using electrospinning. In this study the effect of interleaved GO containing nanofiber on interfacial fracture response of CFRP composites and crystalline morphology change of electrospun nanofibers with the addition of graphene oxide is considered. In addition, by adding GO into the fiber, it was investigated which toughening mechanisms (debonding, bridging and crack pinning) can be activated by the changes in the morphology of the fibers. For this goal, graphene oxide containing Nylon 6 (N6)/Polycaprolactone (PCL) polymers with different N6 mass ratios (60, 80, 100 wt %) are placed mid-plane of the carbon fiber/epoxy laminates and then composites are subjected to double cantilever beam (DCB) test.

CHAPTER 3

MATERIALS AND METHODS

This chapter focuses on the used materials, synthesis methods and applied characterizations involved in the process. In this study, graphene oxide was synthesized while other solvents and materials were purchased from different companies which are explained in the following parts.

3.1. Materials

Several polymer/solvent solutions were prepared for electrospinning to form nanofibers. Polycaprolactone (PCL) pellets which have average molecular weight $\overline{M_W}$~80,000 were purchased from Sigma-Aldrich Co. Ltd. (Germany). Nylon 6 ($C_6H_{11}NO$) with density of 1.084 g/ml at 25˚C pellets were obtained from Sigma-Aldrich (Germany). Dichloromethane (DCM), dimethylformamide (DMF), trifluoroethanol (TFE) solvents for the dissolving the polymers were purchased from Merck (Germany). Tetrahydrofuran (THF) was purchased from Sigma-Aldrich for the purpose of dispersion works. Graphite (~ 44 μm) used for graphene oxide synthesis were purchased from Asbury Carbons in the form of flakes. Potassium permanganate ($KMnO_4$) and sulfuric acid (H_2SO_4, 95-97%) were purchased from Yenilab and Honeywell Co. Ltd. respectively. Hydrochloric acid (HCl, fuming 37%), technical grade acetone, hydrogen peroxide (H_2O_2, 30%) and orthophosphoric acid (Nitric acid, H_3PO_4, 85%) were obtained from Merck. The test samples were produced using the 'VTP H 300 CFA 210 3KT RC35 HS' carbon fiber prepreg (R1) and 'VTP H 300 CFA 200 3KT RC42 HS' carbon fiber prepreg (R2) from SPM Composite Company. Also, the prepregs are 2x2 braided fabrics and the amount of carbon fiber is 210 g/m^2 in R1 (35% wt. resin) and 200 g/m^2 in R2 (42% wt. resin).

3.2. Methods

3.2.1. Synthesis of Graphene Oxide (GO)

Graphite oxide was formed by oxidizing graphite flakes in sulfuric acid, nitric acid for 12 hours by using Tour Method [37]. Graphite powder (1.05 grams,1 weight equivalent) were mixed with $KMnO_4$ (6.30 grams, 6 weight equivalent) in 250 ml volume reactor. Graphite/$KMnO_4$ solid mixture was suspended in a 9:1 mixture (140 ml) of H_2SO_4 and H_3PO_4 by the slow addition of acid mixture to solid mixture under stirring and at this time mixture color is dark green. The reaction was then heated to 50 °C and stirred for 12 h in order to start oxidation process. During this time, oxidation was achieved by lightly increasing reaction temperature and extending reaction time [89] and mixture color was brown. Then, the reaction was cooled to room temperature and 160 ml of ice was added to reaction mixture in a water bath to prevent sudden temperature rise. The H_2O_2 was added slowly into the mixture until the mixture color turned to yellow in order to remove excessive MnO_4^- ions from the system. The obtained solution was then centrifuged (8000 rpm, 20 min) and the supernatant was decanted away. The obtained paste was then washed with 3.4 wt % HCl and acetone. Washing and centrifuge (8000 rpm, 3 min) with HCl was repeated three times, washing and centrifuge (8000 rpm, 20 min) with acetone were carried out four times [90]. The solid obtained after washing was dried using rotary evaporator and dried in a vacuum oven. After removal of solvents from the solid, graphite oxide flakes were obtained with color of brownish yellow. The solid obtained end of the reaction was about 2∼2.5 gram of product. Overall reaction diagram of graphene oxide production is shown in Figure 3.1.

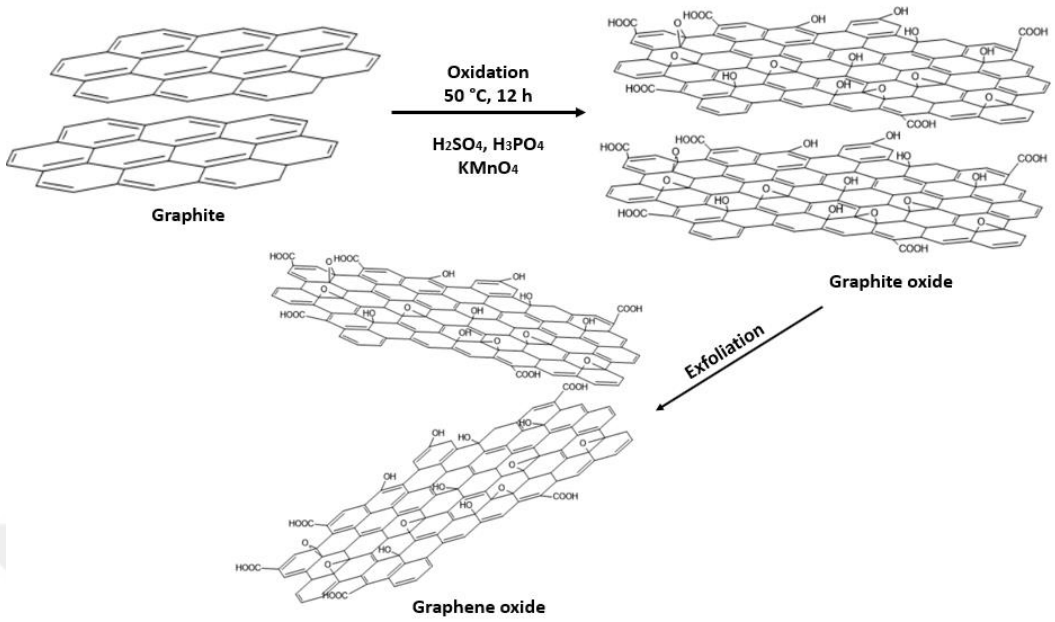

Figure 3.1. Graphene oxide synthesis reaction diagram

3.2.1.1. Graphene Oxide Dispersion in Organic Solvents

Well-dispersed GO sheets in solution to be used for electrospinning is necessary to create hybrid system which is composed of N6 and PCL nanofibers containing GO sheets. It was first necessary to identify a common solvent, for the formation of 2 or 3-component hybrid nanofibers. Several literature reviews and experiments were conducted using various solvents for this purpose. According to literature about GO dispersion, it was found that stable dispersions were left in some solvents such as water, DMF, THF, TFE, ethylene glycol and pyridine [91]. Based on the knowledge that TFE dissolves PCL, N6 polymers and GO, studies on dispersion of GO in TFE and other solvents have been performed and summarized in the follows.

In order to compare the dispersion behavior in different solvents, the same quantity of GO (~2.5 mg) was added to a given volume of solvents (~5 ml), with 0.5 mg/ml concentration. Also, the dispersion of the GO at different concentrations which are 1 mg/ml, 2.5 mg/ml and 6 mg/ml were studied. GO dispersions were tested in the

following organic solvents: DMF, DCM, (DI) Water, DMF/DCM, TFE, THF/Water, HFIP and formic acid/acetic acid. Dispersion experiment results are shown in Section 4.2.

3.2.1.2. Homogeneous Distribution of GO in Solvents and Size Reduction Studies of GO Sheets

Ultrasonic homogenization studies were conducted in order to reduce the size of the GO pieces and provide more homogeneous dispersions of GO sheets in aqueous medium. According to the ultrasonic probe type, duration, centrifugation time and the final average size of GO after ultrasonication process, the GOs used in this study are named. Numerical evaluation for homogenization was performed using Dynamic Light Scattering (DLS) method using Malvern Zetasizer.

An ultrasonic water bath and an ultrasonic homogenizer (probe) were used in the sonication process and the tip-operated process was performed using two different devices seen from Figure 3.2.a and Figure 3.2.b. The properties of the used sonicators are as follows. In the sonication procedures performed with the homogenizer showed in Figure 3.2.a, 80% power (130-Watt, 20 kHz, Probe A- 2.2mm), 1 cycle (50 seconds vibration, 10 seconds waiting) are used. 37% power (74-Watt, 20 kHz, Probe B-12mm), 3 cycles (0,3 seconds vibration, 0,7 seconds waiting) are used in the sonication procedures performed with the homogenizer showed in Figure 3.2.b.

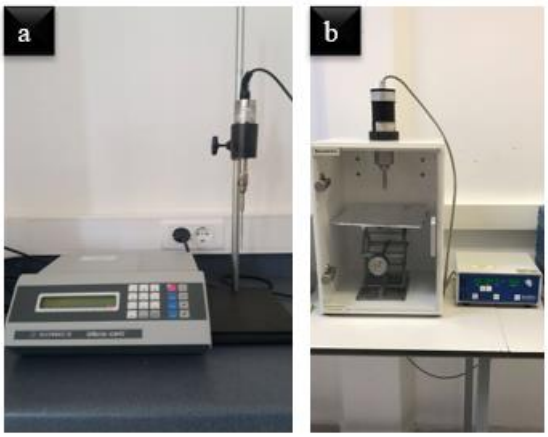

Figure 3.2. Ultrasonic homogenizers with different probe (a) Probe A- 2.2mm, (b) Probe B- 12mm

In probe sonication using 'Probe A', 250 mg GO was first added to the water in 50 ml beaker and the probe was placed in ice bath, 0.5 cm above the bottom of the beaker. The probe sonication was stopped every 10 minutes, and a portion of sample was taken from the beaker and size analysis was performed after the solution was diluted to 0.05 mg/ml.

For the particle size analysis of untreated graphene oxide (GO1), 0.05 mg/ml mixture of GO1/water was prepared, which was sonicated for 15 minutes in a water bath. Zeta sizer analysis results of different sonication times using 0.05 mg GO/ml in water by using Probe A and Probe B are given in Section 4.2.

After the probe sonication was completed by using Probe A and Probe B, the mixtures were centrifuged at 8000 rpm to remove the graphite from the bottom and from the GO with large size. The centrifuge time was determined by the amount of graphite remaining at the bottom. While 20 minutes centrifugation and 30 minutes probe sonication were applied to graphene oxide named as GO2, 40 minutes centrifugation and 120 minutes probe sonication were applied to graphene oxide called GO3. After centrifugation applied to GO3, the graphite and the deep yellow GO sheets appear on the bottom are shown in Figure 3.3.

Figure 3.3. Collapsed graphite (black) and large sheets of GO (dark yellow) after 40 min 8000 rpm centrifugation applied to GO3.

After centrifugation, the above GO/water supernatant was taken into a flask and attached to the freeze dryer. After 3 days, the material in the balloon was checked and the balloon was removed after the material was dry. The dried GO is shown in Figure 3.4.

Figure 3.4. GO's images after drying

The GO must be homogeneous and steady in the solution in which the graphene oxide is present before the electrospinning process is carried out. Therefore, an additional sonication bath step was required, and so additional studies have been conducted to determine the appropriate duration of sonication. These studies were carried out in water and TFE and different sonication times were applied to determine the distribution of GO sheets in these medium. Treatments were applied to the GO2 and GO3. Water was first used as the medium, after GO2 and GO3 in water concentration was set to 0.05 mg/ml, the distribution was performed using a sonication bath 15, 20, 25 and 30 minutes and particle analysis was performed.

3.2.2. Production of the Hybrid System to be Used in the Interface

The hybrid system to be used in the interface consists of graphene oxide-containing nanofiber tulles and these nanofibers are produced by electrospinning process. Before starting the electrospinning process, the solution to be spun was prepared and then nanofiber production was started by installing the appropriate electrospinning setup.

3.2.2.1. Preparation of Electrospinning Solution

Polymers and GO solutions were prepared at determined concentrations one day prior to the electrospinning process. When preparing the polymer solution, the specified number of polymers (PCL, N6 or N6/PCL) are added to the glass vials with black cap and then the TFE solvent is added and then wrapped with parafilm. When preparing the GO solution, the determined amount of GO is added to 10 ml small glass vials and then TFE solvent is added. It should be ensured that the glass containing the GO solution is wrapped around with aluminum foil to prevent receiving light. After the polymer and graphene oxide solutions were prepared, they were separately mixed in the magnetic stirrer for overnight at about 200-300 rpm. The following day, 25 min as determined by optimum sonication time was carried out in sonication bath and then the GO/TFE suspension was immediately added to the N6 or N6-PCL/TFE solution. This mixture was additionally mixed for about 15 minutes in a magnetic stirrer until a

homogeneous appearance was obtained. N6/GO, N6/PCL (60/40)-GO3, N6/PCL (80/20)-GO3 sets were prepared and the amounts of polymer and GO used in these sets are shown in Table 3.1, Table 3.2 and

Table *3.3*. The codes such as C9, C17 shown in the table indicate which composite material is produced. Missing code numbers are samples of my friend who I worked with in the Tübitak project in the laboratory.

Table 3.1. The contents of solutions used in electrospinning experiments in N6/GO system

Code	**GO Type**	**GO (g)**	**GO Media (ml)**	**N6 (g)**	**N6 solvent[2] (ml)**	**GO in Solution (wt %)**	**N6 in Solution (wt %)**	**GO in fiber (wt %)**
C9	**GO1**	0.0100	4.0	1.05	4.0	0.083	8.718	1
C17	**GO1**	0.0192	3.5	0.92	3.5	0.182	8.720	2
C11	**GO2**	0.0220	4.0	1.05	4.0	0.183	8.709	2
C18	**GO3**	0.0220	4.0	1.05	4.0	0.183	8.709	2

Table 3.2. The contents of the solutions used in the electrospinning experiments in N6/PCL (wt/wt: 60/40) - GO3 system

Code	**GO3 (g)**	**GO Media (ml)**	**PCL-N6 solvent (ml)**	**PCL in Solution (wt %)**	**N6 in Solution (wt %)**	**GO in Solution (wt %)**	**GO in fiber (wt %)**
60/40	-	-	10.6	3.73	5.60	-	-
C26	0.0011	3.0	6.0	2.99	4.48	0.008	0.1
C31	0.0031	3.0	6.0	2.99	4.49	0.075	0.3
C24	0.0051	3.0	6.0	2.99	4.48	0.038	0.5
C23	0.0102	3.0	6.0	2.99	4.48	0.076	1.0
C21	0.0153	3.0	6.0	2.99	4.48	0.115	1.5
C19	0.0205	3.0	6.0	2.99	4.48	0.153	2.0

[2]TFE was used as the distribution medium/solvent in all experiments.

Table 3.3. The contents of the solutions used in the electrospinning experiments in N6/PCL (wt/wt: 80/20) - GO3 system

Code	GO3 (g)	GO Media (ml)	PCL (g)	N6 (g)	PCL-N6 solvent (ml)	PCL in Solution (wt %)	N6 in Solution (wt %)	GO in Solution (wt %)	GO in fiber (wt %)
80/20	-	-	0.30	1.20	9.31	2.10	8.40	-	-
C28	0.0053	3	0.21	0.84	6.60	1.50	6.00	0.040	0.5

3.2.2.2. Electrospinning Process and Production of Nanofibers

To produce nanofiber, clean room and electrospinning setup which is shown in Figure 3.5 have been used during the studies. Electrospinning system consists of cabinet, a pump, a power supply having high voltage, syringe filled with polymeric solution, a needle, silicone hose, a grounded collecting plate (rotating mandrel coated with copper plate) and ventilation system. The electrospinning system used in the studies is shown in Figure 3.5. In order to provide homogeneous distribution of nanofibers on copper collector in both axes, the syringe needle moving on the horizontal axis and the rotating collector system at a speed of 100 rpm were designed.

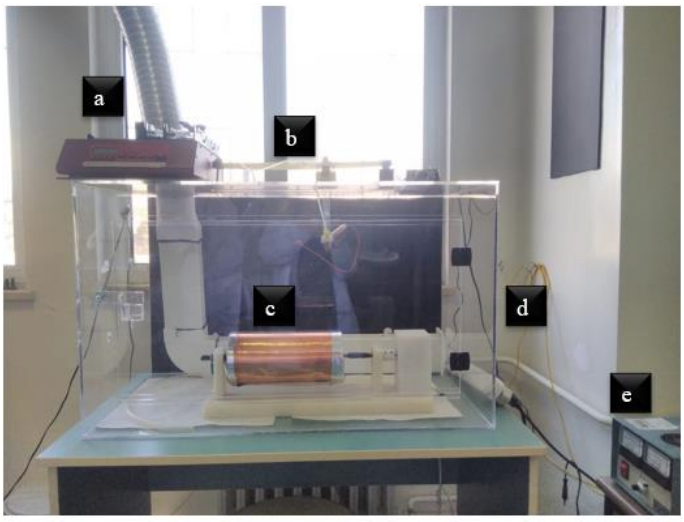

Figure 3.5. Electrospinning system (a) A syringe pump, (b) Moving syringe system, (c) Rotating cylindrical collector, (d) Transparent cabin (e) Voltage power supply

The 18-gauge syringe needle (40 mm, ϕ1.2 mm) moves in both directions at a rate of 1 cm/sec with the aid of a strap (Figure 3.6-a), while the collector consisting of 4 aluminum discs with a diameter of 13 cm rotates at a speed of 100 rpm. Nanofibers were collected on a copper sheet shown in Figure 3.6-c and after the copper plate is cleaned and polished periodically, it is kept in 110 °C vacuum oven for 1 hour and cleaned from oxide layers. Also, an auxiliary electrode made of copper material was used at the needle tip to intensify electric field at needle tip and obtain a more stable polymer jet, Figure 3.6-d.

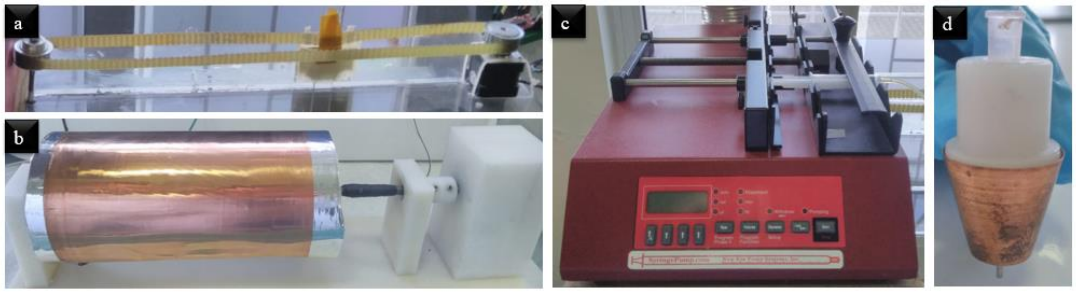

Figure 3.6. (a) moving syringe system, (b) copper plate, (c) a syringe pump, (d) an auxiliary electrode

Nanofiber collection was performed on the copper plate using the above system with specific collection times. To make a comparison between samples, the amount of nanofiber added to the interface must be the same and some calculations have been made for this. In order to ensure that the amounts of fiber to be transferred to the interface are similar in all samples, it is first optimized at which flow rate the fibers can be spun in each production. After the optimization at the first time of each production, the total collection time of nanofibers that can be spun at different flow rates is calculated for each sample. The following equation is used to calculate the collection times in each nanofiber production.

$$t = \frac{100 \times y}{v_{solution} \times \rho_{solution} \times k} \qquad Equation\ 2$$

The symbols used in Equation 2 represent the following expressions;

$t = collection\ time\ (hours)$

$y = amount\ of\ polymer\ targeted\ in\ the\ interface\ (gr)$

$v_{solution} = solution\ flow\ rate\ \left({}^{ml}/_{h}\right)$

$\rho_{solution} = solution\ density\ \left({}^{\mathrm{gr}}/_{\mathrm{ml}}\right)$

$k = percentage\ by\ mass\ of\ polymer\ in\ solution$

After the electrospinning process, the entire surface of the copper plate is covered with the nanofiber layer as shown in Figure 3.7-a. It is important to transfer the fiber collected in the copper plate with the highest efficiency when transferring to the prepreg. However, when the nanofibers collected on the copper plate were transmitted, some nanofiber loss was recorded. In addition, a certain amount of nanofiber residue remains in all corners and middle zone of the copper plate during transferring of nanofibers to prepreg layer, Figure 3.7-b and Figure 3.7-c.

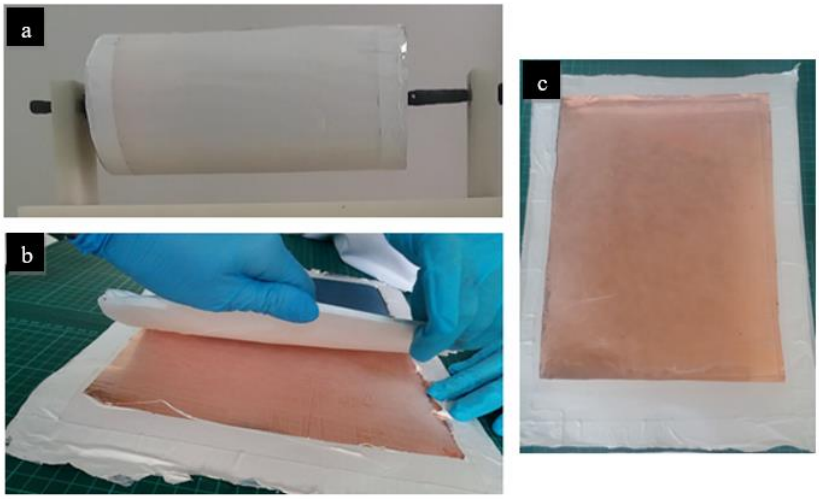

Figure 3.7. After electrospinning; (a) Fiber image collected in the copper plate, (b) transfer of fiber to prepreg layer and (c) Fiber image remaining on the plate after transfer to prepreg

To determine the effective amount of nanofiber (y_{active}) that can be transferred between layers, the mass of nanofiber tulle ($y_{collector}$) remaining on the copper plate and the amount of fiber overflowing ($y_{overflow}$) from the copper collector after transferring was weighed out from the mass of the polymer transferred (y) during the electrospinning period.

$$y_{active} = y - (y_{collector} + y_{overflow}) \qquad Equation\ 2$$

The parameters related to electrospinning processes are given in Table 3.4, Table 3.5 and Table 3.6. The abbreviations shown in these tables refer to the following definitions.

- d: needle tip-collector distance (cm)
- t: collection time (min)
- y: amount collected on the collector (g)
- $y_{collector} + y_{overflow}$: amount of fiber cannot be transmitted (g)
- y_{active}: amount transmitted to interface (g)

Table 3.4. Parameters of electro-spinning and transfer operations of N6/GO system

Code	**Voltage (kV)**	**Flow rate (ml/h)**	**d (cm)**	**t (min)**	**y (g)**	**$y_{collector} + y_{overflow}$ (g)**	**y_{active} (g)**
C9	**18**	1.5	20	206	0.6	0.278	0.322
C17	**19**	2.0	20	155	0.6	0.248	0.352
C11	**16**	1.5	20	165	0.6	0.247	0.353
C18	**19**	1.5	20	206	0.6	0.254	0.346

Table 3.5. Parameters of electro-spinning and transfer operations of N6/PCL (60/40)-GO3 system

Code	Voltage (kV)	Flow rate (ml/h)	d (cm)	t (min)	y (g)	$y_{collector} + y_{overflow}$ (g)	y_{active} (g)
C26	**13**	2.0	20	210	0.7	0.310	0.390
C31	**16**	2.0	20	210	0.7	0.297	0.403
C24	**12**	1.5	20	225	0.7	0.298	0.402
C23	**15**	1.5	20	280	0.7	0.273	0.427
C21	**16**	1.5	20	280	0.7	0.295	0.405
C19	**17**	1.5	20	280	0.7	0.251	0.449

Table 3.6. Parameters of electro-spinning and transfer operations of N6/PCL (80/20)-GO3 system

Code	Voltage (kV)	Flow rate (ml/h)	d (cm)	t (min)	y (g)	$y_{collector} + y_{overflow}$ (g)	y_{active} (g)
C28	**16**	2.0	20	209	0.7	0.297	0.403

3.2.3. Production of Electrospun Nanofiber Toughened Composites and Preparation of Test Samples

Composites were prepared for studying the influence of nano-hybrid system, nanofiber containing graphene oxide, in the interface. ‘VTP H 300 CFA 210 3KT RC35 HS’ code (R1: Reference 1) and ‘VTP H 300 CFA 200 3KT RC42 HS’ code (R2: Reference 2) prepreg rolls obtained from SPM were used, while producing the composites. The properties of these prepregs are given in detail in the 'Materials'

section and the properties of the epoxy and carbon fiber used in these prepregs are given in Table 3.7.

Table 3.7. Properties of fiber and epoxy resin used in prepregs

Carbon Fiber		**Epoxy Resin**	
Tensile Modulus (GPa)	249	Fracture Toughness (Mpa)	0.7-0.8
Tensile Strength (MPa)	4518	Fraction Energy (J/m^2)	130-170
Density (g/cm^3)	1.79	Density (g/cm^3)	1.19
Strain (%)	1.7		

As the DCB test was applied to each of the samples to measure Mode I fracture toughness of composite plies, the samples were prepared in appropriate sizes on the DCB test plate. The Mode I fracture toughness of composites was determined using a testing machine according to the ASTM standard D 5528 and so test specimens were prepared in accordance with this standard in clean room at 18 °C.

Samples were made by placing nano-hybrid system in the middle of the 18 layered prepreg stack and curing them. In other words, DCB specimens were produced by stacking 18 plies prepregs (215x300 mm) on top of each other. After that, the nanofiber collected onto copper plate must be carefully transferred to the one prepreg layer (Figure 3.8-b and Figure 3.8-c). After the nanofiber mat transferred prepreg layer is placed in the middle of the 18-fold, the excess nanofibers remaining on the edge should be cleaned slowly (Figure 3.8-d). The nanofibrous mat was placed between the ninth and tenth plies, since the crack should propagate between the mid-layers of the laminate. To create an initial crack, a 75 μm thick Teflon band (non-adhesive) was introduced at the mid-plane of the laminate during layup over 60 mm (Figure 3.8-a).

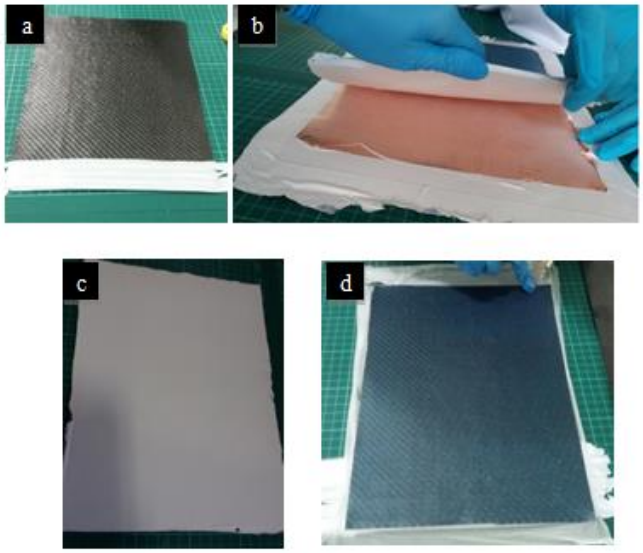

Figure 3.8. Composite sample preparation; (a) 9-fold prepreg with Teflon, (b) transfer of fiber to prepreg layer, (c) nanofiber mat transferred prepreg layer and (d) 18 layered prepreg stack containing nanofiber mat in the midplane

After eighteen layers of prepregs containing nano-hybrid fiber containing graphene oxide in the middle layer were stacked, the stacked prepregs shown in Figure 3.8-d were cured using hot-press. The curing process was carried out at 120 °C by applying 7 atm pressure on the DCB sample. The samples were ramped up at about 2°C/min till 120 °C and held for 90 minutes, and then cooled down to room temperature in 30 minutes before removing from the hot-press at 2°C/min ramp-down rate. Therefore, the curing process takes about 150 min. The temperature-time cycle used for the curing process is given in Figure 3.9.

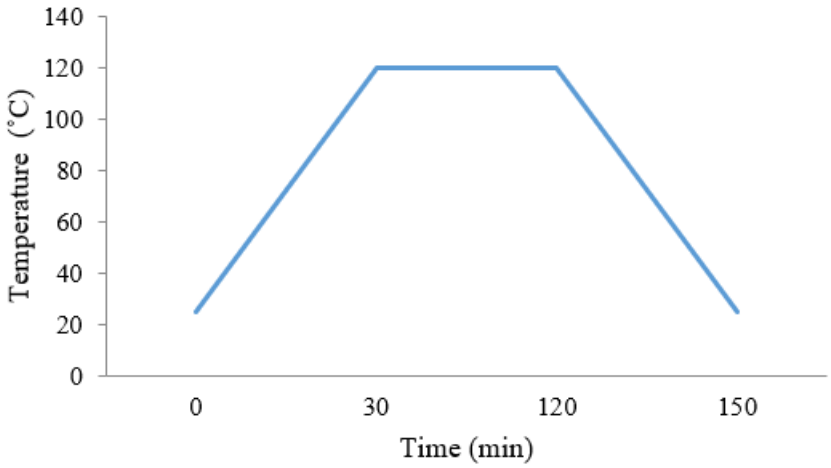

Figure 3.9. Curing cycle used in production of DCB sample

The laminates were placed in the pre-curing press is shown in Figure 3.10-a. Before the sample is placed in the hot-press, the upper and lower surfaces of the press are wiped off with a ‘’mold release agent’’ 2 times in 15 minutes intervals, thus preventing sticking of the sample to the press after curing. The composite laminate prepared using this method is shown in Figure 3.10-b.

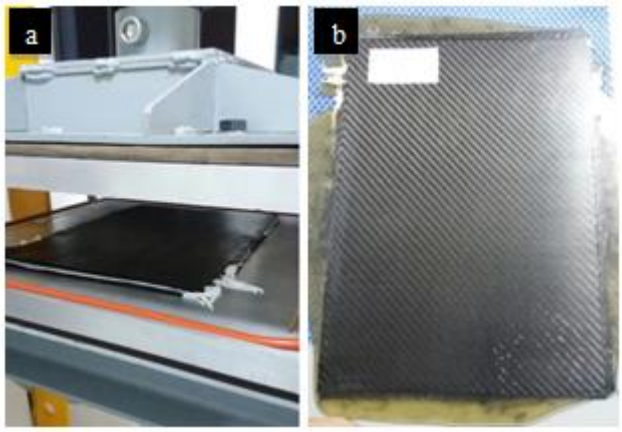

Figure 3.10. (a) Sample placed on the pre-curing press and (b) Composite removed from the press after curing

Samples were cut according to ASTM D-5528 standard sample dimensions. For a smooth cut of the cured plate at suitable sizes, a rotary saw with a diamond tip is used, which rotates at 13,000 rpm. The thickness of the plate after curing is 3.4 mm and after each slab, 6 test coupons were issued and at least 5 of them were tested. The sizes of the coupons are 25 mm wide and 275 mm length in accordance with the standard.

The effect of filler was studied varying the level of graphene oxide doping. The resin/fiber ratios for each sample are given in Table 3.8 and the method of calculating the resin-fiber ratio for a sample is described in Appendix-A.

Table 3.8. Resin/fiber ratio of produced samples

Code	**Reinforced Polymer**	**GO Type**	**GO in fiber (wt %)**	**Hybrid Tulle Field Weight (g/m^2)**	**Resin Ratio (V_{resin}) (%)**	**Fiber Ratio (V_{fiber}) (%)**	**Prepreg roll**
R1	Reference 1	-	-	-	36	64	R1
R2	Reference 2	-	-	-	42	58	R2
C9	N6	GO1	1.0	5.1	37	63	R1
C17	N6	GO1	2.0	5.6	36	64	R1
C11	N6	GO2	2.0	5.6	37	63	R1
C18	N6	GO3	2.0	5.6	34	66	R1
C26	N6/PCL	GO3	0.1	6.1	41	59	R2
C31	N6/PCL	GO3	0.3	6.3	42	58	R2
C24	N6/PCL	GO3	0.5	6.3	41	59	R2
C23	N6/PCL	GO3	1.0	6.7	41	59	R2
C21	N6/PCL	GO3	1.5	6.4	41	59	R2
C19	N6/PCL	GO3	2.0	7.2	35	65	R1
C28	N6/PCL	GO3	2.0	6.3	42	58	R2

3.2.4. Mechanical Test for Interfacial Fracture Toughness Measurement

The mode I interfacial fracture toughness of the composite plies was measured by DCB test according to the ASTM standard D-5528. The process of testing included introduction of known length of crack in the samples and determining the energy required for failing the samples in Mode I fracture.

The size of the DCB samples was 275 x 25 x 3.4 mm^3 with a pre-crack length of 60 mm. Specimens were cut from the cured laminates (Figure 3.10-b) using a rotating diamond disk with 13,000 rpm. To record the crack length, one side of the specimen was marked with white paint every 1 mm for the first 5 mm, and then, every 5 mm (Figure 3.11). 2 pairs of aluminum piano hinges were bonded onto the two sides of the specimen end having the pre-crack to transfer the load to the sample (Figure 3.12-b-2). The width and thickness of each testing specimen were measured from several different points of the specimen by using caliper gage and their average values were calculated. After the sample test equipment prepared in appropriate conditions and dimensions was placed as shown in Figure 3.12-b, the test was carried out by applying force at certain speed and magnitude. For each configuration, 6 test coupons were manufactured and at least 5 of them were tested.

Figure 3.11. DCB test coupon prepared for test

The equipment to be used for testing is shown in Figure 3.12-a. In DCB tests, a load cell (Figure 3.12-b-1) with a capacity of 1 kN was used and the test was performed at 1 mm/min at speed. A camera (Figure 3.12-b-3) with 16:9 W video capture at 1080p resolution (Logitech - HD Pro C920) is used for crack tracking. The test coupons were tested according to ASTM D-5528 test method described in Section 2.1.

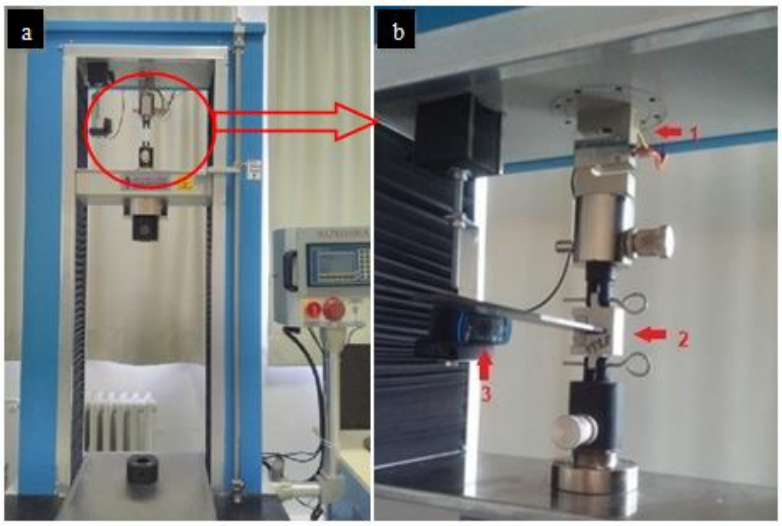

Figure 3.12. (a) DCB testing machine, (b) Equipment used during testing; (1) Load cell, (2) a pair of piano hinges and (3) camera

3.3. Characterizations

3.3.1. Attenuated Total Reflectance-Fourier Transform Infrared Spectroscopy (ATR-FTIR)

Perkin Elmer Spectrophotometer equipment was used for attenuated total reflection Fourier transform infrared spectroscopy measurements. All the analyses were performed in the wave number range of 550-4000 cm^{-1} with 64 scans. ATR-FTIR analysis was used in the studies performed only for graphite and graphene oxide solid samples.

3.3.2. Ultraviolet-visible Spectroscopy (UV-Vis)

Shimadzu UV-2550 spectrophotometer equipment was used for UV-Visible spectrophotometry measurements. The analysis was conducted for graphene oxide and GO-water solution in quartz cuvette was used for UV-Vis analysis.

3.3.3. Dynamic Light Scattering (DLS)

Brownian motion occurs with irregular collisions of objects in a liquid. Brown behavior of particles is measured in the DLS analysis and the dimensions of the

particles are measured from the observed velocities in their environment. Malvern Zeta-sizer ZS series equipment was used in the Hacettepe University Automotive Engineering Materials Laboratory for the analysis of the distribution of GO and the dimensions of GO sheets in GO-water and GO-TFE solutions as well as for measuring zeta potential. When using glass cuvette for the samples prepared using TFE, polystyrene cuvette was used in the samples prepared with water. Measurements were repeated 3 times for each sample, and how many scans were performed at each measurement was determined by the device measurement algorithm.

3.3.4. X-Ray Diffractometer (XRD)

For XRD analysis, the Pananalytical XRD-MPD model X-Ray diffractometer was used in the UNAM Laboratory of Bilkent University to examine the structure of the synthesized material. This analysis was performed for graphite and GO. The X-Ray anode Cu wavelength is approximately 1.54 Angstrom (Å) and 5°-90° angles are used for each sample for approximately 15 minutes. At the end of the analysis, the interlayer spacing for graphite and graphene oxide can be calculated by using following equation of Bragg's Law.

$$\lambda = 2d \times sin\theta \qquad Equation\ 3$$

Where λ is the wavelength of the X-ray beam, d is the distance between layers, and θ is the angle between the molecule surface and incoming beam [41].

3.3.5. Differential Scanning Calorimetry (DSC)

For DSC analyzes, the DSC device (Model: TA Q2000 DSC) operating at the temperature range of -150 to 550 °C was used in the UNAM Laboratory of Bilkent University. The DSC method measures the amount of energy absorbed or emitted while the sample is being heated, cooled or kept at a constant temperature. In this way, changes in the material, melting or glass transition temperatures can be determined. Also, crystal types of nanofibers can be designated, and their quantities can be determined by calculating the area under the melting peaks. The analyzes were

performed with 10 °C increase in temperature per minute up to 250 °C starting from the temperature of 25 °C. In the experiments, the samples were heated and cooled for two cycles and nitrogen was used as ambient gas during the experiments.

Fityk program was used for more detailed peak analysis on DSC data [93]. The analyzes were carried out for all samples using only the values at the first heating time, considering that it better reflects the situation after curing. The melting point of PCL nanofibers ranges from 59-64 °C and has a glass transition temperature (T_g) of -60 °C [94]. For N6 nanofibers, the T_g can vary between 43 °C and 54 °C depending on the moisture and attraction rate of nanofiber during electrospinning process [96]. In hybrid nanofibers samples, the coincidence of the glass transition traces in the DSC data with those of the PCL melting peak caused difficulties in the background process. For this reason, only a qualitative assessment was made in this region. Furthermore, for the analysis of N6 phases which can be crystallized in different regions between about 160 °C and 235 °C, ground value extraction can be done and the peaks can be separated by one of the functions of 'Pearson 7A' and 'Lorentzian A' in Fityk program. The melting temperature of the crystals was determined from the graphs of DSC data plotted in "1 - Heat flow (mW) – Temperature (°C)". Using the graph obtained by plotting the data in "2 - Heat flow (W/g) - Time (seconds)", the area below the peak associated with the temperature determined from the first graph was calculated. By dividing the calculated separated areas by melting enthalpy, the amount of crystalline phase in the fiber structure was determined. Peaks observed between 219 °C-232 °C during the analysis of N6 melting peaks were assumed to belong to" α" phase and peaks observed between 200 °C-217 °C were used to calculate "γ" phase. The peaks seen below 200 °C are called auxiliary side peaks of "γ" phase [96]. These side peaks were not included in the quantity calculations of the "γ'' form crystals as because they were asymmetric and could not fit well and had a negligible small area. In the calculations, the melting enthalpies of "α" and "γ" crystal phases are assumed to be 241 and 239 J/gr, respectively [97]. An example peak analysis is shown in Appendix-B.

3.3.6. Scanning Electron Microscopy (SEM)

The scanning electron microscope with the FEI Quanta 200F brand at the National Nanotechnology Research Laboratory (UNAM) of Bilkent University was used in the analysis of the size and morphology of the nanofibers produced and the structural changes in the fracture surfaces of the coupons after the DCB test. When preparing SEM samples, firstly some amount is cut from the layer deposited in the collector after the electrospinning process. Cut sample was placed on the carbon tape glued aluminum base. For the analysis of the fracture surfaces, the separated layers of the DCB coupon were wrapped with a band to prevent damage up to the moment of analysis. Samples were prepared from both the initial and the progress regions of the crack when preparing the interface samples. The guillotine was used to prepare samples of suitable size and was taped to prevent dust from entering the edges of the samples during the cutting process. The bands were opened just before the SEM analysis.

3.3.7. Transmission Electron Microscopy (TEM)

The transmission electron microscope with the FEI TECNAI F30 model at the National Nanotechnology Research Laboratory (UNAM) of Bilkent University was used to examine the structure of the nanofibers, how the graphene oxide is placed in and over the fiber, and to see if it has a homogeneous distribution. Copper grids were used to prepare TEM samples. Copper grids were placed on the collector and the fibers were allowed to accumulate for about 5 seconds on the grid. The grid was taken from the collector for analysis after it was covered in a thin film.

CHAPTER 4

RESULTS AND DISCUSSION

This study, which was carried out to evaluate the synergetic effect of hybrid nanofiber interleaves on Mode I interlaminar fracture toughness (G_{1C}) of CFRP composites, consists of 4 main steps.

Firstly, GO was synthesized and then it was ultra-sonicated to obtain graphene oxide of different sizes named as GO1, GO2, GO3. Secondly, various weight percent of GO incorporated nanofibers (N6/GO, N6/PCL (60/40)-GO3, N6/PCL (80/20)-GO3) were produced by using electrospinning technique. After that, hybrid nanofibers were placed middle of CFRP composite laminates and then cured. Finally, the specimens were tested with mechanical tests to measure G_{1C}. In Chapter 3, the experiments carried out to achieve this goal were explained in detail. In this section, the results and observations obtained at the end of the experiments were given and discussed.

4.1. Synthesis of Graphene Oxide (GO)

Graphene oxide (GO) was prepared from graphite by Tour method [41], as explained in section 3.2.1 in detail. This method uses a combination of Potassium permanganate ($KMnO_4$) oxidant and sulfuric acid (H_2SO_4)/phosphoric acid (H_3PO_4) mixture. By oxidation of graphite using strong oxidizing agents, oxygenated functional structures expand the layer separation by penetrating the graphite layers and also form C-O bonds [34]. Formation of dimanganese heptoxide (Mn_2O_7) oxidizing agent from $KMnO_4$ in the presence of H_2SO_4 strong acid is shown in following reactions [40];

$$KMnO_4 + 3\,H_2SO_4 \rightarrow K^+ + MnO_3^+ + H_3O^+ + 3HSO_4^-$$

$$MnO_3^+ + MnO_4^- \rightarrow \boldsymbol{Mn_2O_7}$$

In the 12-hour production reaction of graphene oxide, different colors are observed in each process. In the beginning, as a result of the H_2SO_4/H_3PO_4 acid mixture addition to the graphite/$KMnO_4$ solid mixture, dimanganase heptoxide (Mn_2O_7) formed and the color of the mixture becomes dark green. After the 12 h, the color of the mixture changed to dark brown with the consumption of excess $KMnO_4$. The H_2O_2 was added slowly into the mixture until the color of the mixture changes to yellow in order to remove excessive MnO_4^- ions [98]. The obtained mixture was then centrifuged and repeatedly washed in 3.4% HCl and acetone. After this, the solid obtained after washing was dried using rotary evaporator and drying oven. In order to investigate structure and oxidation degree of GO and identify its oxygen containing functional groups, following analysis was conducted.

ATR-FTIR analysis was used to identify functional groups in GO. The FTIR spectra of graphite and GO were shown in Figure 4.1. When the spectrum of GO and graphite was compared, graphite does not contain while GO contains oxygen containing groups which are hydroxyl, carboxylic acid and epoxide groups.

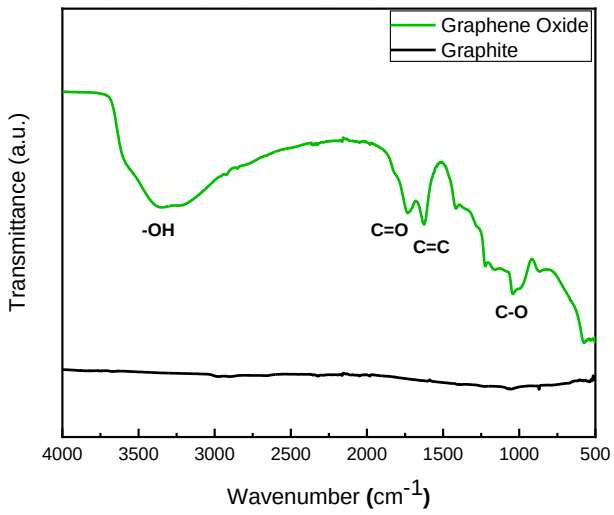

Figure 4.1. ATR-FTIR spectra of graphite and graphene oxide

According to literature, the most characteristic features in the FTIR spectrum of GO are shown in Table 4.1 [41]. When the values in the table below are examined, it is seen that the values obtained from the experiments and the values in the literature are compatible. These results indicate that the GO contains many oxygen containing groups.

Table 4.1. Experimental and literature FTIR data of GO

Wavenumber[1] (cm^{-1})	**Wavenumber[2] (cm^{-1})**	**Functional Group**
3400	3420	O-H stretching vibrations
1730	1720-1740	C=O stretching vibrations
1600	1590-1620	C=C from unoxidized sp^2 CC bonds
1100	1050-1250	C-O vibrations

1 The values are the results of the experiment conducted in this study.

2 The values are from the literature [41].

UV-Vis analysis for the GO has two characteristics, which are a shoulder around 300 nm due to n→ π* transitions of carbonyl groups and a peak around 227-231 nm range due to π → π* transitions of C=C bonding [41]. Performed UV-Vis spectrophotometry shows that characteristic absorbance peaks of synthesized GO are similar to corresponding values from literature, as shown in Figure 4.2.

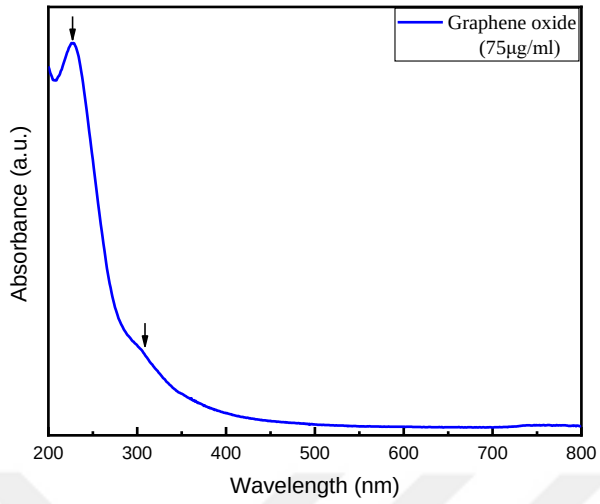

Figure 4.2. UV-Vis spectrum of the synthesized GO

X-Ray diffraction (XRD) patterns of graphite and GO are shown in Figure 4.3. The interlayer spacing (d) can be calculated according to Bragg's law mentioned in section 3.3.4. The XRD pattern of pristine graphite exhibited a basal 002 reflection peak at 2θ = 26˚ (d-spacing = 0.35 nm (3.5 Å)). However, after oxidation of pristine graphite to GO, the reflection peak shifted to the lower angle at 2θ = 9.8˚ (corresponding to a d spacing of 0.94 nm), where the d-spacing increases due to the intercalation of oxygen functional groups in between the basal plane of graphite [99]. In literature, it is said that the appearance of a broad peak centered at about 2θ = 20˚~25˚ indicated the presence of stacked graphene layers, validating the production of few layer graphene [100]. In our experiment, there is a peak centered at 2θ = 21˚ but that is not so sharp and very less in height as compared to the peak at 9.8˚. This may be due to incomplete oxidation of graphite; graphite cannot be oxidized 100 % [101], [41]. In the literature, the spacing of GOs has about 8.0 Å, 9.0 Å and 9.5 Å. The interlayer spacing for the synthesized GO is appropriate with these values taken from the literature [41].

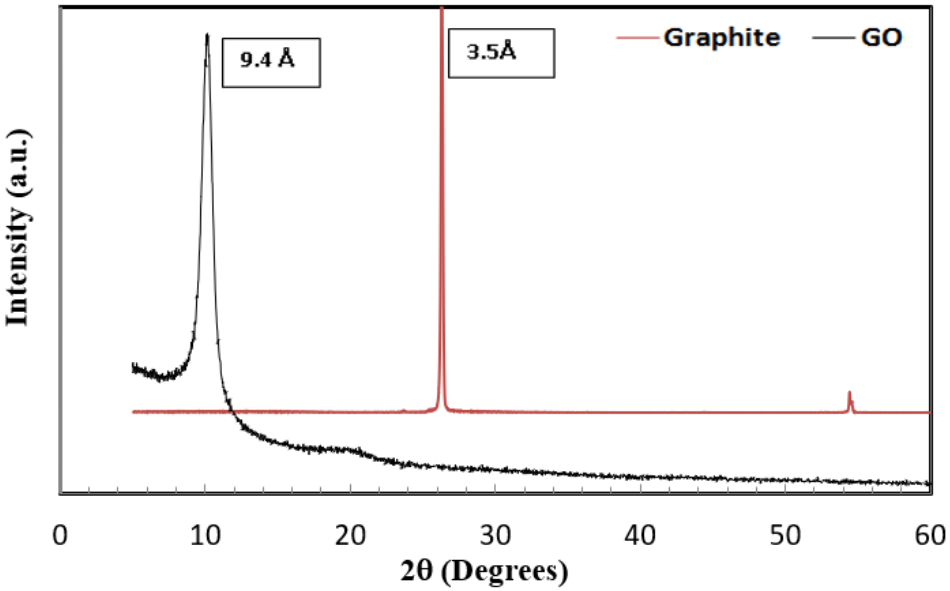

Figure 4.3. XRD spectra of graphite and graphene oxide

After the chemical analysis of GO, SEM and TEM analyzes were performed for better investigation of GO sheets' morphology. SEM and TEM images are given in Figure 4.4.

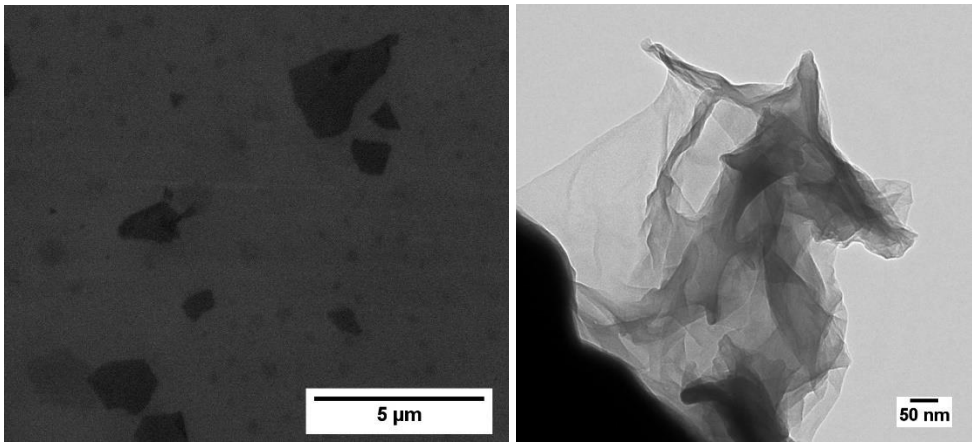

Figure 4.4. SEM (left: 20,000 x) and TEM (right) images of graphene oxide

When SEM image of GO was examined, it was observed that GO has sheet like structure with various dimensions. As can be seen, the sheets have a lateral size. In the SEM analysis performed on a 5-micron scale, there was wide range of GO sheets from nano to micron size (less than 5 microns). It was also thought that the structures with dark color in SEM image could be formed by overlapping some of the GO sheets. In TEM micrograph of GO, the transparency shows that the exfoliated GOs exists in a single layer or a few layers. Also, it is seen that it has a thin leaf structure and this structure folded into each other.

4.2. Size Reduction of GO

In probe sonication using 'Probe A', the results at the end of the probe sonication are summarized in Table 4.2. Graph showing the distribution of different size GO particles by volume graph and result of the report given by the program during analysis are given in the Appendix-C.

Table 4.2. Zeta sizer analysis results of different sonication times using 0.05 mg GO/ml in water by using Probe A

Probe Time (min)	**Peak 1 (nm)**	**Peak 2 (nm)**	**Average Particle Size of GO (nm)**
0	99.57	898.1	466.4[3]
10	638.5	53.42	326.2
20	321.8	4657	265.0
30	297.0	4781	231.8

After the application, the average size of GO1 in water distribution has decreased from 466 nm to 232 nm, but there is no significant change in the ratio of the micron-sized GO1 fragments and micron-level peaks, where a very homogeneous distribution cannot be achieved. As a result of the analysis, it was decided to continue the sonication by using '**Probe A'** for 30 minutes and to separate the size of approximately

[3]Average size of the untreated GO1 sheets

231 nm GO nano sheets from the coarse particles with the additional centrifugation step, and the final GO is named as ‘GO2’.

In probe sonication using **‘Probe B’** the change in particle sizes was followed for a longer time showed in Table 4.3 and volume-size distribution graphs are given in Appendix-D.

The duration of the sonication increases GO average particle size again decreases and appears to fall to about 186 nm. In addition, with the increase in the sonication time, the 3rd peak at the 45th min disappears. After 2 hours of treatment, the amount of GO in the range of about 100 nm and 200 nm was increased, after which the graphene oxide applied was named ‘GO3’.

Table 4.3**.** Zeta sizer analysis results of different sonication times using 0.05 mg GO/ml in water by using Probe B

Probe Time (min)	**Peak 1 (nm)**	**Peak 2 (nm)**	**Peak 3 (nm)**	**Average Particle Size of GO (nm)**
45	513.8	4687	42.09	257.5
60	343.2	50.82	-	219.6
75	386.2	1335	-	218.6
90	90.28	398.0	-	196.5
120	223.9	5121	-	185.4

As a result of the sonication studies, graphene oxides with 3 different particle sizes were designated with different names as GO1, GO2 and GO3 and the processes applied to these graphene oxides and their approximate particle sizes are summarized in Table 4.4.

Table 4.4. Production conditions and particle size of GOs resulting from different processes

GO Type	Probe Type	Probe Time (min)	Centrifuge Speed, Time	Average Particle Size (nm)
GO1	-	-	-	466.4
GO2	Probe A	30	8000 rpm, 20 min	231.8
GO3	Probe B	120	8000 rpm, 40 min	185.4

The results of the particle analysis in bath sonication are given in Table 4.5 and it can be said that the changes were not significant after 25 min for GO1. However, there was a 5.4% change for GO2.

Table 4.5. Change in average dimensions of GO2 and GO3 in water after sonication

GO Type	Bath Sonication Time (min)	Average Particle Size (nm)
GO2	15	215.9
	20	209.8
	25	202.5
	30	191.5
GO3	15	174.2
	20	172.4
	25	169.1
	30	169.9

The distribution behavior of GO2 and GO3 in TFE was monitored for 40 minutes, as the distribution indicators in TFE identified as the common solvent and dispersant of GO in N6-PCL mixtures were better represented by the electrospinning solutions. Analyzes of GO2 and GO3 at a concentration of 0.05 mg/ml in TFE were summarized in Table 4.6 with the corresponding distribution histograms.

When the distribution of GO2 and GO3 in the TFE at different times is examined, the average size of the bath sonication to a certain time decreases, it was observed that the increase in the mean size due to the expansion of the distribution when the bath sonication time increased. Volume-size distribution graphs are given in Appendix-E and F. In both types of GO, a homogeneous and narrow distribution can be obtained in 25 minutes.

Table 4.6**.** Change in average dimensions of GO2 and GO3 in TFE after sonication

GO Type	Bath Sonication Time (min)	Peak 1 (nm)	Peak 2 (nm)	Average Particle Size (nm)
GO2	15	787.9	165.5	763.9
	20	878.2	-	878.2
	25	444.3	-	586.5
	30	501.5	-	738.6
	35	476.4	-	535.7
	40	5649	-	695.0
GO3	15	447.7	-	798.1
	20	901.2	5146	613.4
	25	523.5	-	617.8
	30	610.3	-	608.1
	35	542.8	-	649.5
	40	600.0	-	631.5

While the untreated graphene oxide was named GO1, GOs with different ultrasonication processes were named GO2 and GO3. Size reduction of GO was observed with DLS measurements and particle size distribution of GO1, GO2 and GO3 are shown in Figure 4.5. These graphs shown in Figure 4.5 were drawn by using *'Origin Program'*.

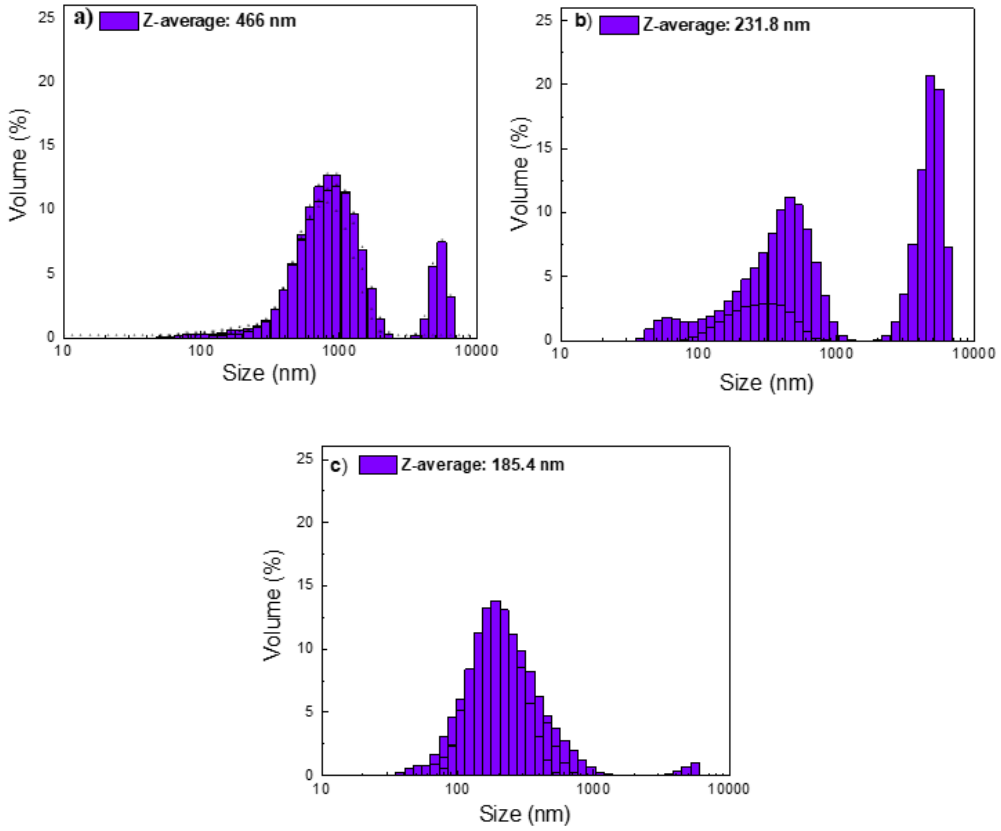

	Size (nm)	Volume (%)	Size (nm)	Volume (%)	Size (nm)	Volume (%)
Z-average	**a) 466 nm**		**b) 231.8 nm**		**c) 185.4 nm**	
Peak 1	99.57	1.4	297.0	26.1	223.9	97.1
Peak 2	898.1	98.6	4781	73.9	5121	2.9

Figure 4.5. Particle size distribution of (a) GO1, (b) GO2 and (c) GO3

To produce GO2 and GO3, enough probe sonication and centrifugation time are applied, and these duration times are shown in Table 4.4. Also, average particle sizes of GOs are shown in same table.

Figure 4.5-a shows the size distribution of pristine GO1 solution and this solution was prepared by dispersing GO1 in water about 15 minutes in an ultrasonic bath. Thus, it was observed that the mean particle size of GO1 was about 466 nm and 2 peaks with

dimensions of approximately 99 nm and 898 nm were observed. When these results were evaluated, GO sheets with various particle sizes were formed as a result of oxidation of graphite at random and different ratios during the production of graphene oxide. To ensure more homogeneous distribution of graphene oxide into nanofibers, the graphene oxide has been sonicated by using probe-sonicator and the size reduction operation can be controlled by sonication and centrifuge processes. Figure 4.5-b shows the size distribution of GO2 and it was observed that the mean particle size of GO2 was about 231.8 nm. As in GO1, 2 peaks were observed about 297 nm and 4781 nm, but the first observed peak shifted to lower particle sizes compared to the peak observed in GO1. When Figure 4.5-c is examined, when the applied probe and centrifugation time is increased to a certain time, a more uniform distribution was obtained and the percentages of the larger particles of GO sheets were reduced considerably. A uniform distribution of GO3 sheets with a mean particle size of 185.4 nm was achieved with determination of optimum times.

4.3. Reference Samples (R1 and R2)

The composite samples produced in these studies, two types of prepreg were used and properties of the prepregs used are summarized in the following table.

Table 4.7. Properties of reference samples

PREPREG CODE	Reference Code	Fiber amount	Epoxy weight
VTP H 300 CFA 210 3KT RC35 HS	R1	210 g/m^2	35%
VTP H 300 CFA 200 3KT RC42 HS	R2	200 g/m^2	42%

These prepregs were taken from SPM firm and it was aimed to use the same prepreg in all studies. After the first prepreg roll is finished, it is requested to send the prepreg with the same properties but in the last order, the prepreg is sent with more resin content. Each composite sample produced with these rolls estimated to be mechanically different will be compared with the reference value obtained from the

roll from which it was produced. Table 3.8 shows which prepreg rolls were used in the composite samples produced and which reference to compare these samples.

While the average load-extension curves of the reference plates are shown in Figure 4.6-a, the toughness (G_{1C}) with crack length in the DCB testing are plotted in Figure 4.6-b. Also, the toughness ($G_{1C\text{-}in}$ and $G_{1C\text{-}prop}$) values of reference plates are summarized in Table 4.8.

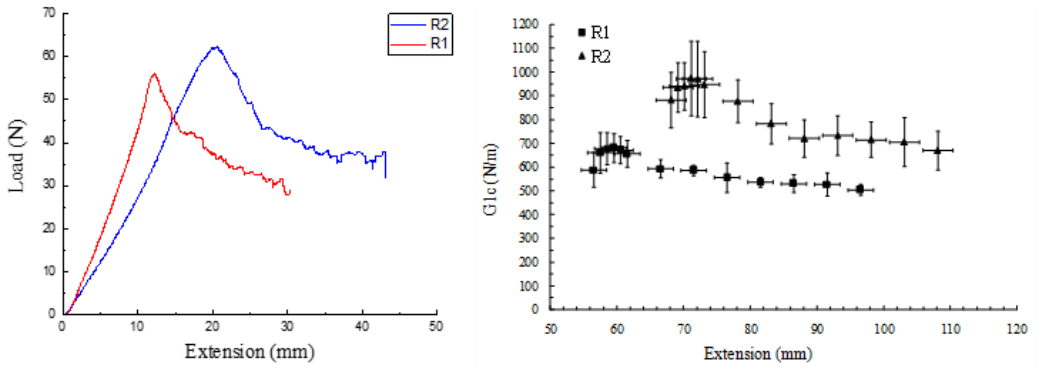

Figure 4.6. (left) Load vs. extension and (right) G_{1C} vs. crack length plots of R1 and R2 reference plates

Table 4.8. G_{1C} and standard deviation (STD) values of reference plates at crack initiation and propagation

Reference Plate	**$G_{1C\text{-}in}$ ± STD (N/m)**	**$G_{1C\text{-}prop}$ ± STD (N/m)**
R1	589 ± 73	599 ± 48
R2	883 ± 117	832 ± 105

When the values in Table 4.8 are examined, R2, which was produced by prepreg with high resin amount, has higher G_{1C} values than R1. However, increase of epoxy amount in the prepreg led to an increase in the standard deviation value.

The fracture surfaces of R1 and R2 specimen after the Mode I test were examined by SEM analysis for a better investigation of the interface properties of the references.

SEM and energy dispersive X-Ray (EDX) images are shown in Figure 4.7 and Figure 4.8.

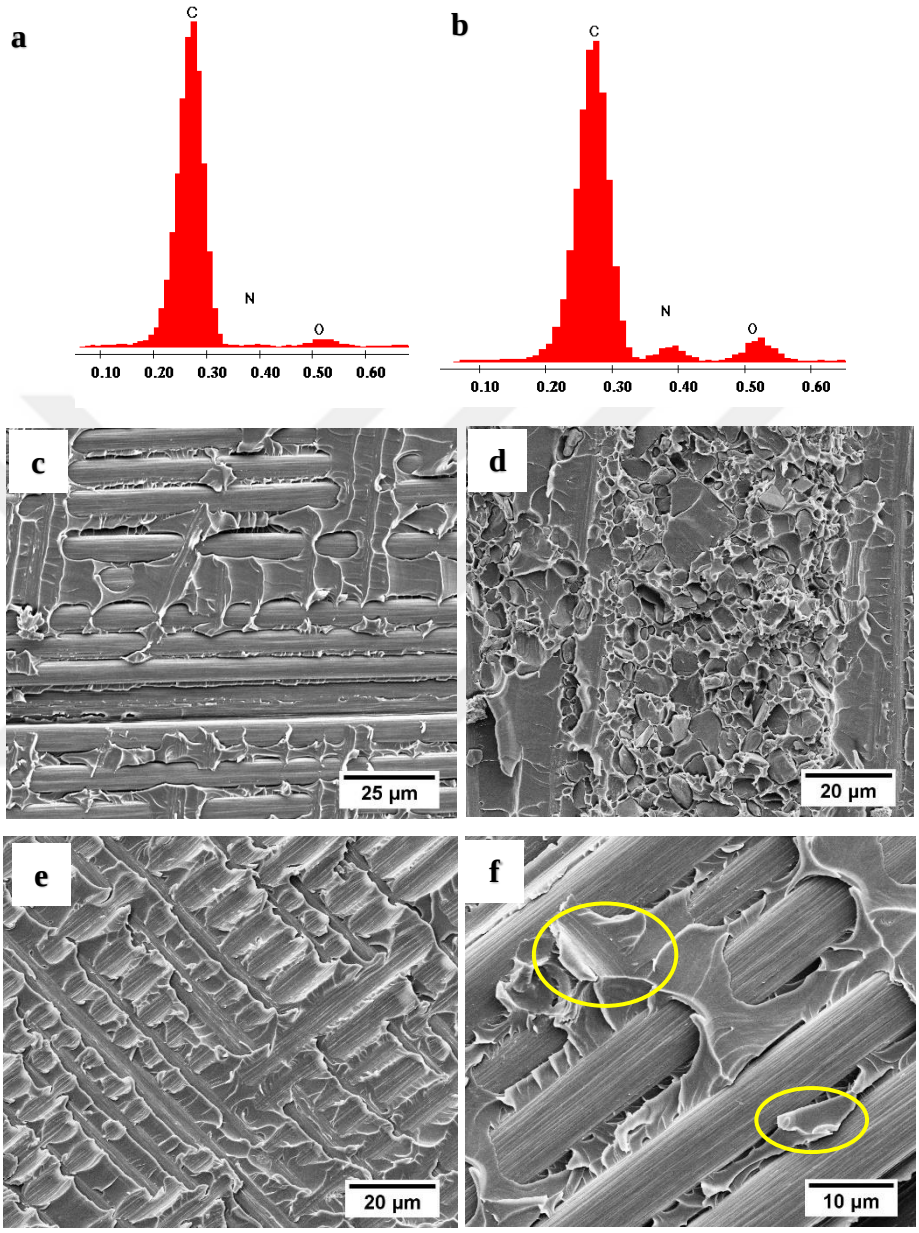

Figure 4.7. (a, b) EDX and SEM images of fracture surfaces of R1 at (c: 1,000 x, d: 2,500 x) initiation and (e: 2,500 x, f: 5,000 x) propagation

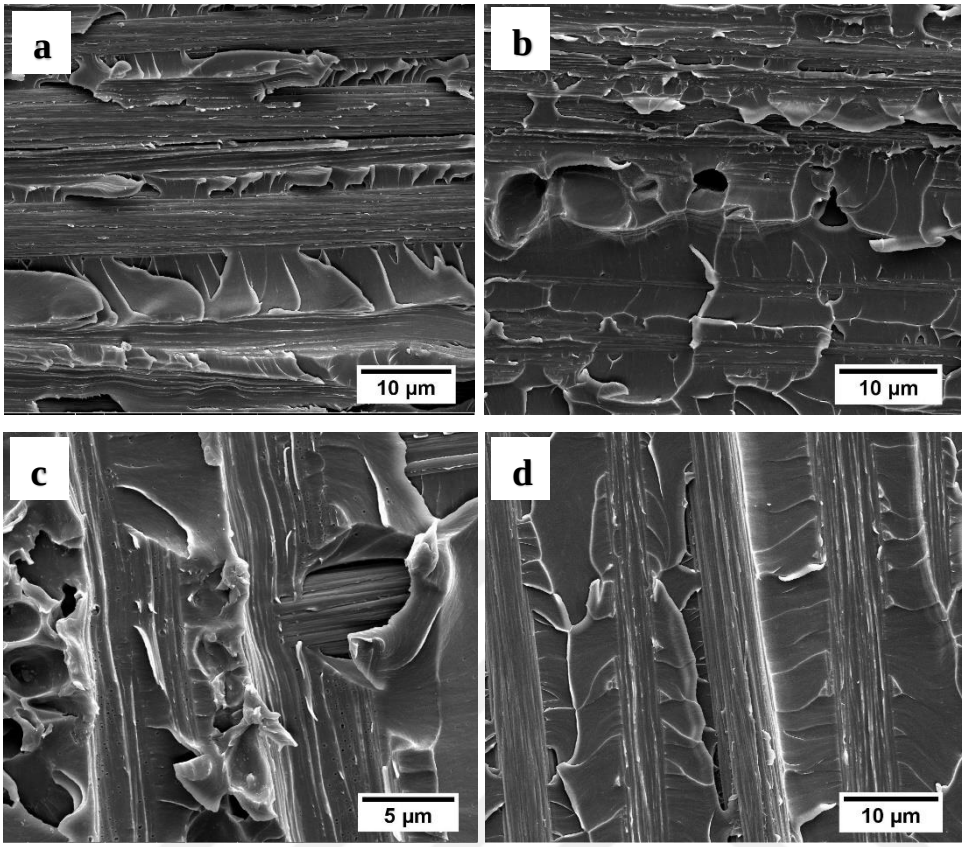

Figure 4.8. SEM images of fracture surfaces of R2 at (a: 5,000 x, b: 5,000 x) initiation and (c: 10,000 x, d: 5,000 x) propagation

As it is known, the main drawback of an epoxy matrix is its inherent brittleness, which makes it sensitive and leads to composites with low toughness. Carbon fiber-containing epoxy matrix composites often have a brittle fracture resulting from limited plastic strain [74].

In Figure 4.7 and Figure 4.8, it was seen that the characteristic structures on the fracture surfaces of R1 and R2 are similar to the brittle fracture surfaces seen in the CFRP composites. Compared to Figure 4.7-f and Figure 4.8-d, the amount of epoxy-free or uncoated carbon fiber with epoxy, which was seen after breakage in the interface, was further exposed in R1, and this was one of the images that revealed the difference in the amount of inter-epoxy between the composites. R1 compared with R2, the carbon fibers and epoxy resin are clearly visible, and the surface of carbon

fiber is very clean even though very tiny particles of epoxy resin are remained on the surface (Figure 4.7-f, yellow circle). Apparently, for carbon fiber/epoxy (CF/EP) system, the matrix on the fiber is largely peeled off, exposing the inside fibers with quite smooth surface [102]. This situation has taken place in our system and is clearly seen in Figure 4.7-c, f and Figure 4.8-a, c, d.

In addition to SEM analysis, energy dispersive X-Ray (EDX) analysis was performed to identify the elemental composition of material for R1 sample because some bunching particles were seen in the interface of the R1. Figure 4.7-a and b are EDX analyzes of Figure 4.7-c and d, respectively.

The EDX analysis was performed on the clean area (Figure 4.7-c) and the areas that were thought to be dirty (Figure 4.7-d), and about 5% nitrogen element was found in the structure of the particles. These structures were consulted about the company and it has been determined that these agglomerated particles may be amine-based hardening particles that are unreacted in curing. When the R2 interface with a larger amount of resin shown in Figure 4.8 is examined, it can be said that these structures are relatively less.

4.4. Composite Plates

4.4.1. Morphology of Nanofibers

SEM is mostly used in the examination of morphological structures of nanofibers. However, the distribution of nanofibers containing GO in the fiber is difficult to detect by SEM analysis [70]. TEM is used to examine how the GOs are distributed in the fiber. The numbers on the SEM and TEM figures shown in below that refers to the percentage by weight of the GO in the fibers.

The morphologies of the nanofibers added between the composites were examined in detail by SEM and TEM analyzes. In this section, morphologies of N6/GO, N6/PCL (60/40)-GO3 and N6/PCL (80/20)-GO3 nanofibers sets were examined separately.

The change in the morphology of the fiber by adding different weight and size of GO into the nanofibers was investigated. The images of the fibers of these sets are respectively shown below.

4.4.1.1. N6 nanofibers veils containing different types of GO (N6/GO)

SEM and TEM images of N6 nanofibers containing different amounts and types of GOs which were added to the interface of the composites are given in Figure 4.9 and Figure 4.10, respectively.

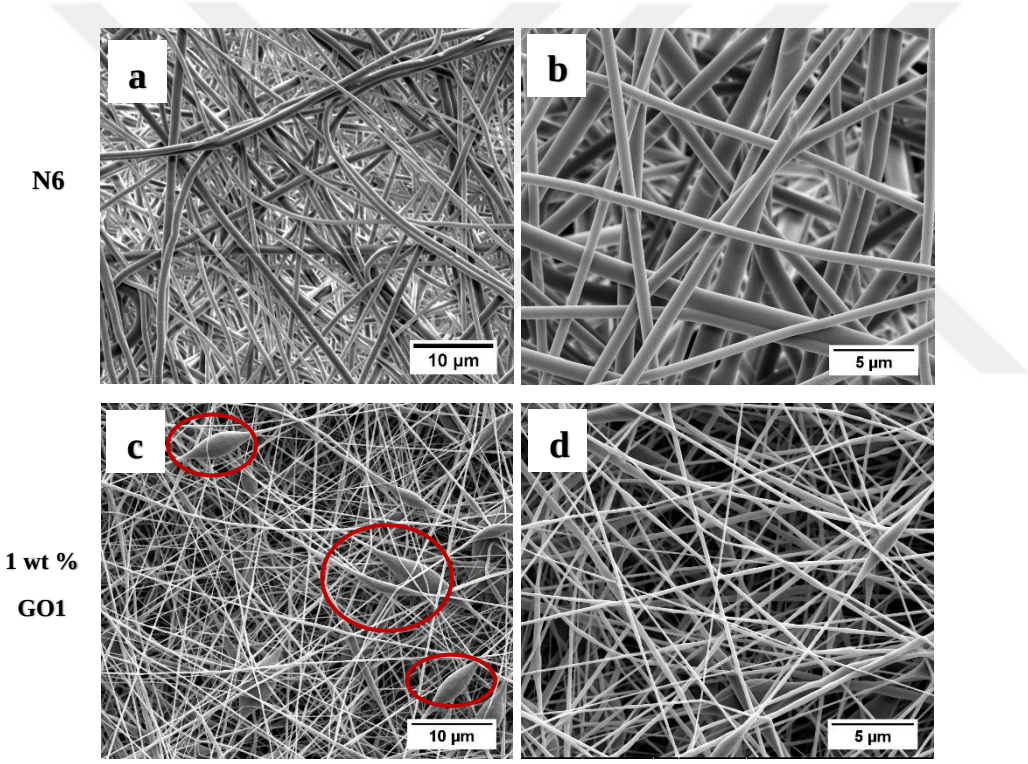

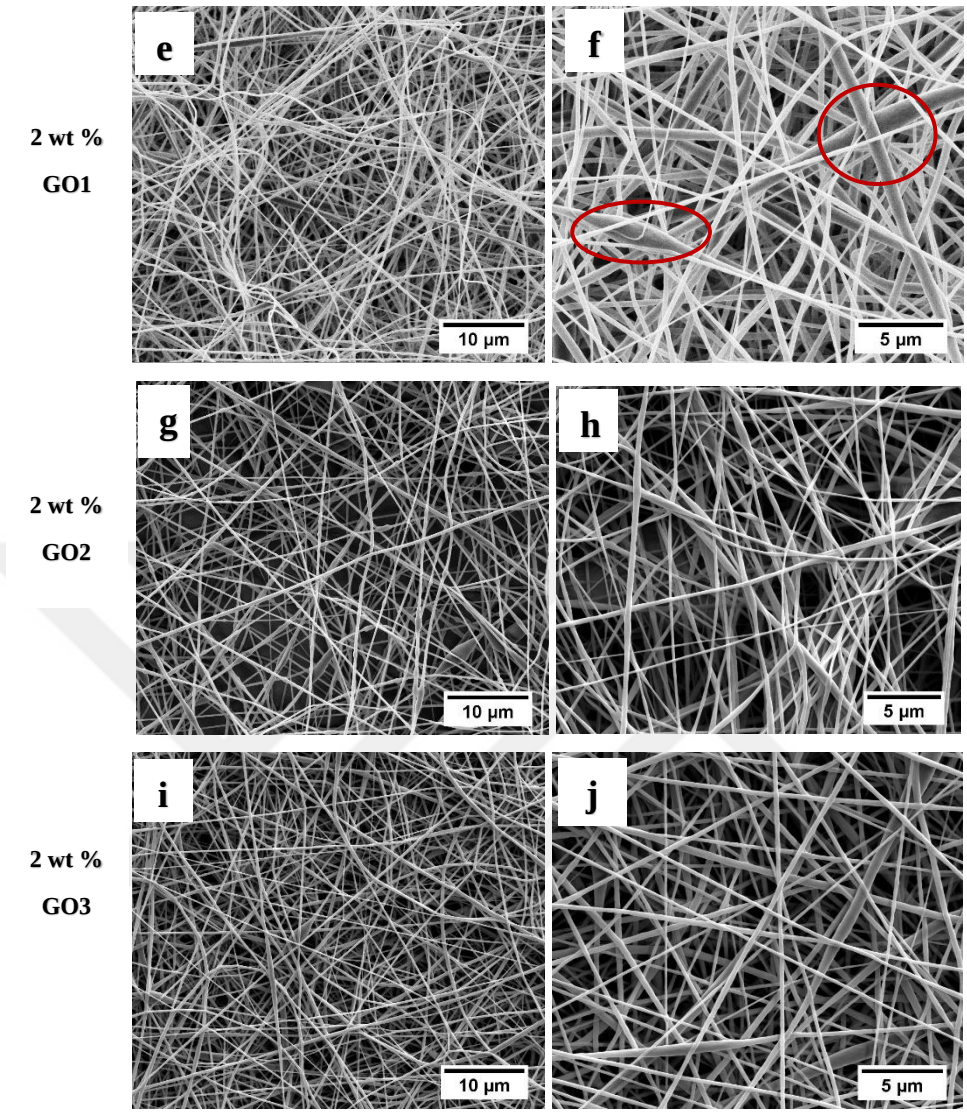

Figure 4.9. SEM images of N6 and N6/GO nanofibers (a, c, e, g, i: 5,000 x and b, d, f, h, j: 10,000 x)

In Figure 4.9, it is observed that nanofiber structures with different morphology were formed. The structure of pristine N6 nanofiber, shown in Figure 4.9-a and b, changed by adding 1% and 2% of GO1 into the N6 nanofiber (Figure 4.9-c, d, e, f). GO1 (average particle size of 466 nm) which contains different sizes of GO sheets are the cause of beads in the fiber structure. These structures formed in the fibers are shown with red circles in Figure 4.9-c and f. It has been observed that relatively homogeneous

and smooth fibers without bead defect were fabricated by incorporating the reduced size of GO2 and GO3 into the fiber structure. When these results were analyzed, the treated GO2 and GO3 did not disturb the morphological structure of the nanofibers, whereas the untreated GO1 containing GO sheets of any size negatively affected the morphological structure of the fibers and caused the formation of beaded nanofibers.

TEM images of N6/GO nanofibers added to the interfaces of composites are given in Figure 4.10.

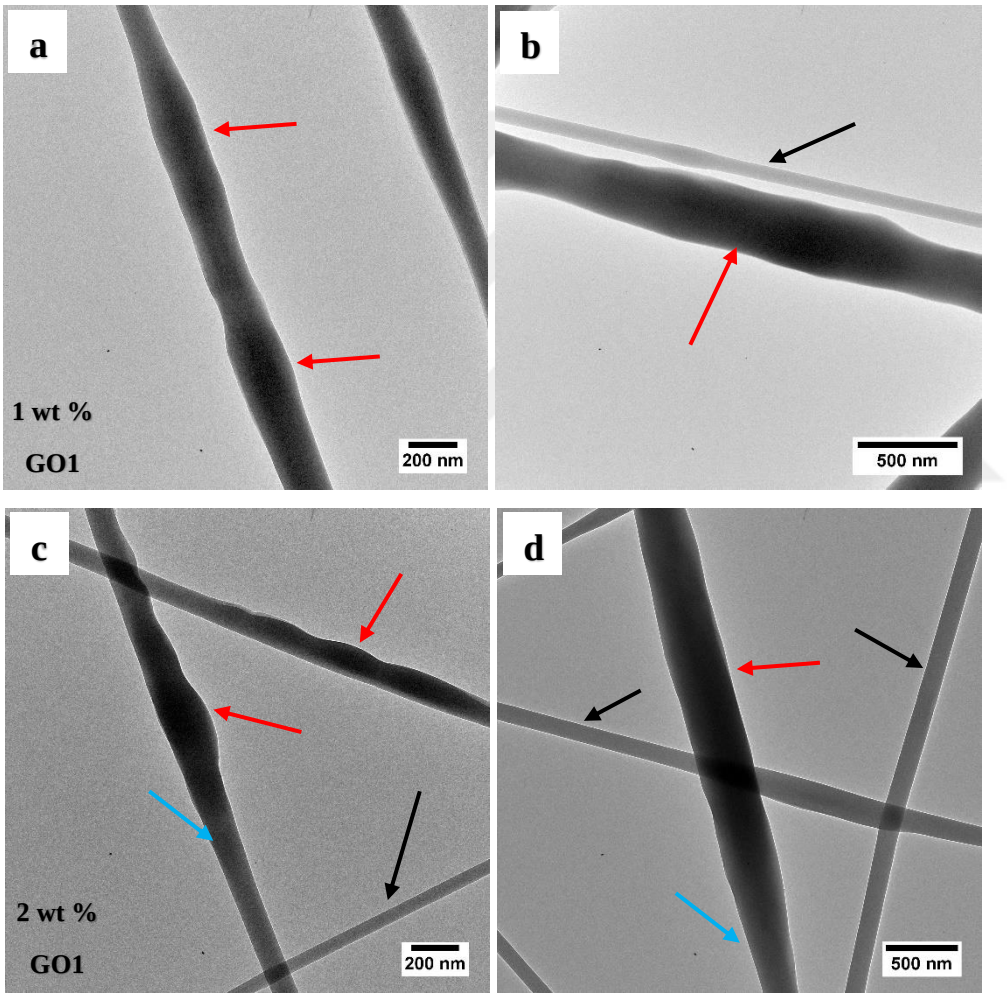

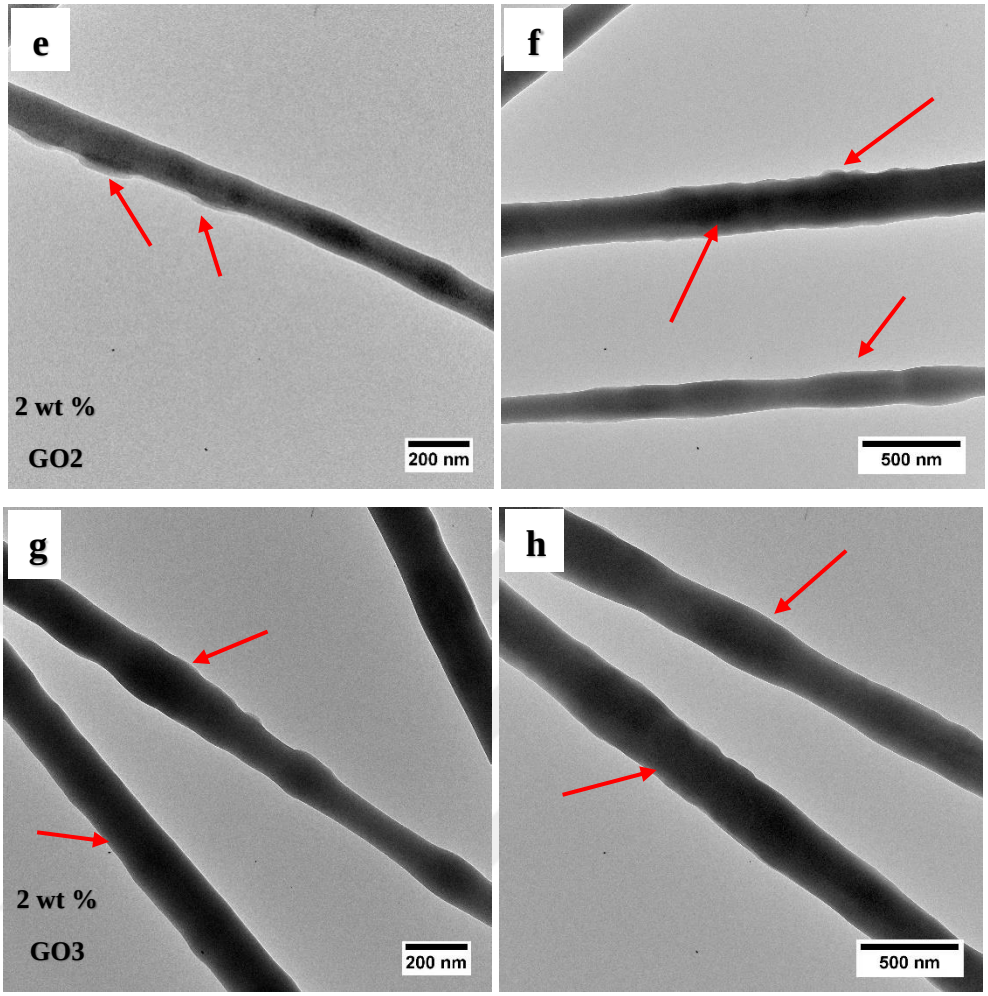

Figure 4.10. TEM images of N6/GO nanofibers

In Figure 4.10, TEM images of fibers electrospun from solution N6 solution at presence of 1and 2 wt % GO confirms the appearance of GO nanosheets along the fibers which are shown with red arrows. In N6 nanofibers containing GO1, the GO sheets were not embedded in some fibers and these regions are indicated by black arrows (Figure 4.10-a, b, c, d). In addition, these areas were observed to be knotted and transparent. In the regions indicated by the blue arrows, GO was evaluated as reflecting the transition from the dense region to the GO-free regions.

In one study, it is mentioned that the GO may sometimes be folded in the fiber or may be present in a stacked manner [103]. In the darker areas of the N6 fiber, it is evaluated

that the GO1 containing the GO sheets in a wide size distribution could be folded in the fiber or in a stuck together.

In Figure 4.10-e, f, g, h, it is observed that the fibers become knotty at more points. In addition, it was concluded that the small structures coming out of the sides of the fibers were GO [104]. As a result of these images, it can be said that GO2 and GO3 are more homogenously distributed throughout the fiber.

4.4.1.2. N6/PCL-60/40 and N6/PCL-80/20 nanofibers reinforced with GO3

First, N6/PCL (60/40) containing different amounts of GO3, added to the interface of the composites, were fabricated and SEM/TEM images of pre-cured structures of the obtained nanofibers are shown in Figure 4.11 and Figure 4.12, respectively.

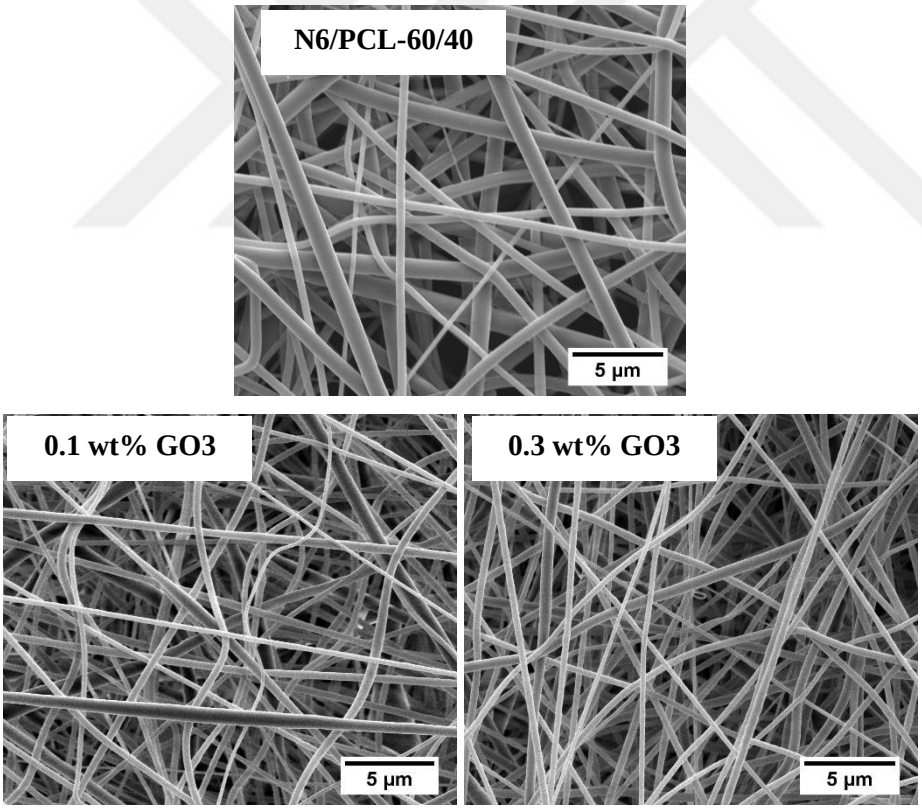

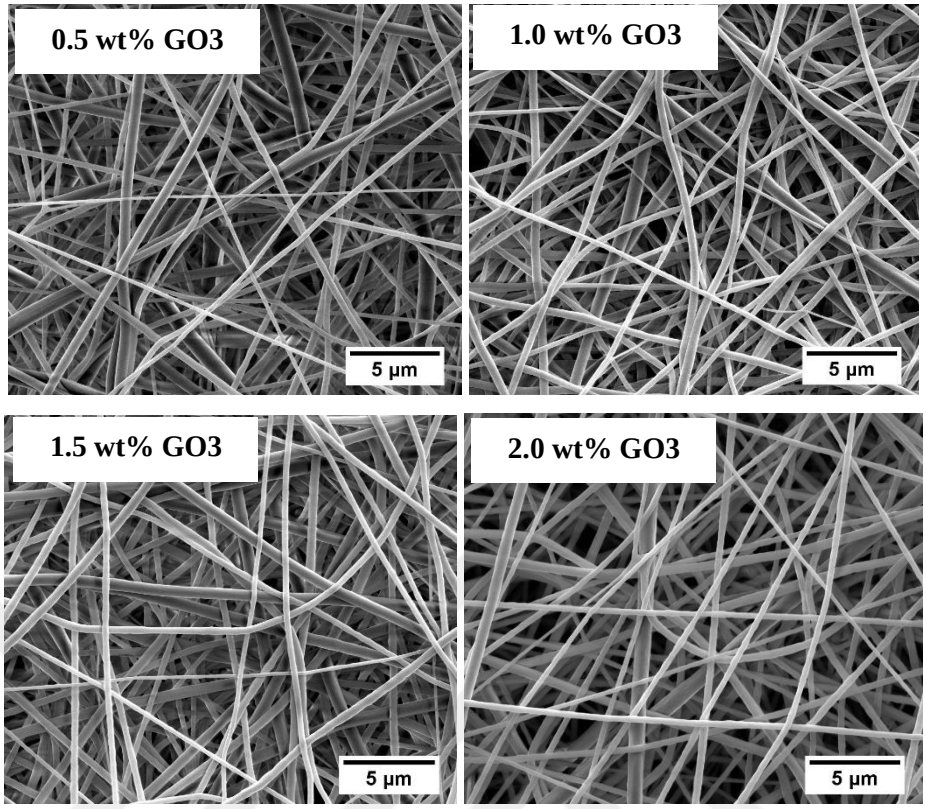

Figure 4.11. SEM images of pristine N6/PCL-60/40 nanofibers and N6/PCL-60/40 nanofibers reinforced with various weight of GO3 (mag of all images: 10,000 x)

When the nanofiber morphologies given in Figure 4.11 are examined, it is observed that smooth fibers without bead were fabricated. There was also no deterioration in fiber morphology by increasing the amount of GO3 from 0.1% to 2.0% in a 60/40 in nanofiber structure.

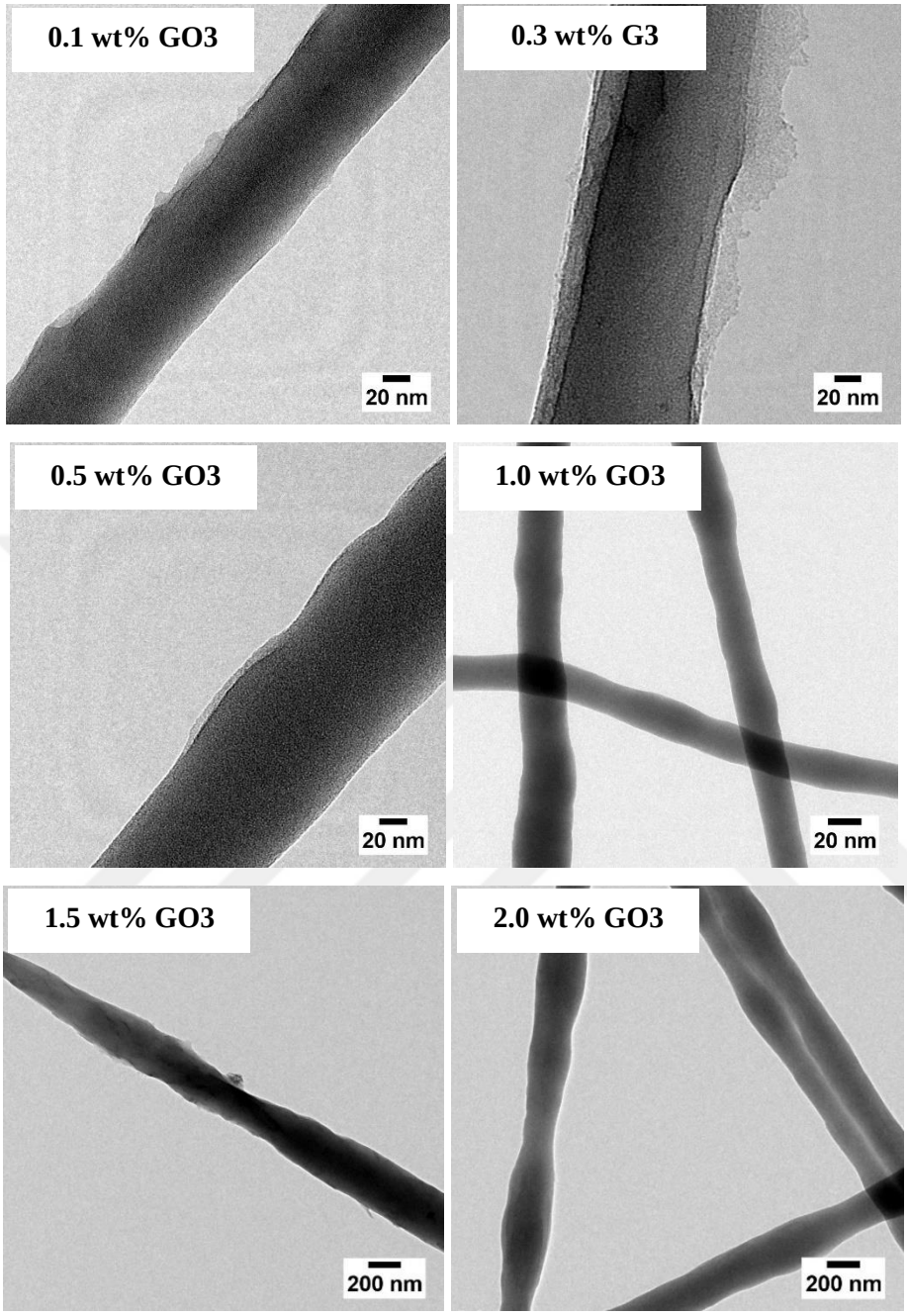

Figure 4.12. TEM images of N6/PCL (60/40)-GO3 nanofibers

In Figure 4.12, TEM images of fibers electrospun confirms the appearance of GO3 nanosheets along the fibers which are shown in all figures. When the fiber structures are examined, it is thought that GO3 sheets overflowed out of the fiber structure in

some regions and it is assumed that these structures can establish a strong bond with epoxy.

SEM and TEM images of the pre-curing structure of the tulle obtained from N6/PCL-80/20 nanofibers containing 0.5 wt % GO3 are given in Figure 4.13.

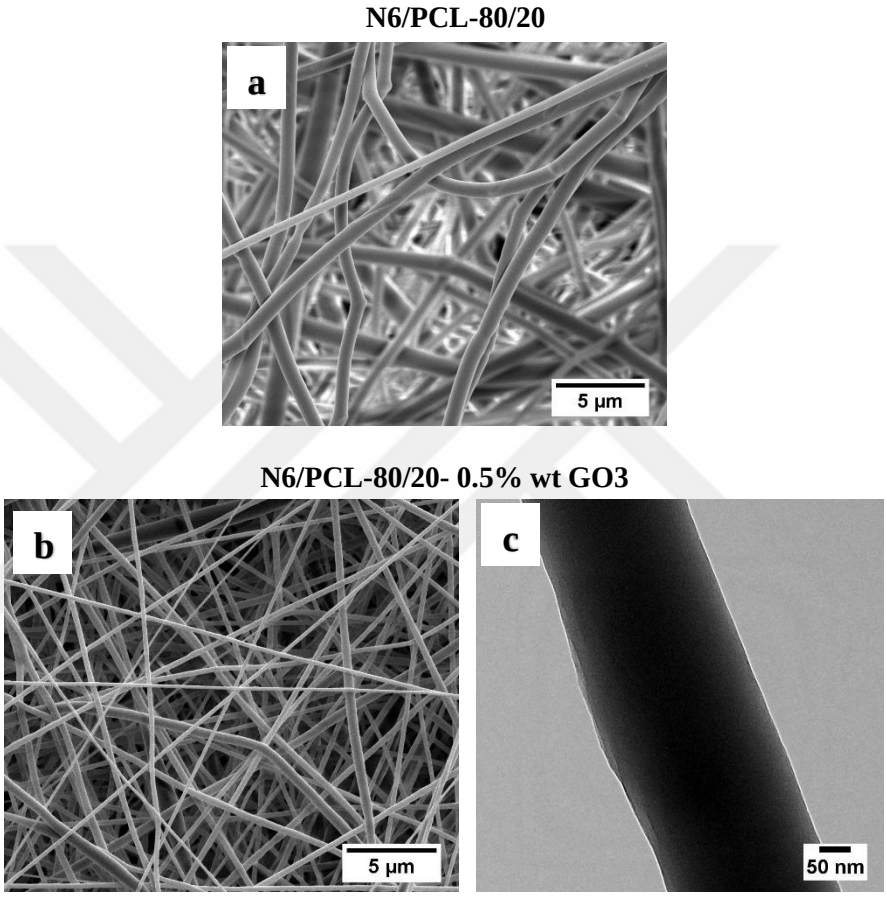

Figure 4.13. SEM images (mag 10,000 x) of (a) N6/PCL-80/20, (b) N6/PCL-80/20-0.5 wt % and TEM image of (c) N6/PCL-80/20-0.5 wt % nanofibers

It is observed that smooth beadless fibers were produced during electrospinning process under certain condition. The addition of GO3 to 80/20 nanofibers at 0.5 wt % did not disrupt the fiber structure and the fibers maintained their smooth morphology (Figure 4.13-b). The knotty fiber structures seen in the TEM image show that the GO3 has been successfully placed into the nanofiber structure (Figure 4.13-c).

4.4.2. DCB Tests

In this section, mechanical results for DCB test are presented for different composites. These composites were fabricated with incorporation of N6/GO, N6/PCL (60/40)-GO3 and N6/PCL (80/20)-GO3 nanofibers interleaf into the interface of CFRP laminates.

4.4.2.1. Composites interleaved with N6 nanofibers veils containing different types of GO (N6/GO)

First of all, Force (N)-Displacement (mm) curves and G_{1c} values resulting for both virgin (R1) and N6/GO nanofibers modified configuration are shown in Figure 4.14 and Table 4.9.

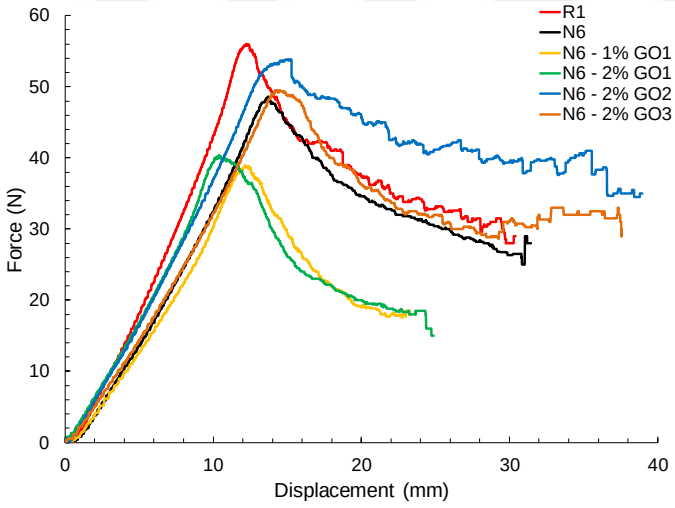

Figure 4.14. Force–displacement curves of R1, N6 and N6/GO laminates

Changes in G_{1C} initiation and propagation values according to the amount and type of GO are given in Figure 4.15 and numerical values are given in Table 4.9 in detail.

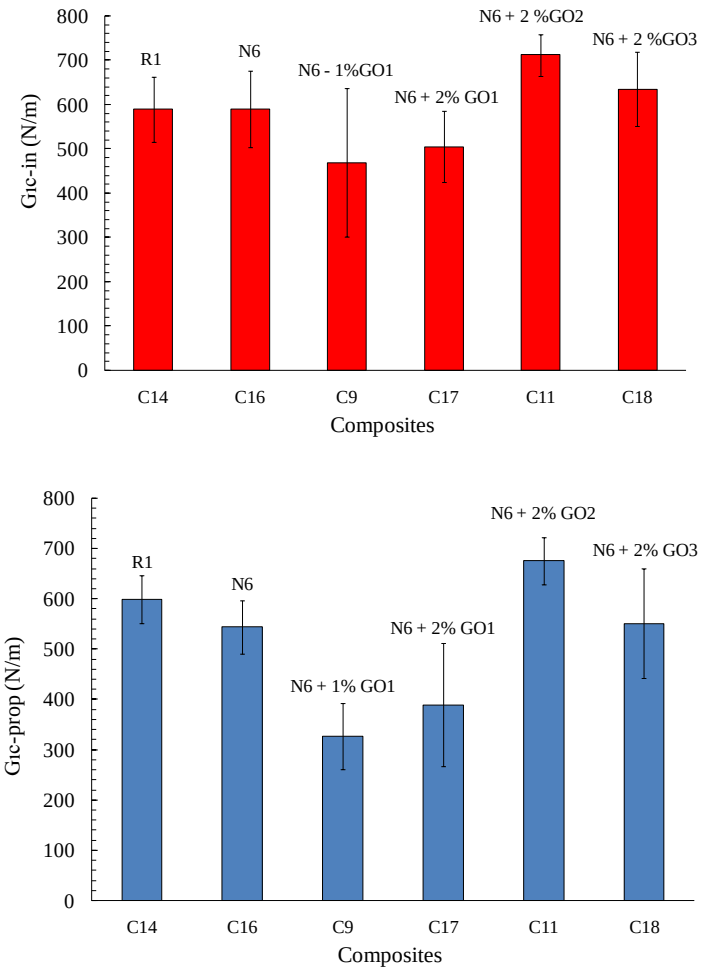

Figure 4.15. G_{1C} values of R1, N6 and N6/GO composites; (top) initiation, (bottom) propagation

Table 4.9. G_{1C} of R1, N6 and N6/GO composites according to the amount and type of GO for the initiation and propagation region and percentages of change according to R1

Code	GO Type	GO wt %	$G_{Ic\text{-}in}$ (N/m)	$G_{Ic\text{-}in}$ (STD)	$G_{Ic\text{-}in}$ (% variance)	$^4\Delta G_{Ic}$ (N/m)
C14-R1	-	-	589	73	-	-10
C16-N6	-	-	590	86	0	46
C09	GO1	1.0	469	167	-20	143
C17	GO1	2.0	505	81	-14	116
C11	GO2	2.0	712	47	**21**	36
C18	GO3	2.0	635	84	8	84
Code	**GO Type**	**GO wt %**	$G_{Ic\text{-}in}$ (N/m)	$G_{Ic\text{-}in}$ (STD)	$G_{Ic\text{-}in}$ (% variance)	
C1-R1	-	-	599	48	-	
C16-N6	-	-	544	53	-9	
C09	GO1	1.0	326	66	-45	
C17	GO1	2.0	389	123	-35	
C11	GO2	2.0	676	47	**13**	
C18	GO3	2.0	551	109	-8	

When Table 4.9 is examined, the change in G_{1c} initiation ($G_{1C\text{-}in}$) and propagation ($G_{1C\text{-}prop}$) values does not always show the same behavior. In other words, while the $G_{1c\text{-}in}$ value is increased, the $G_{1C\text{-}prop}$ value may decrease. Figure 4.15-a and b clearly show that 1.0 wt % and 2.0 wt % GO1 containing N6 interleaves in carbon fiber/epoxy composites leads to a dramatic 20% and 14% decrease in $G_{1C\text{-}in}$ and 45% and 35% decrease in $G_{1C\text{-}prop}$ values compared to the R1 baseline laminate without interleaves respectively. However, this behavior has changed in the sample containing 2.0 wt % GO2 and G_{1C} values have reached maximum level (according to reference in initiation +%21, in propagation +%13). At the same ratio, but this time with GO3 sample

$^4\Delta G_{Ic} = G_{Ic\text{-}in}$ (N/m) - $G_{Ic\text{-}prop}$ (N/m)

addition; there is an increase of 8% in $G_{1C\text{-}in}$ value compared to the reference and decrease of 8% in $G_{1C\text{-}prop}$ value.

When the variations between the samples are compared, it is seen that the highest standard deviation **(STD)** is in the sample with 1.0 wt % GO1 which showed the worst performance. Best performance with samples containing 2.0 wt % GO2, variation between samples is low compared to other samples. When the differences between $G_{1C\text{-}in}$ and $G_{1C\text{-}prop}$ values **(ΔG_{ic})** are examined, it can be said that; in high performance samples the difference is low in N6/GO hybrid systems containing 2.0 wt % GO2 and 2.0 wt % GO3, whereas in low performance samples 1.0 wt % and 2.0 wt % GO1, the difference is higher.

In a study conducted by Daelemans *et al.* in 2016, it was stated that the G_{1c} values of the composite were almost never changed by adding N6 nanofibers to the system [20]. As mentioned in the earlier sections, a hybrid system in which graphene oxide is introduced into N6 nanofibers by electrospinning method to improve interfacial fracture toughness has not been found in the literature.

Consistent with the literature, N6 nanofibers did not produce any improvement in $G_{1C\text{-}in}$ value but caused a decrease in the propagation value of G_{1C}. However, changes in mechanical performance have been observed by incorporating GO into this system. While GO1-containing systems did not provide an increase in $G_{1C\text{-}in}$ and $G_{1c\text{-}prop}$ values, GO2 and GO3 were found to significantly increase G_{1C} values relative to the R1 and N6 containing system. The effect of the GO size distribution on the mechanical performance can be related to the fact that GO1 is not homogeneously distributed within the fiber and is not present in each region of the fiber, whereas GO2 and GO3 are more uniformly distributed throughout the fiber.

However, in order to make the reasons for this contribution more clearly, the thermal phase transformation behaviors of fiber tulles were investigated by DSC analysis. The behavior of the N6/GO hybrid tulles in the first heating cycle for the N6 melting zone

is given in Figure 4.16. DSC analysis could not be performed for N6 hybrid tulles containing 1 wt % GO1 because enough sample was not separated from this sample.

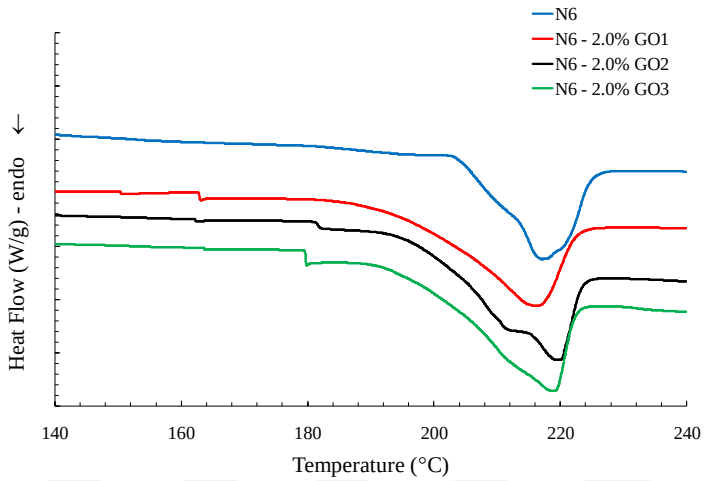

Figure 4.16. DSC first heating scans of N6 and N6/GO hybrid nanofibers

As previously mentioned in Section 3.3.5, Nylon 6 nanofibers have two common crystalline forms, α- and γ-forms, and these two crystalline forms coexist in N6 fibers in various percentages depending on processing conditions.

In the thermodynamically more stable α crystals, hydrogen bonding is formed between anti parallel chains. In the less stable γ crystal, molecular chains have to twist away from the zigzag planes to form hydrogen bonding between parallel chains [105]. As a result, the crystal density of the γ crystal is less than the density of the crystal α. In neighboring amidic groups in which hydrogen bonds are formed, the distance between these groups is longer in the γ crystal than in the α crystal. As a result, interchain interaction in the γ crystal is weaker than α crystal [106].

In one study, it was concluded that the addition of CNF into N6 nanofibers favors the formation of γ crystal. An explanation is that the decrease in the mobility of the polymer chains at the nanofiber-matrix interface promotes the formation of γ

crystallites. Also, this literature highlights the following features of crystals; α-form has a higher modulus and hardness, whereas γ-form is tougher [107].

The DSC data of the N6 melting zone given in Figure 4.16 and the areas under the melting peaks were analyzed; the amounts of the N6 crystal and crystal types were calculated. The results are given in Figure 4.17 and Table 4.10.

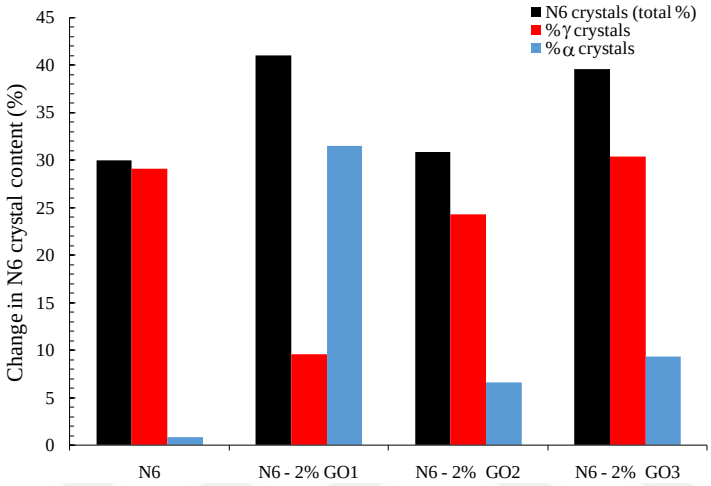

Figure 4.17. Variation of N6 crystal types and quantities according to GO type in N6, N6/GO hybrid tulles

Table 4.10. N6 crystal types and quantities in N6, N6/GO hybrid tulles

Code	N6/PCL	GO wt %	GO Type	γ Crystals (%)	α Crystals (%)	N6 Crystals (total %)
C16	100/0	-	-	29.1	0.80	29.9
C17	100/0	2.0	GO1	9.50	31.5	41.0
C11	100/0	2.0	GO2	24.3	6.60	30.9
C18	100/0	2.0	GO3	30.3	9.30	39.6

Pure N6 nanofibers electrospun as in almost all of the γ phase had been identified in previous work performed in our group [108]. When Figure 4.17 and Table 4.10 are

examined, it is clear that the crystal regions in N6 have changed and this indicates an interaction between N6 and GO. With the addition of GO, there was a significant increase in the α phase and total N6 crystallization in N6 nanofibers. In the N6 fiber containing 2 wt % GO1, the amount of γ crystal (9.5%) decreased significantly compared to the amount of crystal in pure N6 (29.1%) and the amount of α crystal increased (31.5%). This great change in the structure of the N6 fiber was thought to be due to the fact that the GO1 did not show a very good distribution in the N6 nanofiber. It is possible that the increase in the draw ratio in the regions where sudden fiber diameter changes occur at the ends of heterogeneous GO knot regions cause an increase in α crystal.

In the N6 hybrid tulle containing 2 wt % GO2 and GO3, it can be said that as GO relatively homogeneously distributed throughout the fiber, reducing the movement of the polymer chains generally more effectively and thereby increases the formation of the γ crystal regions. The formation of the α crystal region together with the γ crystal provided a balance between the toughness and hardness properties of the system. Compared to pure N6, which contains almost all γ crystals, an increase in G_{1C} values was achieved in N6 systems containing GO2 with α and γ phases together. Besides, it is thought that one of the factors that increase the G_{1c} values will be through the GOs which are overflowed out of the fiber (Figure 4.10-e, f, g, h). It is expected that, the functional groups on the GO are expected to reinforce the bond that the epoxy matrix and N6 cannot establish, and delay the debonding, leading to increased toughness. In fact, it is consistent with this expectation that the overgrown sheets of graphene oxide, which are reflected in TEM images of GO2-containing fibers and which are higher than GO3-containing fibers, have provided a better increase in toughness.

In terms of production steps, GO3 can be produced in larger quantities and also shows structures similar to GO2 in terms of overflow to the fiber wall. Therefore, the use of GO3 was preferred in the subsequent studies of the study using graphene oxide.

4.4.2.2. Composites interleaved with N6/PCL (60/40) nanofibers veils containing different weight of GO3

The Force (N)-Displacement (mm) curves of the composites interleaved with N6/PCL (60/40) nanofibers containing GO3 are given in Figure 4.18.

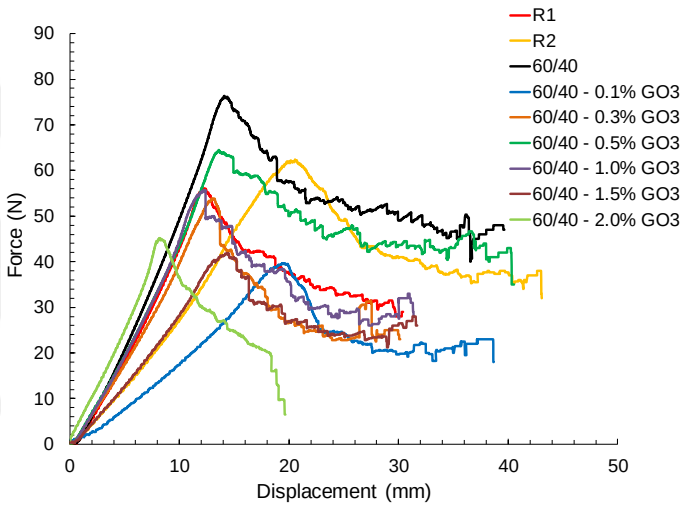

Figure 4.18. Force–displacement curves of R1, R2, 60/40 and 60/40-GO3 laminates

Changes in G_{1C} initiation and propagation values according to the amount of GO3 are given in Figure 4.19 and numerical values are given in Table 4.11 in detail.

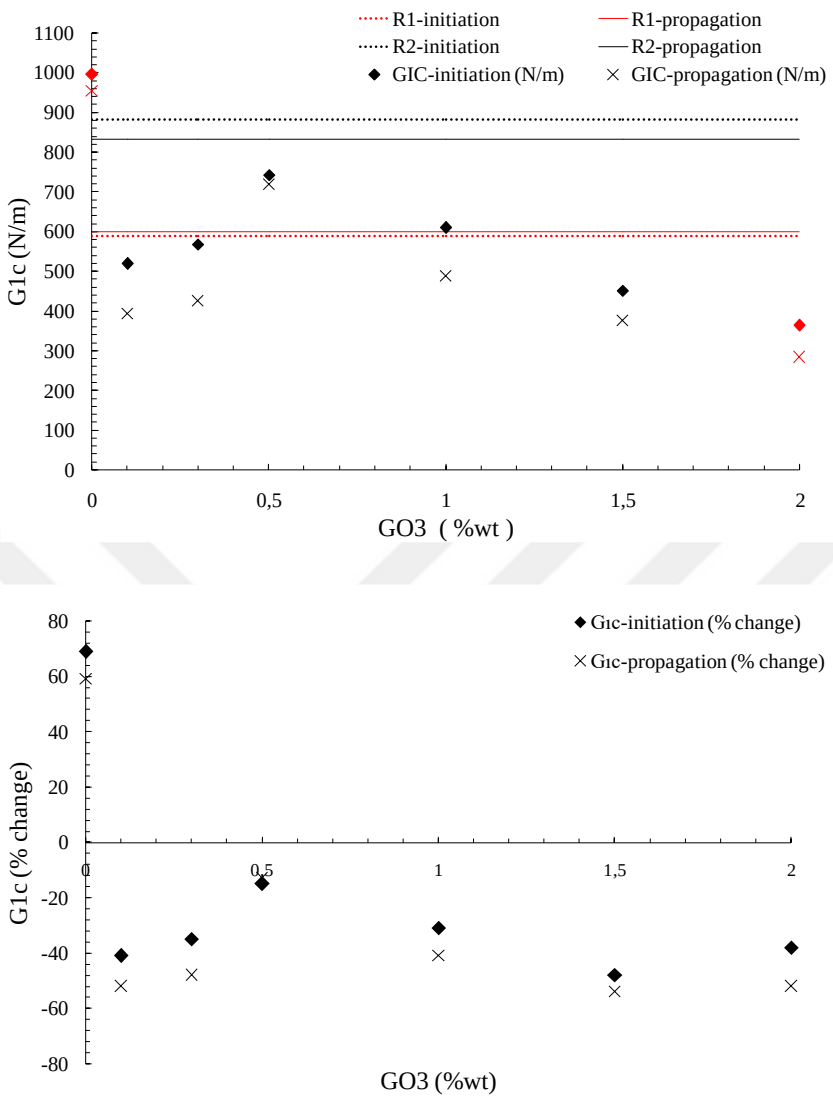

Figure 4.19. G_{1C} values of plates R1, R2 and CSET2; (top) variations for the initiation and propagation region with increasing GO3 in the fiber, (bottom)[5] percentages of variation relative to the reference sample

[5]During the production of this set, due to the depletion of R1 roll, it was necessary to produce with R2. Therefore, in order to better understand the change of G_{1C} values with different amounts of GO3 addition, Figure 4.19-b should be preferred instead of Figure 4.19-a.

Table 4.11. G_{1C} values of R1, R2 and N6/PCL (60/40)-GO3 plates, depending on the increased amount of GO3 for the initiation and propagation region and the percentage of change relative to the references

Code	N6/PCL	GO Type	GO wt %	$G_{Ic\text{-}in}$ (N/m)	$G_{Ic\text{-}in}$ (STD)	$G_{Ic\text{-}in}$ (% variance)	ΔG_{Ic} (N/m)
C14-R1	-	-	-	589	73	-	-10
C29-R2	-	-	-	883	117	-	51
60/40	60/40	-	-	996	74	69	42
C26	60/40	GO3	0.1	519	77	-41	126
C31	60/40	GO3	0.3	568	44	-35	143
C24	60/40	GO3	0.5	742	183	-15	24
C23	60/40	GO3	1.0	610	119	-31	122
C21	60/40	GO3	1.5	451	207	-48	75
C19	60/40	GO3	2.0	364	77	-38	80
Code	**N6/PCL**	**GO Type**	**GO wt %**	$G_{Ic\text{-}prop}$ (N/m)	$G_{Ic\text{-}prop}$ (STD)	$G_{Ic\text{-}prop}$ (% variance)	
C14-R1	-	-	-	599	48	-	
C29-R2	-	-	-	832	105	-	
60/40	60/40	-	-	954	72	59	
C26	60/40	GO3	0.1	393	62	-52	
C31	60/40	GO3	0.3	425	80	-48	
C24	60/40	GO3	0.5	718	219	-13	
C23	60/40	GO3	1.0	488	119	-41	
C21	60/40	GO3	1.5	376	156	-54	
C19	60/40	GO3	2.0	284	56	-52	

In previous work performed in our group, it was the N6/PCL hybrid system where the sample PCL ratio was 40% with the highest increase in both G_{1C} values relative to the reference sample [108]. For this reason, changes in G_{1C} were investigated with the addition of GO3 at different weight ratios to the sample where N6/PCL were mixed at 60/40 and the causes of these changes were investigated.

With the addition of GO3 to the 60/40 hybrid system, G_{1C} values could not be increased. When the samples in this set were compared with the non-additive samples

(R1 or R2) made from the reference rollers to which they were related (Figure 4.19-b), there was a sudden drop in $G_{1C\text{-}in}$ and $G_{1C\text{-}prop}$ values with 0.1 wt % GO3 addition, followed by an increase of up to 0.5 wt %. When the differences between $G_{1C\text{-}in}$ and $G_{1C\text{-}prop}$ values are examined, it can be said that the difference between the samples with the best performance of 0.5 wt % GO3 is less and the difference with 0.3 wt % GO3 is higher in the sample.

With the addition of GO3 to the system, in order to understand the internal structural changes in the N6/PCL hybrid system in 60/40 ratio, the thermal phase transformation behaviors of the fiber tulles were examined by DSC. The behavior of hybrid tulle produced in the first heating cycle is given in Figure 4.20.

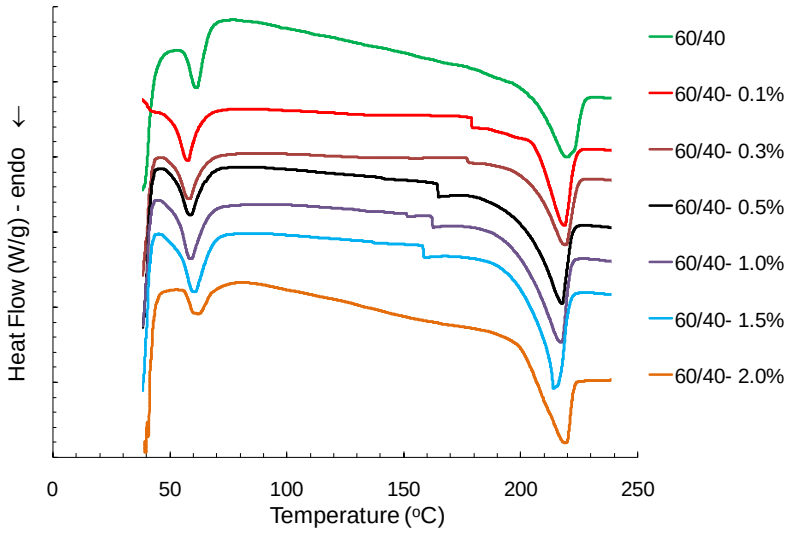

Figure 4.20. DSC first heating scans of 60/40 and 60/40-GO3 hybrid nanofibers

It was observed that 60/40 nanofiber sample without GO3 addition melted at about 60 °C and melting point decreased to about 56-57°C by adding different amounts of GO3 to the nanofiber. This decrease is due to the fact that PCL crystal formations start from the graphene oxide sheets; that is, graphene oxide in hybrid fibers and PCL crystals with melt potential during curing can be said to be related and close to each other. As a result, it can be predicted that the phase-separated PCL crystals which have the

potential to melt during curing, together with the melting, will expose the adjacent GO regions to the epoxy.

When the amount of GO3 reaches 2%, it is noticed that 2 different types of crystal zones are formed which melt at low and high temperatures. Furthermore, it can be said that the amount of PCL crystal in the 60/40 sample increased with the addition of GO3 to the mixture.

In order to investigate the effect of GO3 on the N6 melting points, the N6 melting zone data were analyzed using the peak separation method. The DSC data of the N6 melting zone are presented in Figure 4.21. For the calculation of the amounts of N6 crystal, which are separated according to the crystal types, the areas under the melting peaks are analyzed and the results are given in Figure 4.22 and the values are given in Table 4.12.

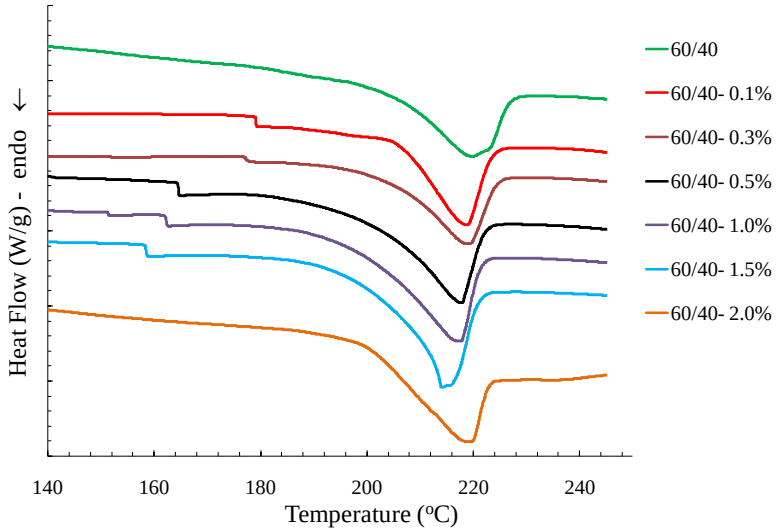

Figure 4.21. The first heating cycle behaviors normalized to the sample weight of the 60/40 and GO3 added 60/40 hybrid tulles at the N6 melting zone

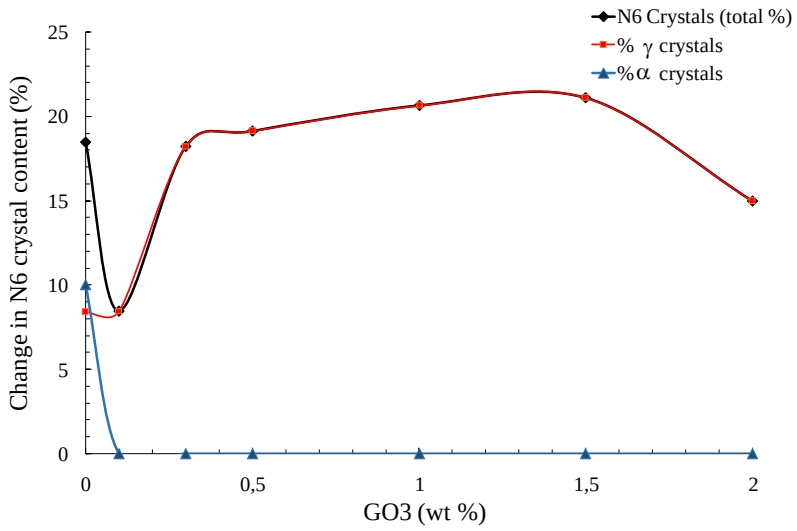

Figure 4.22. Variation of N6 crystal types and amounts in GO3 added 60/40 hybrid tulles according to amount of GO3

Table 4.12. N6 crystal types and quantities in 60/40 and N6/PCL (60/40)-GO3 nanofibers

Code	N6/PCL	GO3 (wt %)	γ Crystals (%)	α Crystals (%)	N6 Crystals (total %)
C08	60/40	-	8.41	10.04	18.45
C26	60/40	0.1	8.47	0	8.47
C31	60/40	0.3	18.24	0	18.24
C24	60/40	0.5	19.12	0	19.12
C23	60/40	1.0	20.63	0	20.63
C21	60/40	1.5	21.09	0	21.09
C19	60/40	2.0	19.48	0	19.48

With the addition of different amounts of GO3 to the N6/PCL (60/40) hybrid system, α crystal region were almost completely disappeared, while significant changes were observed in the amount of γ crystals. With the addition of 0.1 wt % GO3, a sudden decrease was observed in the total crystallization amount of N6 and there was an increase in the total crystallization amount of N6 by adding 0.3 wt % and more GO3

to the mixture. There was no significant change, except for the drop in the 2 wt % addition of GO3. The complete disappearance of the α phase and subsequent increase of the γ phase can be explained by the decrease in the mobility of the polymer chains at the GO-polymer interface, as in the carbon nanotubes-polymer interface [107]. Accordingly, it has been found that both PCL crystals and relatively unstable γ crystals tend to be more nucleated on the surfaces of the GO3.

There appears to be a strong correlation between performance degradation with the addition of graphene oxide to the complete disappearance of α phase. The formation of γ phase increased with increasing graphene oxide and it is seen that there is a relationship between the increase of gamma phase and performance. It was mentioned in the previous sections that the formation of certain ratios of α and γ crystals in N6 fibers, optimizes mechanical performance and positively affects. By adding GO3 to the 60/40 fibers, it can be said that the complete disappearance of α crystal regions negatively affects resistance in the longitudinal axis of the fibers.

4.4.2.3. Composites interleaved with N6/PCL (80/20) nanofibers veils containing 0.5 wt % of GO3

Since the best performance in the 60/40-GO3 nanofibers hybrid system was achieved with 0.5 wt % GO3, the study in this set was carried out by adding 0.5 wt % GO3 in the 80/20 mixture.

The Force (N)-Displacement (mm) curves of the composites interleaved with N6/PCL (80/20) nanofibers containing 0.5 wt % GO3 are given in Figure 4.23. Changes in G_{1C} initiation and propagation values are given in Table 4.13 in detail.

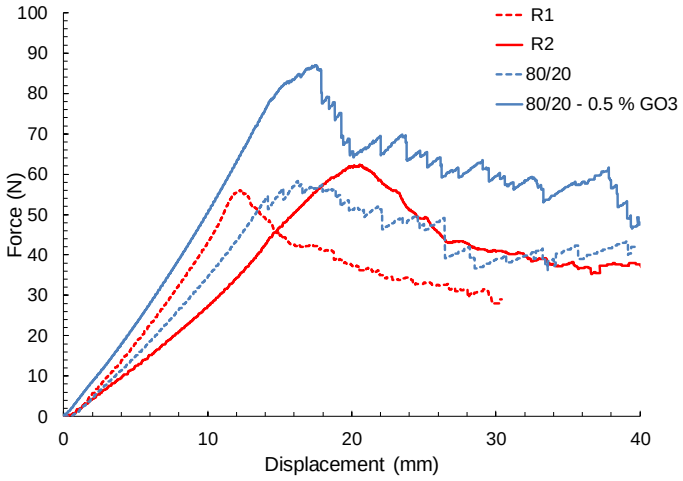

Figure 4.23. Force–displacement curves of R1, R2, 80/20 and 80/20-GO3 laminates

Table 4.13. G_{1C} values of R1, R2, N6/PCL (80/20) and N6/PCL (80/20)-GO3 plates, depending on the 0.5 wt % of GO3 for the initiation and propagation region and the percentage of change relative to the references

Code	**N6/PCL**	**GO Type**	**GO wt %**	**$G_{Ic\text{-}in}$ (N/m)**	**$G_{Ic\text{-}in}$ (STD)**	**$G_{Ic\text{-}in}$ (% variance)**	**Prepreg Roll**	**ΔG_{Ic} (N/m)**
C14-R1	-	-	-	589	73	-	R1	-10
C29-R2	-	-	-	883	117	-	R2	51
[6]C07	80/20	-	-	765	204	30	R1	70
C28	80/20	GO3	0.5	1108	160	26	R2	-69
Code	**N6/PCL**	**GO Type**	**GO wt %**	**$G_{Ic\text{-}prop}$ (N/m)**	**$G_{Ic\text{-}prop}$ (STD)**	**$G_{Ic\text{-}prop}$ (% variance)**	**Prepreg Roll**	
C14-R1	-	-	-	599	48	-	R1	
C29-R2	-	-	-	832	105	-	R2	
C07	80/20	-	-	696	124	16	R1	
C28	80/20	GO3	0.5	1177	179	42	R2	

[6]The test results of the 80/20 hybrid fiber (C7) are based on previous work performed in our group.

With the addition of GO3 to the 80/20 mixture, both $G_{1C\text{-}in}$ and $G_{1C\text{-}prop}$ values were improved according to the corresponding reference plate results (initiation 26%, propagation 42%). Considering that the 80/20 mixture without the GO3 additive, according to the R1, achieves a development of $G_{1C\text{-}in}$ and $G_{1C\text{-}prop}$ values about 30% and only 16% respectively, it is seen that the development of the crack propagation region is noteworthy with the addition of 0.5 wt % GO3 in the 80/20 nanofiber system.

The behavior of 80/20 and 0.5% GO3 added 80/20 hybrid tulles in the first heating cycle are given in Figure 4.24.

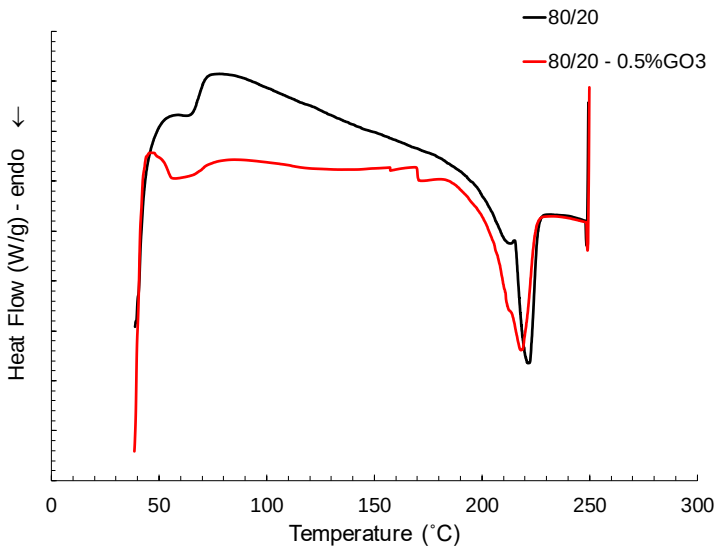

Figure 4.24. DSC first heating scans of 80/20 and 80/20-GO3 hybrid nanofibers

When Figure 4.25 examined, it can be seen that behavior of the N6 crystal region varies considerably with the addition of GO3. It was found that the side peaks of the gamma phase observed below 200 °C as a result of the GO3 additions to 60/40 also appeared in this example. The change in the crystal structure of N6 was investigated by peak separation analysis and the results are given in Figure 4.26 and numerical values are given in Table 4.14.

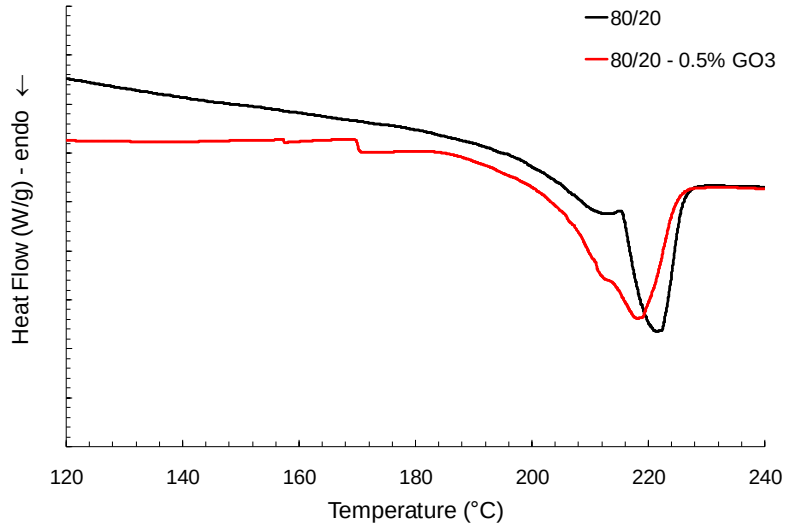

Figure 4.25. The first heating cycle behaviors normalized to the sample weight of the 80/20 and GO3 added 80/20 hybrid tulles at the N6 melting zone

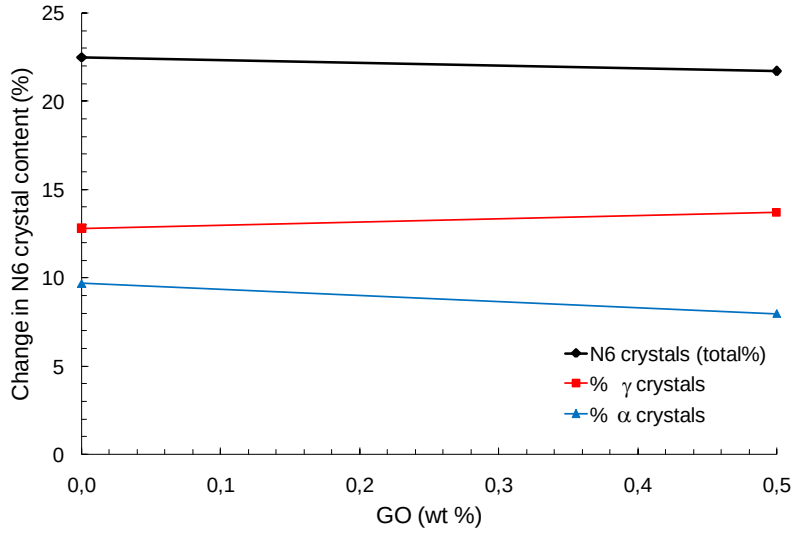

Figure 4.26. Variation of N6 crystal types and quantities in 80/20 and GO3 added 80/20 hybrid tulles with GO3 content

Table 4.14. N6 crystal types and quantities in 80/20 and 80/20-GO3 nanofibers

Code	N6/PCL	GO3 (wt %)	γ Crystals (%)	α Crystals (%)	N6 Crystals (total %)
C08	80/20	-	12.8	9.7	22.5
C28	80/20	0.5	13.7	8.0	21.7

Unlike the 60/40 mixture, there is not significant change in α, γ and N6 total crystallization amounts by adding GO3 to the 80/20 hybrid nanofibers. By adding GO3 to the 80/20 hybrid fiber, the internal crystal structure is not highly affected and may be associated with performance improvement.

4.4.3. Fracture Surface of Composite Plates

In order to understand which mechanisms showed in Figure 1.2 are active during interface separation, SEM analysis on the fracture surface of composite specimens was examined.

4.4.3.1. Composites interleaved with N6/PCL (60/40) nanofibers veils containing different weight of GO3

In 60/40 sets, it is seen that debonding traces and broken fiber ends (Figure 4.27-a, red arrow). In this example, it is seen that the phase-separated PCL crystals could act as foundation for fibers in the bridging position by forming a locally localized interpenetrating network (IPN) structure during epoxy curing. The fact that the broken fibers do not undergo excessive stretching and physical change can be explained by the fact that the α phase with higher mechanical stability of the N6 crystal regions in the fibers is greater in quantity. Also, after a limited debonding, fibers with homogeneous lengths and presumably similar breaks are present due to the stable mechanical phase weighted internal structure.

It can be said that some of the PCL-weighted regions, which are thought to be plastic deformation in the matrix, come into prominence at the time of fracture and activate

the crack capture mechanisms (Figure 4.27-b, red circles). As a result, in this sample, due to the balanced and stable phase weighted internal structure, additional mechanisms arising from the plasticization of the matrix resulting from the IPN formed on the wall of the fibers and the crack initiation and propagation resistance are formed due to the simultaneous breakage of the fibers.

The addition of GO3 to the 60/40 system showed significant changes in the structure of the fiber and the differences observed as a result of interface separation were evaluated for some examples, as shown in Figure 4.27.

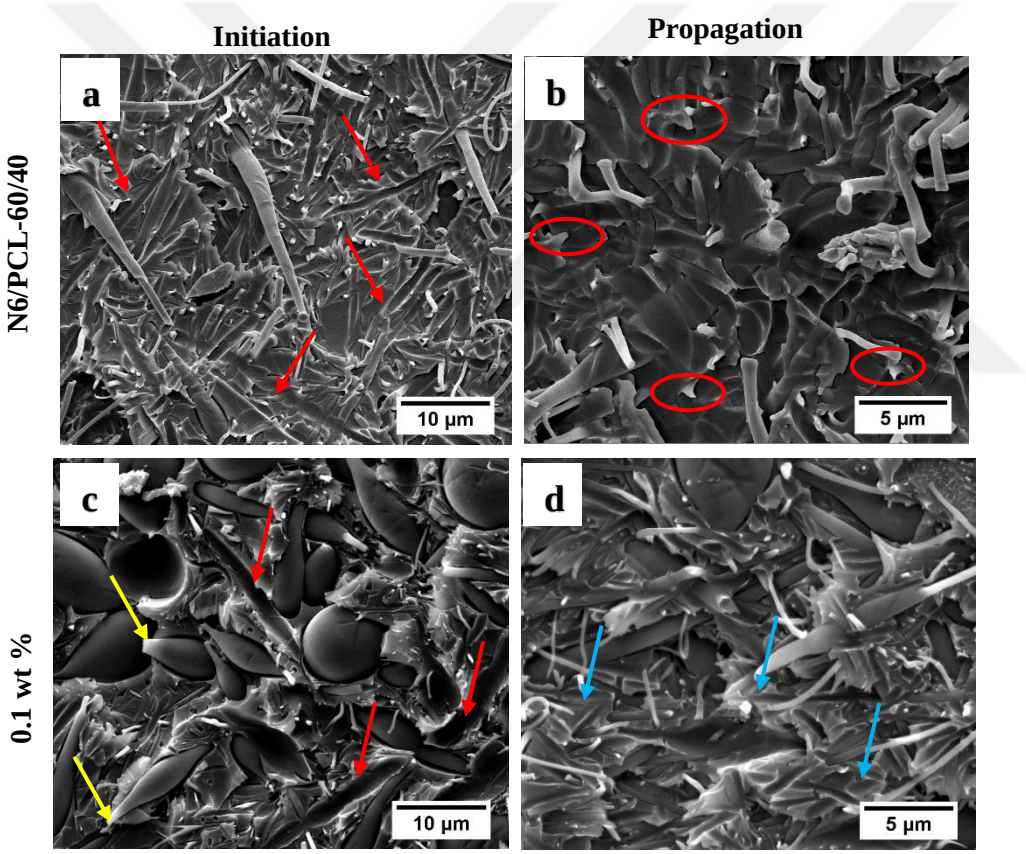

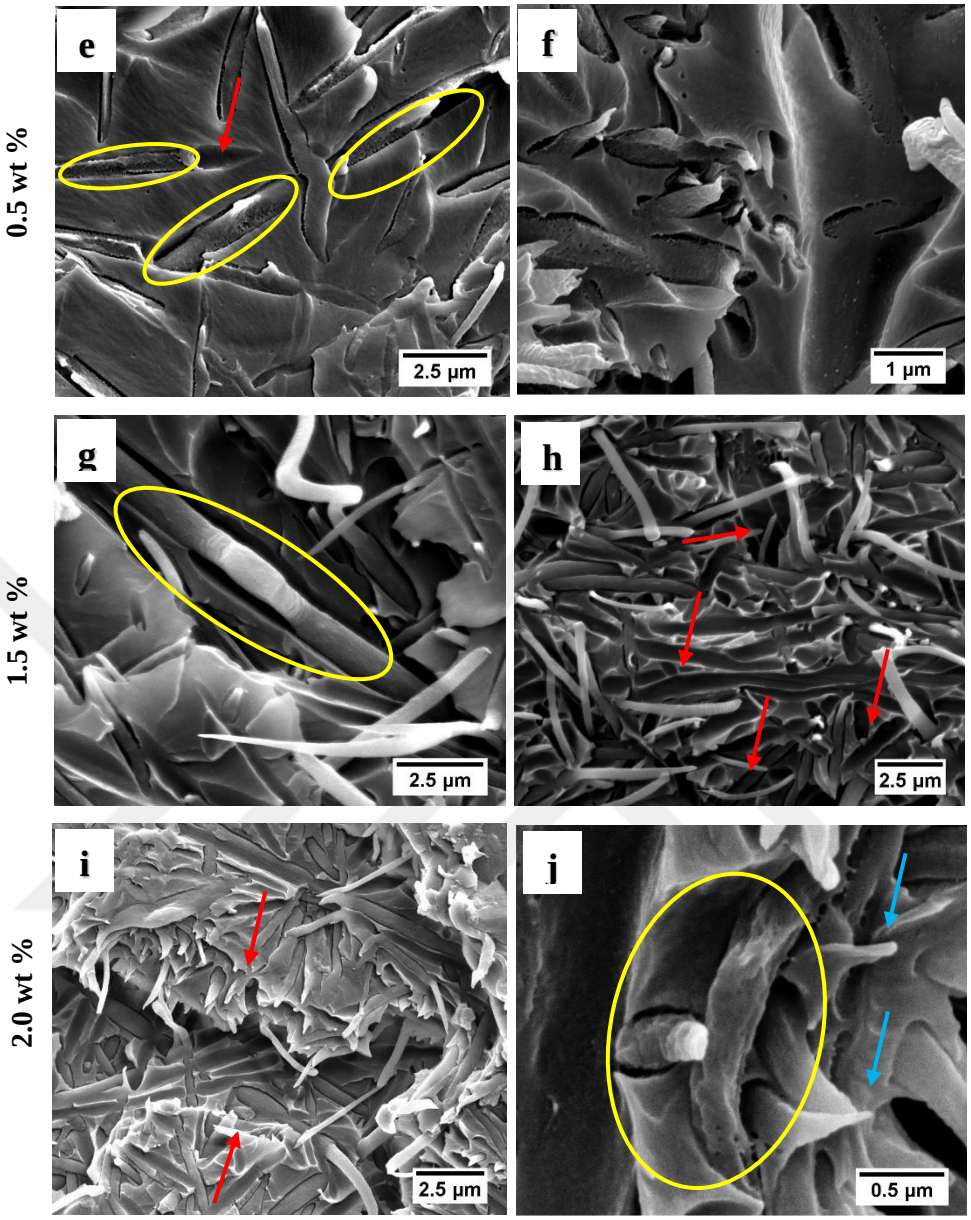

Figure 4.27. SEM images of fracture surface of specimens interleaved with N6/PCL (60/40) nanofibers veils containing different weight of GO3, (a, c: 5,000 x - b, f: 40,000 x - d: 10,000 x - e, g: 20,000 x - i: 15,000 x and j: 100,000)

When the GO3 addition of the N6/PCL (60/40) system, limited debonding traces (Figure 4.27-c, e, h, i, j, red arrows) as well as heterogeneous fiber strain and rupture tip traces (Figure 4.27-d, j, blue arrows) were found in all images. In the pure 60/40, thin roughing debonding traces and fibers are observed (Figure 4.27-a, b), with the addition of GO3, it is seen that the debonding traces and fiber walls become either irregularly rough (Figure 4.27-e, yellow circle) or smooth (Figure 4.27-c, e, h, i, j, red arrows).

In GO3-added samples, PCL phase regions are likely to be close to the GO3 and there will be more intense dissolution along such regions. It is clear that this situation will increase the bond with epoxy in those regions (obstruct debonding) but weaken the remaining fiber structure (Figure 4.27-g, yellow circle). These regions that are considered as examples of these are shown in the Figure 4.27-e, yellow circle.

By adding 0.1% GO3 to the system, the beaded structures formed in the fibers could not carry the load and broke (Figure 4.27-c, yellow arrows).

The damaged perforated fiber structure will not be able to carry the load and immediately break when it is loaded onto it. Fibers containing more γ phases in the structure will extend disproportionately (Figure 4.27-h, d, j general view). The difference in the broken fiber lengths also indicates that the fiber breakages are not synchronized along the crack line. It can be said that the good bond between epoxy and GO, which occurs with the dissolution of, has reduced the number of fibers that can come into bridging position after debonding.

In the sample with 2 wt % GO3, a region with excessive dissolution and loss of integrity in the fibers is shown in a higher magnifier ratio (Figure 4.27-j, yellow circle).

The increase in the interaction between the fiber surfaces and the epoxy is to cause the fibers to remain in the debonding phase, or to cause break away immediately in the GO3-loaded region, and to cause the over-extended break in the non-region. The relative increase of heterogeneous loading and deterioration of the synergistic

relationship between the debonding/fiber bridging mechanisms explain the cause of the poor mechanical performance in N6/PCL (60/40)-GO3 systems.

4.4.3.2. Composites interleaved with N6/PCL (80/20) nanofibers veils containing 5 wt % of GO3

In the fracture interface of the sample with 20% PCL, it is seen debonding traces and smooth fiber surfaces in all SEM images.

The fibers are loaded along the long axis after stripping, resulting in an increased number of flexed, broken, and post-ruptured beads that contractively shrink. It was observed that some fibers flexed under load and some others stretched under load and contracted back after elongation (Figure 4.28-a, b, d- red arrows). However, the presence of deformed and severed fibers which are broken after stretching (Figure 4.28-c, d- red arrows) or half broken (like half-moon shaped fibers) (Figure 4.28-a, yellow circle), show that deformation is heterogeneous at different levels in each fiber.

The predominantly mechanically unstable γ phase in the internal structure of these fibers causes the fibers to not undergo strain at the same time. In this sample, PCL remains largely in admixture with N6 without chain-level crystallization, which means that there is a better chance of better bonding along the fiber length than N6 (Figure 4.28-a, c-yellow circles).

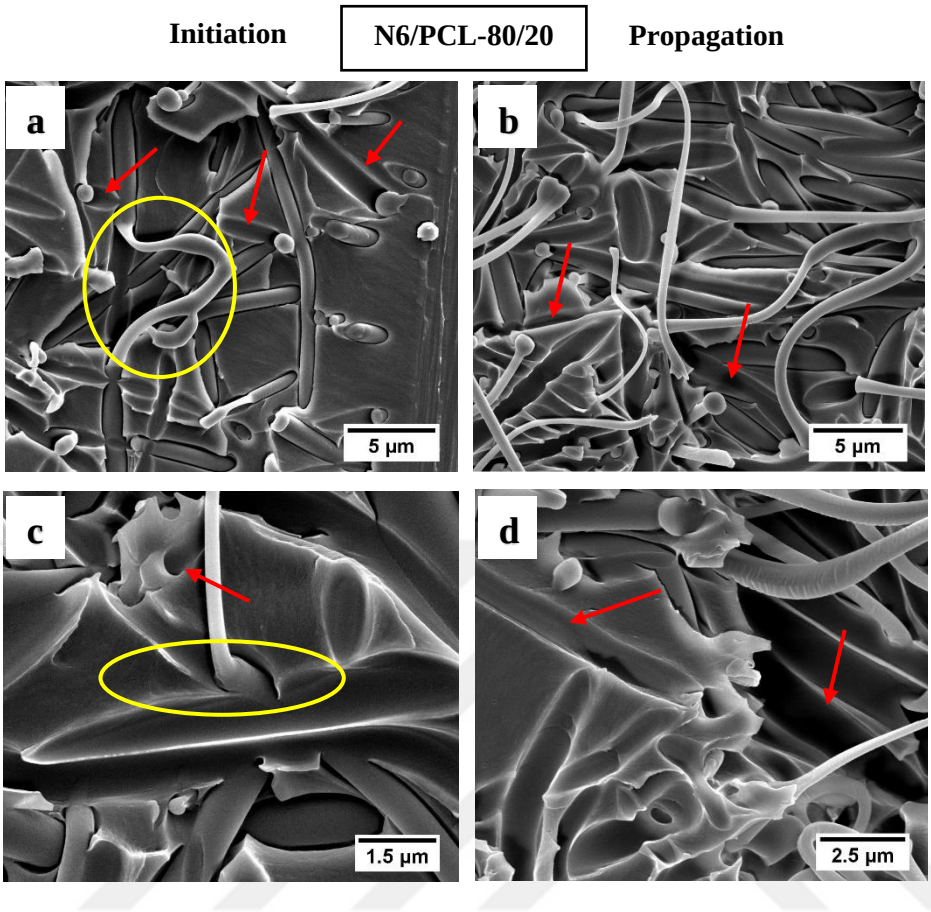

Figure 4.28. SEM images of fracture surface of specimens interleaved with N6/PCL (80/20) nanofibers veils, (a, b: 10,000 x – c: 30,000 and d: 20,000)

In the interface of the 80/20 composite with 0.5% GO3, as in the same 80/20 example, debonding traces are encountered (Figure 4.29-all micrographs), and some fine rough areas (Figure 4.29-d, red arrow) as well as smooth areas (Figure 4.29-b, red arrow) are observed on the peel surfaces of fibers. Due to the small amount of PCL crystals that appear to be formed by the addition of GO to the 80/20 mixture, the characteristics of the fibers were decomposed during curing and the regional bridging characteristics of the fibers were changed. Particularly in the crack propagation region, PCL is observed to bond with the epoxy as fine protrusions along the fiber in the wall of the fiber structure (Figure 4.29-d, red circles). In such regions, where fiber integrity is also lost, it is observed that the fibers break without elongation as seen in the 60/40-GO3 samples (Figure 4.29-d, yellow arrows).

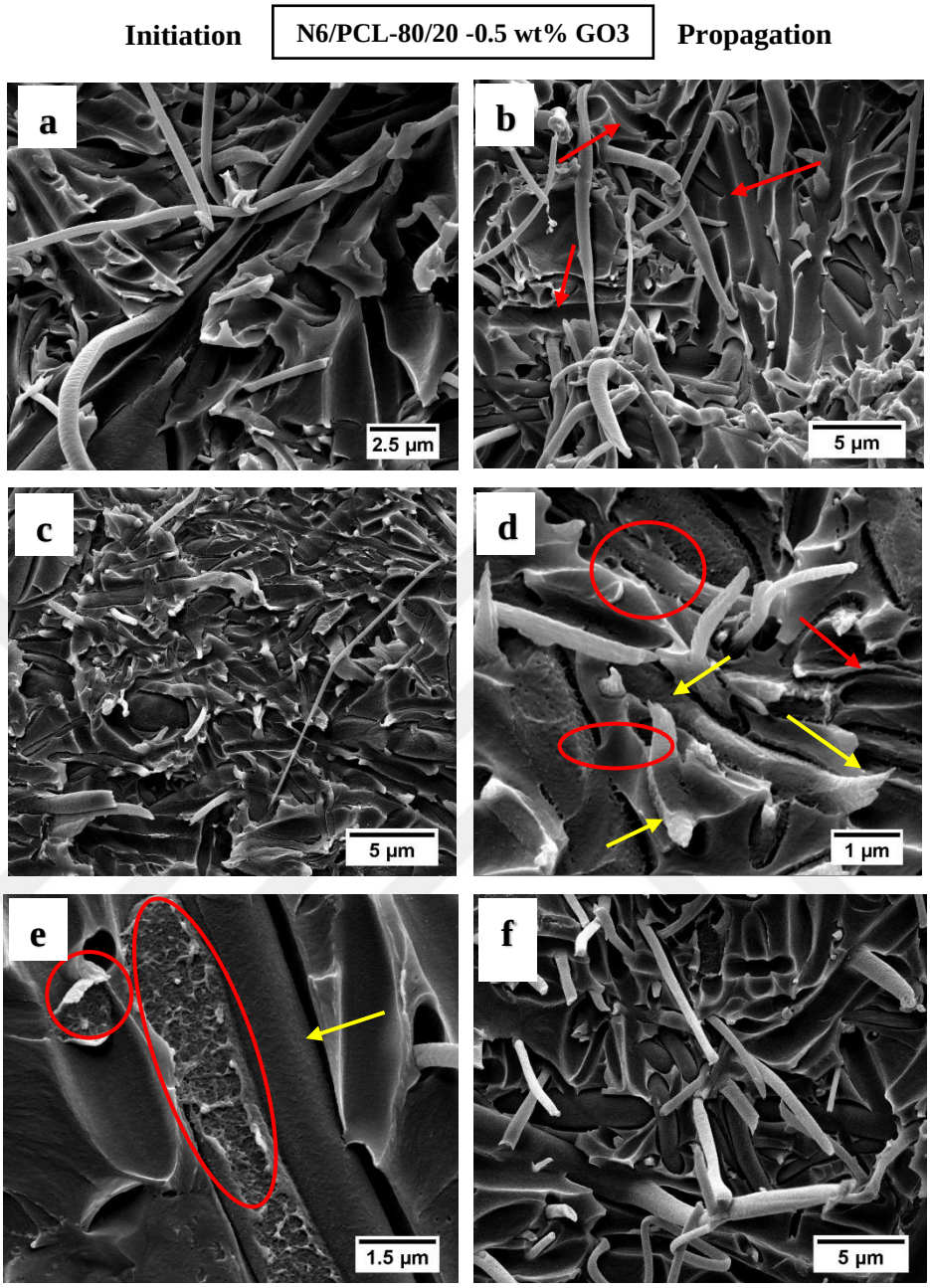

Figure 4.29. SEM images of fracture surface of specimens interleaved with N6/PCL (80/20) nanofibers veils containing 0.5 wt % GO3, (a: 15,000 x – b, c, f: 10,000 x – d: 40,000 x, e: 30,000 x)

It has been determined in the crack initiation zone that the fibers that break without observing the elongation are more in amount than in the progression region (Figure

4.29-c). It is evident that the rupture characteristics (in terms of the end structure) of the fibers that break out in the crack propagation region are similar to the 60/40 sample but have not been able to capture the 60/40 sample in terms of homogeneity (Figure 4.29-f).

Structures in a micrograph from the initiation section should be examined in detail (Figure 4.29-e). On the twin fiber bundle seen here, the yellow arrow is shown to be easily debonding ones, and the red circles also show that half of the broken fibers remain on the other coupon side. These structures, indicated by red circles, show that significantly higher forces can also be applied to the fibers along their diameter axes, either by melting the PCL-containing regions or by attaching the GO leaf tips to the epoxy along the long axis. The majority of the fibers cannot reach the position where they can carry the load along their long axis in the crack initiation state, or they break without elongation. The crack stability in the progress region is particularly important in applications where fatigue performance is critical.

CHAPTER 5

CONCLUSIONS

In this study, it is aimed to increase Mode I interlaminar fracture toughness (G_{1c}) of carbon fiber reinforced polymer (CFRP) composites by using Nylon 6 (N6), N6/PCL (wt/wt: 60 /40), N6/PCL (wt/wt: 80/20) electrospun hybrid nanofibers containing different weight and particle size of graphene oxide (GO) as interleave.

To succeed this aim, firstly GO was synthesized and then some characterization tests were applied to analyze the GO. Therefore, GO, consisting some functional groups such as hydroxyl, epoxide, carbonyl and carboxylic, is easy to fabricate at low cost and has many physical properties. The functionalities on the surface of GO can provide the dispersion of GO in polymeric matrices and the interfacial interaction between GO and polymeric matrices. Also, nano-sized GO sheets were produced by the usage of ultrasonication and centrifuge processes and three different size of GO (approximately 466 nm=GO1, 230 nm=GO2, 165 nm=GO3) were obtained. The addition of sonication steps in the 2-hour probe sonication and 25 min water bath to the GO production steps resulted in a more homogeneous distribution of the GO sheets in the spinning solution and in the nanofibers. The interlayer of CFRP composites was hybridized by GO containing electrospun nanofibers by using N6/PCL polymers with different N6 mass ratios (60, 80, 100 wt %).

In the N6/GO composite sets, while treated GO2 and GO3 did not disarrange the morphological structure of the fiber, untreated, GO1 containing graphene oxide sheets of all sizes negatively affected the morphological structure of the fiber and caused the formation of beaded fiber structures. In cases where N6 was used alone in the interface, the easy peel-off resulting from the weakness of the epoxy-N6 interaction caused poor performance. The addition of 2 wt % GO2 to N6 fibers resulted in an

increase in $G_{1c\text{-}in}$ and $G_{1c\text{-}prop}$ with 21% and 13% respectively relative to reference sample. The reasons for this are; (i) bonding of GO2 with epoxy through portions of N6 fiber surfaces that overflow and carry functional groups makes it difficult to debonding and peel of the fibers and (ii) stabilize the amount of γ/α crystal in the N6 internal structure with addition of GO2 to the system.

In N6/PCL (60/40)-GO3 composite sets, addition of GO3 to 60/40 hybrid system could not increase the G_{1C}. By adding GO3; (i) N6 began to crystallize only γ phase, (ii) PCL phase separation sites were concentrated around the GO3 and (iii) GO3 was present in each region along the fiber and overflowed from some regions. Also, there is a relationship between increased formation of γ phase and relative increased performance in this system. The relative increase of heterogeneous loading and deterioration of the synergistic relationship between the debonding/fiber bridging mechanisms cause the poor mechanical performance in N6/PCL (60/40)-GO3 systems.

In the 80/20-GO3 composite sets, $G_{1C\text{-}in}$ and $G_{1C\text{-}prop}$ values were increased by 26% and 42% according to reference with 0.5 wt % GO3 addition. The change in the character of dissolving PCL crystals to form ‘'bridge’’ and the bonding of graphene oxide with epoxy through the fiber increased mechanical performance, as opposed to the 60/40 mixture. In this system, balanced and stable amount of γ/α phase in internal structure of fibers, synergistic relationship between the debonding/fiber bridging mechanisms provide interfacial toughening of CFRP composites.

In conclusion, graphene oxides dispersed homogeneously in the fiber and overflowed to the fiber surface in some regions reinforced electrospun N6 and N6/PCL (80/20) interleaving resulted in improvement of the interfacial fracture toughness under Mode I load, G_{1C}, of carbon fiber/epoxy laminates. At the same time, in N6/PCL (60/40)-GO3 system, a good relationship was established between the crystal structure of fibers and mechanic performance and this relationship was examined by interface images after fracture. Results showed that fibers containing GO can be produced by electrospinning process and can be used in interface toughening studies.

CHAPTER 6

RECOMMENDATIONS

There are some recommendations depend on conducted studies for the future work. These suggestions can be as follows;

- By using different polymer combinations, different toughening mechanisms can be activated by synergistic effect.
- New hybrids can be produced by adding GO in 0.5% or less to mixtures containing PCL of less than 20% or between 20% and 40% but without phase separation. Thus, with the controlled melting of PCL, the very strong interaction of the released graphene oxide sheets with the epoxy can be reduced in a controlled manner. Thus, the number of fibers that can be brought into the bridging position after the debonding can be increased.
- Further studies can be carried out to make the distribution of graphene oxide in the fiber more homogeneous.
- With the addition of graphene oxide at rates much lower than used ratios, it is possible that graphene oxide can be dispersed in the fiber in such a way that it does not choke and does not overflow from the surface.

REFERENCES

[1] R. M. Jones, *Mechanics Of Composite Materials*, Second Edition ed., 1999.

[2] T. K. O' Brien, "Delamination of Composite Materials," *Fatigue of Composite Materials*, 1990.

[3] M. R. Wisnom, "The role of delamination in failure of fibre-reinforced composites," vol. 370, pp. 1850-1870, 2012.

[4] A. P. L. Mouritza, K.H. and I. Herszberg, "A review of the effect of stitching on the in-plane mechanical properties of fibre-reinforced polymer composites," *Composite Part A*, vol. 28A, pp. 979-991, 1997.

[5] W. Trabelsi, L. Michel, and R. Othomene, "Effects of Stitching on Delamination of Satin Weave Carbon-Epoxy Laminates Under Mode I, Mode II and Mixed-Mode I/II Loadings," *Applied Composite Materials*, vol. 17, pp. 575-595, 2010.

[6] B. S. O. Jamal Seyyed Monfared Zanjani, Yusuf Ziya Menceloglu, Mehmet Yildiz, "Nano-engineered design and manufacturing of high-performance epoxy matrix composites with carbon fiber/selectively integrated graphene as multi-scale reinforcements," *RSC Adv.*, vol. 6, pp. 9495-9506, 2016.

[7] B. B. J. A. J. Kinloch, R. D. Mohammed, A. C. Taylor, S. Sprenger, "Toughening mechanisms in novel nano-silica epoxy polymers," in *5th Australasian Congress on Applied Mechanics (ACAM 2007)*, Brisbane, Australia, 2007, pp. 441-446.

[8] D. A. Hawkins and A. Haque, "Fracture Toughness of Carbon-Graphene/Epoxy Hybrid Nanocomposites," *Procedia Engineering*, vol. 90, pp. 176-181, 2014.

[9] F. J. McGarry, B. Zhu, and D. E. Katsoulis, "Silicone Resin Based Composites Interleaved for Improved Toughness," United States Patent US 6,660,395 B2, 2003.

[10] A. M. L. Becu, H. Sautereau, J. F. Gerard, "Fracture Behavior of Epoxy Polymers Modified with Core-Shell Rubber Particles," *Journal of Applied Polymer Science,* vol. 65, pp. 2419-2431, 1996.

[11] R. Sager, "A Characterization of the Interfacial and Interlaminar Properties of Carbon Nanotube Modified Carbon Fiber/Epoxy Composites," Texas A&M University, 2008.

[12] X. F. Wu, "Fracture of Advanced Polymer Composites with Nanofiber Reinforced Interfaces," PhD, Department of Engineering Mechanics, University of Nebreska, 2003.

[13] S. C. T. W. Jiang, P. K. Chu,R. K. Y. Li, J. K. Kim,Y. W. Mai, "Interlaminar Fracture Properties of Carbon Fibre/Epoxy Matrix Composites Interleaved with Polyethylene Terephthalate (PET) Films," *Polymers and Polymer Composites,* vol. 9, pp. 141-145, 2001.

[14] P. Y. B. J. Dejan Stevanovic, Adrian Lowe & Shankar Kalyanasundaram, "The Influence of Rubber Particle Concentration on Fracture Toughness of Interlayer Toughened Vinyl-Ester/Glass Fibre Composite," 1999.

[15] K. L. White and H.-J. Sue, "Delamination toughness of fiber-reinforced composites containing a carbon nanotube/polyamide-12 epoxy thin film interlayer," *Polymer,* vol. 53, pp. 37-42, 2012.

[16] P. J. Hogg, "Developments in Toughening Composites," *Materials Science and Engineering: A,* vol. 412, pp. 97-103, 2005.

[17] D. H. R. Yuris A. Dzenis, "Delamination resistant composites prepared by small diameter fiber reinforcement at ply interfaces," US Patent, 2001.

[18] J.-S. Kim and D. H. Renekeer, "Mechanical Properties of Composites Using Ultrafine Electrospun Fibers," *Polymer Composites,* vol. 20, pp. 124-131, 1999.

[19] Y. A. Ozge Kaynan, E.Ö. Yeniguna, H. Cebeci, "Mixed Mode delamination in carbon nanotube/nanofiber interlayered composites," *Composites Part B,* vol. 154, pp. 186-194, 2018.

[20] S. v. d. H. Lode Daelemans, Ives De Baere, Hubert Rahier, Wim Van Paepegem, Karen De Clerck, "Damage-Resistant Composites Using Electrospun Nanofibers: A Multiscale Analysis of the Toughening Mechanisms," *ACS Applied Material Interfaces,* vol. 8, pp. 11806-18, May 11 2016.

[21] G. W. Beckermann and K. L. Pickering, "Mode I and Mode II interlaminar fracture toughness of composite laminates interleaved with electrospun nanofibre veils," *Composites Part A: Applied Science and Manufacturing,* vol. 72, pp. 11-21, 2015.

[22] F. Bovicelli, Saghafi, H., Brugo, T. M., Belcari, J., Zucchelli, A., Minak, G., "On Consideration the Mode I Fracture Response of CFRP Composite Interleaved by Composite Nanofibers," *Procedia Materials Science,* vol. 3, pp. 1316-1321, 2014.

[23] Y. L. Huiming Ning, Ning Hu, "Improvement of interlaminar mechanical properties of CARALL based on nanofiller interface reinforcement and other fabrication techniques," 2013, June 16-21 2013.

[24] A. Shekhawat and R. O. Ritchie, "Toughness and strength of nanocrystalline graphene," *Nat Commun,* vol. 7, p. 10546, 2016.

[25] J. H. B. Chang Yeong Lee, Tae-Yoon Kim, Seung-Hwan Chang, Soo Young Kim "Using silane-functionalized graphene oxides for enhancing the interfacial bonding strength of carbon/epoxy composites," *Composites Part A: Applied Science and Manufacturing,* vol. 75, pp. 11-17, 8// 2015.

[26] D. R. Bortz, E. G. Heras, and I. Martin-Gullon, "Impressive Fatigue Life and Fracture Toughness Improvements in Graphene Oxide/Epoxy Composites," *Macromolecules,* vol. 45, pp. 238-245, 2012.

[27] J. L. Huiming Ning , Ning Hu, Cheng Yan, Yaolu Liu, Liangke Wu, Feng Liu, Jianyu Zhang "Interlaminar mechanical properties of carbon fiber reinforced plastic laminates modified with graphene oxide interleaf," *Carbon,* vol. 91, pp. 224-233, 9// 2015.

[28] A. Hirsch, "The era of carbon allotropes," *Nature Materials,* vol. 9, pp. 868-871, 2010.

[29] V. C. Shan Liu , Zhiguang Xu , David Hui , Hao Wang "A review of extending performance of epoxy resins using carbon nanomaterials," *Composites Part B,* pp. 197-214, 2018.

[30] M. K. Roksana Muzyka, Lukasz Smędowski, Noel Diez, Grażyna Gryglewicz, "Oxidation of graphite by different modified Hummers methods," *New Carbon Materials,* vol. 32, pp. 15-20, 2017.

[31] P. V. M. S. Syama, "Comprehensive Application of Graphene: Emphasis on Biomedical Concerns," *Nano-Micro Letters,* vol. 11, p. 31, 2019.

[32] J. L. B. Edgar Jimenez-Cervantes Amieva, Ana Laura Martínez-Hernández and Carlos Velasco-Santos, *Graphene-Based Materials Functionalization with Natural Polymeric Biomolecules,* 2016.

[33] M. P. Chun Kiang Chua, "Chemical reduction of graphene oxide: a synthetic chemistry viewpoint," *The Royal Society of Chemistry,* vol. 41, pp. 291-312, 2014.

[34] M. S. Eluyemi, M. A. Eleruja, A. V. Adedeji, B. Olofinjana, O. Fasakin, O. O. Akinwunmi, "Synthesis and Characterization of Graphene Oxide and Reduced Graphene Oxide Thin Films Deposited by Spray Pyrolysis Method," *Graphene,* vol. 05, pp. 143-154, 2016.

[35] Y. Z. Xiao Han, Jian-ming Sun, Ye Li, Jin-dong Zhang, Yue Hao, "Effect of graphene oxide addition on the interlaminar shear property of carbon fiber-reinforced epoxy composites," *New Carbon Materials,* vol. 32, pp. 48-55, 2017.

[36] K. L. Velram Balaji Mohan, David Hui, Debes Bhattacharyy, "Graphene-based materials and their composites: A review on production, applications and product limitations," *Composites Part B,* vol. 142, pp. 200-220, 2018.

[37] S. B. Tapas Kuilla , Dahu Yao , Nam Hoon Kim,Haswata Bose , Joong Hee Lee, "Recent advances in graphene based polymer composites," *Progress in Polymer Science,* vol. 35, 2013.

[38] H. R. Pant, C. H. Park, L. D. Tijing, A. Amarjargal, D.-H. Lee, and C. S. Kim, "Bimodal fiber diameter distributed graphene oxide/nylon-6 composite nanofibrous mats via electrospinning," *Colloids and Surfaces A: Physicochemical and Engineering Aspects,* vol. 407, pp. 121-125, 2012.

[39] H. F. Da Chen, Jinghong Li, "Graphene Oxide: Preparation, Functionalization, and Electrochemical Applications," *Chemical Reviews,* vol. 112, pp. 6027-6053, 2012.

[40] S. P. Daniel R. Dreyer, Christopher W. Bielawski and Rodney S. Ruoff, "The chemistry of graphene oxide," *Chemical Society Reviews,* 2009.

[41] D. V. K. Daniela C. Marcano, Jacob M. Berlin, Alexander Sinitskii, Zhengzong Sun, Alexander Slesarev, Lawrence B. Alemany, Wei Lu, and James M. Tour, "Improved Synthesis of Graphene Oxide," *American Chemical Societ,* vol. 4, pp. 4806-4814, 2010.

[42] D. Y. Guolong Wang , Ajit D. Kelkar , Lifeng Zhang, "Electrospun nanofiber: Emerging reinforcing filler in polymer matrix composite materials," *Progress in Polymer Science,* vol. 75, pp. 73-107, 2017.

[43] S. R. Vishnu Vijay Kumar, Jeremy Lee Kong Yoong, and S. S. Rasoul Esmaeely Neisiany, Gurusamy Balaganesan, "Electrospun nanofiber interleaving in fiber reinforced composites—Recent trends," 2018.

[44] X. Y. Yun-Ze Long, Xiao-Xiong Wang, Jun Zhang, Miao Yu, "Electrospinning: The Setup and Procedure," pp. 21-52, 2019.

[45] R. R. Nagavally, "Composite Materials- History, types, fabrication techniques, advantages, and applications," *International Journal of Mechanical And Production Engineering,* vol. 5, 2017.

[46] A. K. Kaw, *Mechanics of Composite Materials* vol. 29. London: Taylor & Francis Group, 2006.

[47] B. Harris, *Engineering Composite Materials*. London: Institute of Metals, 1999.

[48] F. C. Campbell, "Inroduction to Composite Materials," in *Structural Composite Materials*, ed: ASM International, 2010, p. 630.

[49] D. Tenney and R. B. Pipes, "Advanced Composites Development for Aerospace Applications," in *Advanced Composites Development for Aerospace Applications*, 2001.

[50] J. W. W. Daniel C. Davis, Jiang Zhu, Daniel O.O. Ayewah "Improvements in mechanical properties of a carbon fiber epoxy composite using nanotube science and technology," *Composite Structures*, vol. 92, pp. 2653-2662, 2010.

[51] R. Palazzetti, "Electrospun nanobrous interleaves in composite laminate materials," Master of Science, Meccanica e scienze avanzate, Degli Studi di Bologna, 2012.

[52] G. Seshasai, "Selective Toughening of Carbon/Epoxy Composites Using Graphene Oxide," Master of Science, Mechanical Engineering, Osmania University, India, 2008.

[53] T. Tay, "Characterization and analysis of delamination fracture in composites: An overview of developments from 1990 to 2001," vol. 56, 2003.

[54] ASTM-International, "Standard Test Method for Mode I Interlaminar Fracture Toughness of Unidirectional Fiber-Reinforced Polymer Matrix Composites," ed, 2013.

[55] W. Trabelsi, "Effects of stitching on delamination of satin weave carbon-epoxy laminates under mode I, mode II and mixed-mode I/II loadings," *Applied Composite Materials*, vol. 17, 2010.

[56] N. J. Pagano, "The Influence of Stacking Sequence on Laminate Strength," *Journal of Composite Materials*, vol. 5, 1971.

[57] M. A. Rahman, "Fabrication and mechanical characterization of novel hybrid carbon-fiber/epoxy composites reinforced with toughening/selfrepairing nanofibers at interfaces," Master of Science, Mechanical Engineering, North Dakota State University, 2012.

[58] V. C. P.S. Shivakumar Gouda , P.K. Barhai, Dayananda Jawali, Sameer Rahatekar,M.R. Wisnom "Improved fracture toughness in carbon fibre epoxy composite through novel pre-preg coating method using Epoxy Terminated Butadiene Nitrile rubber," *Materials & Design*, vol. 62, pp. 320-326, 2014.

[59] K. X. Cheng Yan, Lin Ye and Yiu-Wing Mai, "Numerical and Experimental Studies on the Fracture Behavior of Rubber-toughened Epoxy in Bulk Specimen and Laminated Composites " *Journal of Materials Science,* vol. 37, pp. 921-927, 2002.

[60] S. F. N.Chikhi, M. Bakar, "Modification of Epoxy Resin Using Reactive Liquid (ATBN) Rubber," *European Polymer Journal,* vol. 38, pp. 251-264, 2002.

[61] A. A. B. Ferdandez, E. Diaz, and I. Mondragon, "Influence of Polyethersulfone Modification of a Tetrafunctional Epoxy Matrix on the Fracture Behavior of Composite Laminates Based on Woven Carbon Fibers," *Polymer Composites,* vol. 25, pp. 480-488, 2004.

[62] H. C. K. Soo-Jin Park, "Thermal Stability and Toughening of Epoxy Resin with Polysulfone Resin," *Polymer Physics,* vol. 39, pp. 121-128, 2000.

[63] Y. Z. Yaping Zhenga , Rongchang Ninga, "Effects of nanoparticles SiO2 on the performance of nanocomposites," *Materials Letters,* vol. 57, pp. 2940-2944, 2003.

[64] M. Q. Z. Guang Shi, Min Zhi Rong, Bernd Wetzel, Klaus Friedrich "Sliding wear behavior of epoxy containing nano-Al2O3 particles with different pretreatments," *Wear,* vol. 256, pp. 1072-1081, 2004.

[65] P. R. Bernd Wetzel , Frank Haupert, Klaus Friedrich, "Epoxy nanocomposites – fracture and toughening mechanisms," *Engineering Fracture Mechanics,* vol. 73, pp. 2375-2398, 2006.

[66] Y. I. Tomohiro Yokozeki , Masaru Ishibashi, Takashi Yanagisawa, Kazunari Imai, Masahiro Arai, Tatsuhiro Takahashi, Kiyoshi Enomoto "Fracture toughness improvement of CFRP laminates by dispersion of cup-stacked carbon nanotubes," *Composites Science and Technology,* 2009.

[67] S. Sprenger, A. J. Kinloch, and A. C. Taylor, "Fibre Reinforced Composites Optimized by the Synergy Between Rubber-Toughening and Sio2-Nanoparticles," 2009.

[68] Y.-J. W. Long-Cheng Tang, Dong Yan, Yong-Bing Pei, Li Zhao, Yi-Bao Li, Lian-Bin Wu , Jian-Xiong Jiang , Guo-Qiao Lai, "The effect of graphene dispersion on the mechanical properties of graphene/epoxy composites," *Carbon*, pp. 16-27, 2013.

[69] H. Z. Xusheng Du, Weifu Sun, Hong-Yuan Liu , Guangnan Zhou , Huamin Zhou , Yiu-Wing Mai "Graphene/epoxy interleaves for delamination toughening and monitoring of crack damage in carbon fibre/epoxy composite laminates," *Composite science and Technology*, vol. 140, pp. 123-133, 2017.

[70] S. H. B. M. Goodarz, M. Sadighi, and S. Saber-Samandari, "The influence of graphene reinforced electrospun nano-interlayers on quasi-static indentation behavior of fiber-reinforced epoxy composites," *Fibers and Polymers*, vol. 18, pp. 322-333, 2017.

[71] O. I. N. Sela, L. Banks-Sills, "The effect of adhesive thickness on interlaminar fracture toughness of interleaved CFRP specimens " *Composites* vol. 20, pp. 257-264, 1989.

[72] Y. G. W. Nam Gyun Yuna, Sung Chul Kimb, "Toughening of Epoxy Composite by Dispersing Polysulfone Particle to Form Morphology Spectrum," vol. 52, pp. 365-372, 2004.

[73] S. M. Masaki Hojo, Mototsugu Tanaka, Shojiro Ochiai, Atsushi Murakami, "Mode I delamination fatigue properties of interlayer-toughened CF/epoxy laminates," *Composite Science and Technology*, vol. 66, 2006.

[74] L. L. Doris W.Y. Wong , P. Terry McGrail , Ton Peijs , Paul J. Hogg "Improved fracture toughness of carbon fibre/epoxy composite laminates using dissolvable thermoplastic fibres," *Composites: Part A*, vol. 41, 2010.

[75] E. S. Elisa Borowski , Usama F. Kandil and Mahmoud Reda Taha, "Interlaminar Fracture Toughness of CFRP Laminates Incorporating Multi-Walled Carbon Nanotubes," *Polymers*, vol. 7, pp. 1020-1045, 2015.

[76] J. Zhang, T. Lin, and X. Wang, "Electrospun nanofibre toughened carbon/epoxy composites: Effects of polyetherketone cardo (PEK-C) nanofibre diameter and interlayer thickness," *Composites Science and Technology,* vol. 70, pp. 1660-1666, 2010.

[77] A. Y. Volkan Eskizeybek , Ahmet Avcı "CNT-PAN hybrid nanofibrous mat interleaved carbon/epoxy laminates with improved Mode I interlaminar fracture toughness," *Composites Science and Technology*, vol. 157, 2018.

[78] M. L. F. Andrea Zucchelli, Chiara Gualandi and Seeram Ramakrishn, "Electrospun nanofibers for enhancing structural performance of composite materials," *Polymer Advanced Technology,* 2010.

[79] C.-E. P. Woo-Nyon Kım, Charles M.Burns, "Ternary Blends of Poly(arnide-6)/ Polycarbonate/Poly(e-caprolactone)," *Applied Polymer Science,* vol. 49, pp. 1003-1011, 1993.

[80] L. P. Li Gang, Yu Yunhua, Jia Xiaolong, Zhang Shen, Yang Xiaoping, Ryu Seungkon, "Novel carbon fiber/epoxy composite toughened by electrospun polysulfone nanofibers," *Materials Letters,* vol. 62, pp. 511-514, 2/15/ 2008.

[81] T. Y. Jin Zhang, Tong Lin, Chun H. Wang "Phase morphology of nanofibre interlayers: Critical factor for toughening carbon/epoxy composites," *Composites Science and Technology,* vol. 72, pp. 256-262, 2012.

[82] K. Magniez, C. De Lavigne, and B. L. Fox, "The effects of molecular weight and polymorphism on the fracture and thermo-mechanical properties of a carbon-fibre composite modified by electrospun poly (vinylidene fluoride) membranes," *Polymer*, vol. 51, pp. 2585-2596, 5/28/ 2010.

[83] K. Magniez, T. Chaffraix, and B. Fox, "Toughening of a Carbon-Fibre Composite Using Electrospun Poly(Hydroxyether of Bisphenol A) Nanofibrous Membranes Through Inverse Phase Separation and Inter-Domain Etherification," *Materials*, vol. 4, pp. 1967-1984, 2011.

[84] R. Palazzetti, A. Zucchelli, C. Gualandi, M. L. Focarete, L. Donati, G. Minak, "Influence of electrospun Nylon 6,6 nanofibrous mats on the interlaminar

properties of Gr–epoxy composite laminates," *Composite Structures*, vol. 94, pp. 571-579, 2012.

[85] A. Z. H. Saghafi, R. Palazzetti, G. Minak, "The effect of interleaved composite nanofibrous mats on delamination behavior of polymeric composite materials," *Composite Structures*, vol. 109, pp. 41-47, 2014.

[86] H. L. Shay Hamer, Anthony Green, Ron Avrahami, Eyal Zussman, Arnon Siegmann, Dov Sherman "Mode I and Mode II fracture energy of MWCNT reinforced nanofibrilmats interleaved carbon/epoxy laminates," *Composites Science and Technology*, vol. 90, pp. 48-56, 2014.

[87] S. H. B. M. Goodarz, M. Sadighi, and S. Saber-Samandari, "The Influence of Graphene Reinforced Electrospun Nano-Interlayers on Quasi-Static Indentation Behavior of Fiber-Reinforced Epoxy Composites," *Fibers and Polymers*, 2017.

[88] D. L. Peng Li, Bo Zhu, Bo Li, Xiaolong Jia, Lili Wang, Gang Li, Xiaoping Yang "Synchronous effects of multiscale reinforced and toughened CFRP composites by MWNTs-EP/PSF hybrid nanofibers with preferred orientation," *Composites Part A: Applied Science and Manufacturing*, vol. 68, pp. 72-80, 2015.

[89] Y. Z. Yan Wang, Tianjiao Bao, Xiang Li, Yuqin Su, Yuexin Duan, "Preparation of Ni-reduced graphene oxide nanocomposites by Pd-activated electroless deposition and their magnetic properties," *Applied Surface Science*, vol. 258, pp. 8603-8608, 2012.

[90] J. L. Franklin Kim, Rodolfo Cruz-Silva, Laura J. Cote, Kwonnam Sohn, Jiaxing Huang, "Self-Propagating Domino-like Reactions in Oxidized Graphite," *Advanced Functional Materials*, vol. 20, pp. 2867-2873, 2010.

[91] A. S. Mohammad Saleem Khan, Gul Tiaz Khan, Sabiha Sultana and Abid Zia, "A Study of Stable Graphene Oxide Dispersions in Various Solvents," *journal of chemistry society pakistan*, vol. 37, pp. 62-67, 2015.

[92] M. F. Ashby, *Materials Selection in Mechanical Design*, 4th Edition ed. United States: Elsevier, 2011.

[93] M. Wojdyr, "Fityk: a general-purpose peak fitting program," *Journal of Applied Crystallography,* vol. 43, pp. 1126-1128, 2010.

[94] L. M. Eva Kuzelova Kostakova, Gabriela Maskova, Lenka Blazkova,Tamas Turcsan, and David Lukas, "Crystallinity of Electrospun and Centrifugal Spun Polycaprolactone Fibers: A Comparative Study," *Journal of Nanomaterials,* vol. 2017, p. 9, 2017.

[95] Y. P. Khanna, W. P. Kuhn, and W. J. Sichina, "Reliable Measurements of the Nylon 6 Glass Transition Made Possible by the New Dynamic DSC," *Macromolecules,* vol. 28, pp. 2644-2646, 1995/04/01 1995.

[96] D. Cho, E. Zhmayev, and Y. L. Joo, "Structural studies of electrospun nylon 6 fibers from solution and melt," *Polymer,* vol. 52, pp. 4600-4609, 2011.

[97] T. D. Fornes and D. R. Paul, "Crystallization behavior of nylon 6 nanocomposites," *Polymer,* vol. 44, pp. 3945-3961, 2003.

[98] M. S. Adolfo Senatore, Klaus D. Sattler, "Carbon Nanomaterials Sourcebook," *Graphene, Fullerenes, Nanotubes, and Nanodiamonds,* .

[99] N. K. Suman Thakur, "Green reduction of graphene oxide by aqueous phytoextracts," *Carbon 50,* pp. 5331-5339, 2012.

[100] J. S. Adhiraj Dasgupta, Manosij Ghosh, Amartya Bhattacharya, Anita Mukherjee, Dipankar Chattopadhyay, Krishnendu Acharya, "Green conversion of graphene oxide to graphene nanosheets and its biosafety study," *PLOS-one,* p. 20, 2016.

[101] S. M. Swarnima Kashyap, and Shantanu K. Behera, "Aqueous Colloidal Stability of Graphene Oxide and Chemically Converted Graphene," *Hindawi,* p. 6, 2014.

[102] H. Z. Yan Tian, Zhong Zhang, "Influence of nanoparticles on the interfacial properties of fiberreinforced-epoxy composites," *Composites: Part A,* vol. 98, pp. 1-8, 2017.

[103] C. O. G. Cesar Leyva-Porras, M. Miki-Yoshida, Yazmın I. Avila-Vega, Javier Macossay, Jose Bonilla-Cruz "EELS Analysis of Nylon 6 Nanofibers Reinforced with Nitroxide-Functionalized Graphene Oxide," *Carbon N Y,* vol. 70, pp. 164-171, 2014.

[104] S. Ramazani and M. Karimi, "Study the molecular structure of poly(epsilon-caprolactone)/graphene oxide and graphene nanocomposite nanofibers," *J Mech Behav Biomed Mater,* vol. 61, pp. 484-92, Aug 2016.

[105] L. C. Yi Liu, Fangxiao Guan, Yi Gao Nyle E. Hedin, Lei Zhu, and Hao Fong, "Crystalline Morphology and Polymorphic Phase Transitions in Electrospun Nylon 6 Nanofibers," *Macromolecules,* vol. 40, pp. 6283-6290, 2007.

[106] M. Ito, K. Mizuochi, and T. Kanamoto, "Effects of crystalline forms on the deformation behaviour of nylon-6," *Polymer,* vol. 39, pp. 4593-4598, 1998/09/01/ 1998.

[107] C. L. T. Shu Huang, Liping Yang, Silei Phua, Rui Zhou, Aravind Dasari, Xuehong Lu, "Reinforcing nylon 6 via surface-initiated anionic ring-opening polymerization from stacked-cup carbon nanofibers," *Composites Science and Technology,* vol. 93, pp. 30-37, 2014.

[108] M. Kılıçoğlu, "Use of Nano-hybrid Systems in Carbon Fiber Reinforced Polymer Matrix Composites (CFRP) for Interfacial Toughening," Master of Science, Hacettepe University, 2018.

APPENDICES

A. Calculation of fiber-resin ratios in composite plates

The prepreg specification information is primarily used to calculate the ratio of the mass of nanofiber tulle placed between the layers within the entire composite structure. Prepreg rolls used the project are as follows; VTP H 300 CFA 210 3KT RC35 HS (R1) and VTP H 300CFA 200 3KT RC42 HS (R2). The RC35 and EC42 codes in the naming of the rolls mean "resin content 35%" and "resin content 42%". So, 35% or 42% by mass of the unit m^2 prepreg fabric consists of epoxy resin.

After the entire mass of the plate (m_{total}) for the DCB test is weighed, the epoxy resin mass ($m_{epoxy\_calculated}$) in the plate is calculated by multiplying the percentage of resin in it by the total mass of the plate. After the epoxies overflowed from the edges shown in Figure 33-b are cut off, the cut pieces ($m_{epoxy\_overflowed}$) are weighed. When the protruded mass is removed from the calculated value, the epoxy mass remaining ($m_{epoxy\_remaining}$) in the DCB plate is calculated. Fiber mass in the plate is obtained by subtracting m_{total} from $m_{epoxy\_calculated}$.

$$m_{epoxy-remaining} = m_{epoxy-calculated} - m_{epoxy-overflowed}$$

The weight of the nanofiber tulle is calculated by using the electrospinning parameters. During the electrospinning process, the flow rate (ml/ h) of the pump is multiplied by the electrospinning time (hours), the amount of solution used in the process is calculated in ml. The m_{fiber} value is then calculated by proportioning this value to the polymer mass in the total solution.

An exemplary calculation for the N6 - 1.0 wt. % GO1 sample produced with R1 roll is as follows:

Of a 389.7 gram (m_{total}) weighed DCB test plate, 35 % by mass is epoxy resin. In this case, the mass of the epoxy resin ($m_{epoxy\_calculated}$) is 136.4 grams. After the plate exited the hot press, the overflowed epoxies were weighed and this value ($m_{epoxy\_overflowed}$) was recorded as 39 g. In this case, the $m_{epoxy\_remaining}$ value is 97.4 grams. m_{fiber} value is 253.3 gram.

Using prepreg data (fiber density = 1,779 g/cm^3, resin density = 1.19 g/cm^3), fiber volume is calculated as 141.5 cm^3 and epoxy volume as 82.2 cm^3.It is concluded that 37 % of the total volume is resin (V_{resin}) and 63 % is fiber (V_{fiber}).

Electrospinning parameters are used to determine the amount of fiber transferred to prepreg. 1.05 g of N6 polymer, 7.0 ml of solvent was used for the electrospun N6 - 1.0 wt % GO1 sample. The density of the solvent is 1.39 g/ml (7 ml of solvent is 9,73 grams). There are 1.05 grams of polymer with 10 grams of solution transferred to the syringe and since electrospinning is carried out for 3 hours 26 minutes (206 minutes) at a flow rate of 1.5 ml/h, 0.6 g of polymer is dispensed when 6.3 ml of solution is flushed during the procedure.

After this operation, nanofiber tulle which cannot be transferred to prepreg was weighed 0.278 grams. In this case, the polymer (y_{active}) transferred between the layers is 0.322 grams.

The area of the 215mm x 300mm plate is 0.645m^2.

In this case, the nanofiber tulle transferred to the unit area is calculated as $\frac{0.322}{0.645} = 0.499$.

$\frac{y_{active}}{composite} =$ value can be calculated as $\frac{0.322}{(389.7-39)} x100 = \%\ 0.1$.

B. Crystallinity Analysis with Fityk Program

While the DSC data were analyzed, firstly the raw data consisting of 3 columns (time-min, temperature -°C, heat flow - mW) were normalized according to the correct units (time - seconds) and weight of the sample. In Fityk program; melting temperature was obtained from heat flow (mW) – temperature (°C) graph (1) and melting enthalpy was measured from heat flow (W/g) - time (sec) (2) graph. In the first graph, the ‘’Pearson 7a’’ function used in the peak separation was applied in the second pair. Samples in this analysis will be given on DSC data of N6 nanofiber containing 2 wt % GO3.

The regions that are to be studied on the chart are marked and the region to be extracted is marked with gray color. In all data points, the biggest peak is of our interest, so remaining points are deactivated. The green lines are the data region selected for the study and the red color is the value line to be extracted. The heat flow/temperature data obtained from DSC analysis were transferred to Fityk program and plotted. This plot is shown in Figure B1.

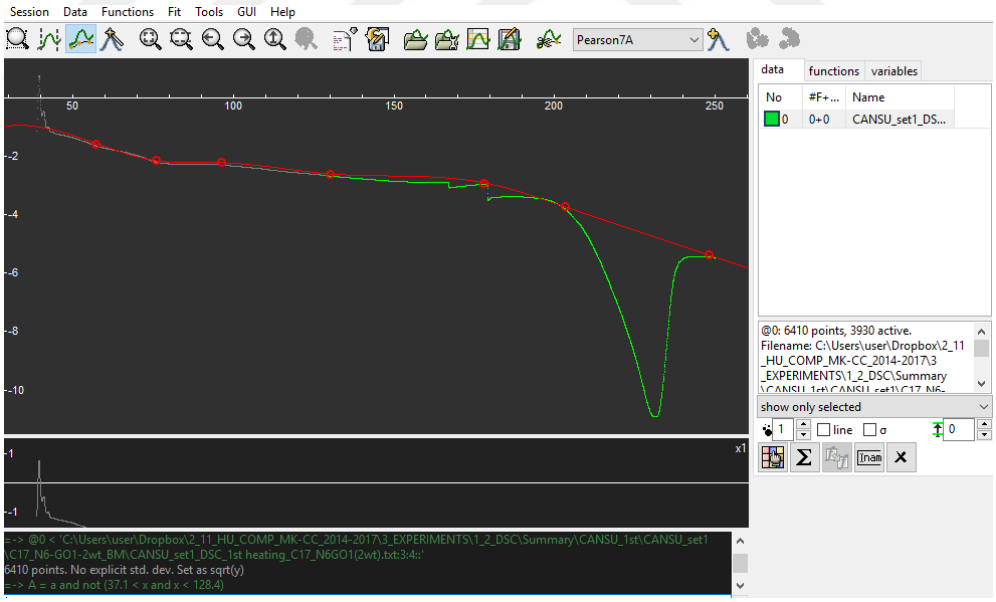

Figure B1. Heat flow (mW) – temperature (°C) plot

Raw data in the region of interest after subtraction is shown in Figure B2.

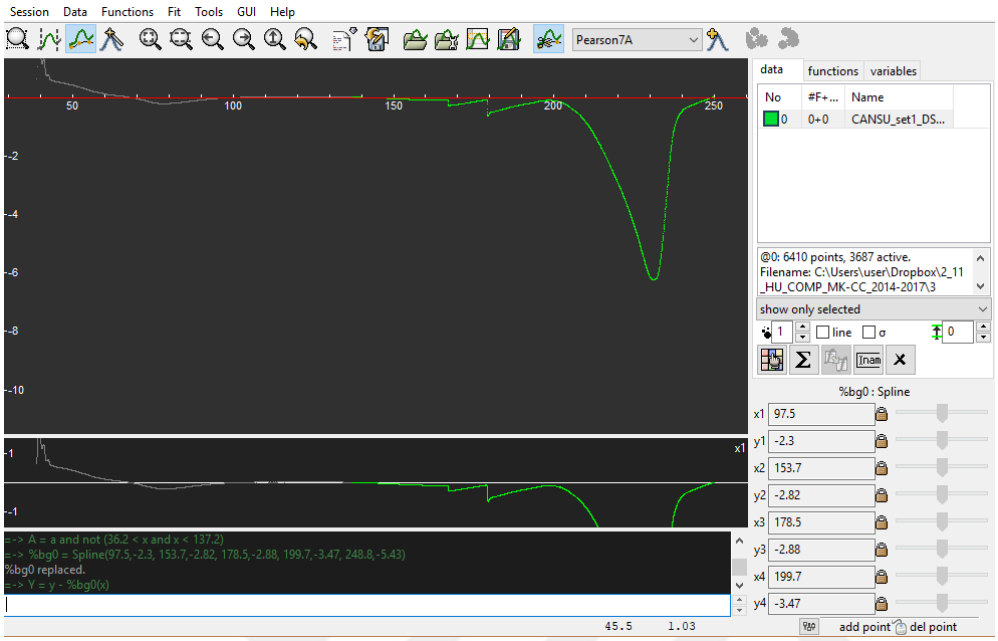

Figure B2. Raw data in the region of interest after subtraction

Next step is to define a peak with reasonable initial values and fit it to the data. Green color shows raw data, while red and yellow peaks show manually placed peaks and total peaks, respectively. These peaks are shown in Figure B3.

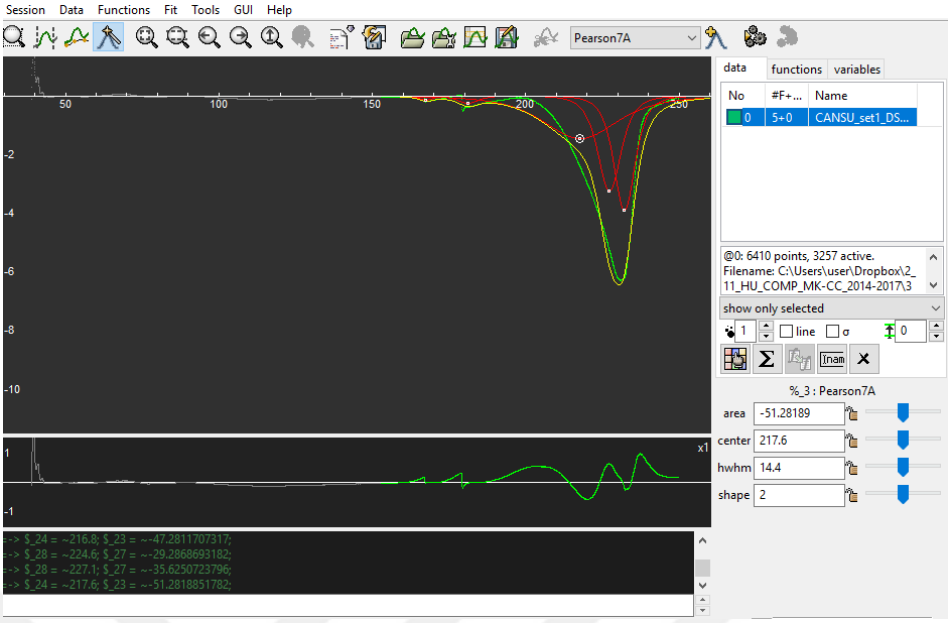

Figure B3. First peaks placement; green peak: raw data, yellow peak: total and red peaks: manually placed peaks

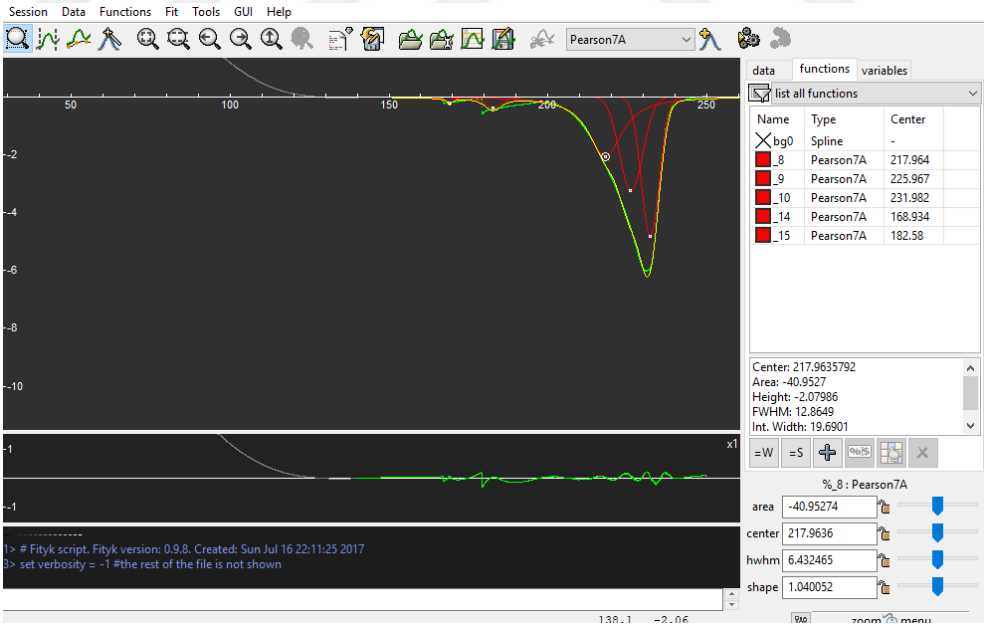

Figure B4. Approaching/fitting the yellow and green lines after running the alignment algorithm

After this step, the data of the center point (data set 1) and area (data set 2) of each peak are transferred to an Excel table. For example, the calculations made in the melting zone of N6 nanofiber containing 2% GO are given below.

a- In the first data set (heat flow (mW) – temperature (°C)), melting temperature data of nanofibers containing GO in different composition;

Table B1. Melting temperatures of each crystals

	Melting Temperatures, °C (POWER vs TEMPERATURE)						
			N6 - γ shoulder	**N6- γ shoulder**	**N6-γ**	**N6-α**	
N6	-	-	-	210.5	217.2	221.5	-
N6-2% GO1	168.9	182.6	-	-	217.9	225.9	231.9
N6-2% GO2	164.8	184.3	-	212.2	-	219.4	-
N6-2% GO3	166.9	182.7	200.9	208.3	214.3	219.0	-

b- In the second data set (heat flow (W/g) - time (sec)), area of peaks seen in nanofibers containing GO in different composition;

Table B2. Calculated area under the peaks for each crystal region

Area, J/g (POWER vs TIME)						
		N6 - γ shoulder	**N6- γ shoulder**	**N6- γ**	**N6 -α**	
-	-	-	-16.4	-53.1	-2.0	-
-0.43	-	-	-	-22.7	-55.5	-20.4
-	-	-	-58.0	-	-15.9	-
-	-4.3	-19.9	-24.0	-28.6	-22.3	-

c- Table of enthalpy and crystallinity values

Crystals amounts (x_c) is calculated by the ratio of $\Delta H_m / \Delta H_m°$ where $\Delta H_m°$ is the average of $\Delta H_m°$ (α) and $\Delta H_m°$ (γ) listed in following table, i.e. 239 J/g and 241 J/g [98].

ΔH values are based on amount of pure N6 within the composite sample.

$$\% \, x_c = \frac{\Delta H_m}{\Delta H_m°} x \, 100 \qquad Equation \, 4$$

Table B3. Calculated enthalpy and crystallinity values

Total Area (J/g)	**Main Peaks Total Area (J/g)**	**ΔHγ (J/g)**	**ΔHα (J/g)**	**% γ-crystals**	**% α-crystals**	**Total % N6 Crystallinity**
-71.5	-71.5	239	241	29.1	0.8	29.9
-99.0	-98.6	239	241	9.5	31.5	41.0
-73.9	-73.9	239	241	24.3	6.6	30.9
-99.1	-94.8	239	241	30.3	9.3	39.6

C. Sonication Studies Using 'Probe A'

Malvern Zeta-Sizer program graphs of GO + water mixture at a concentration of 0.05 mg/ml with (a) 15 min sonication in water bath, (b) 10 min probe sonication (c) 20 min probe sonication and (d) 30 min probe sonication

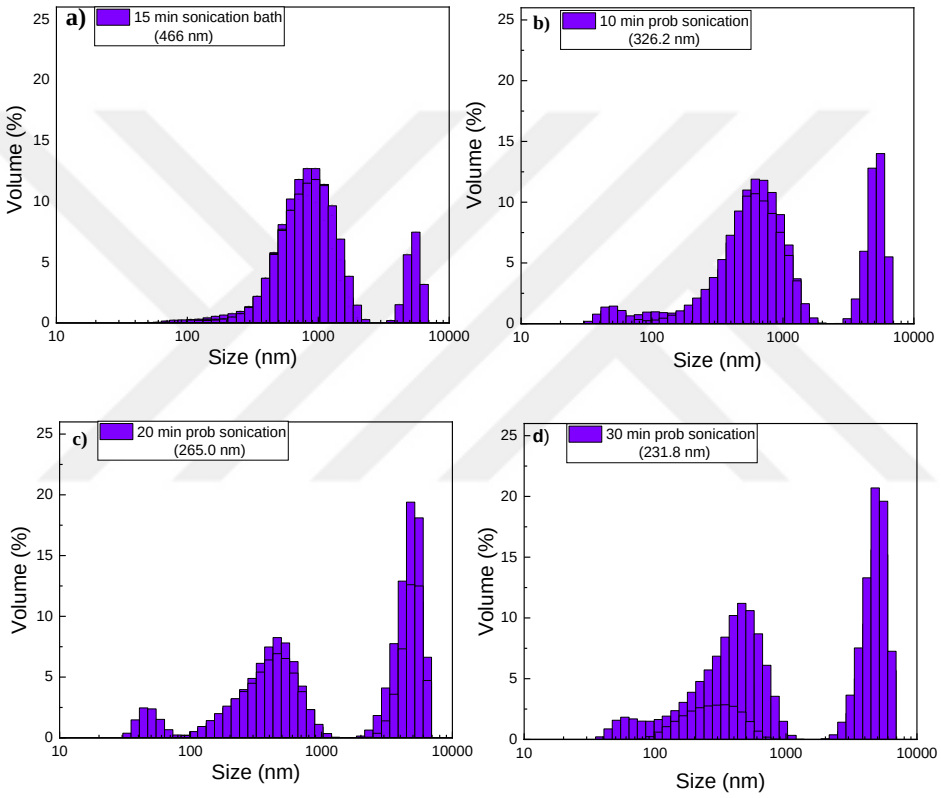

Figure C1. Particle size distribution of GO + water mixture at different sonication times using Probe A

D. Sonication Studies Using 'Probe B'

Malvern Zeta-Sizer program graphs of GO + water mixture at a concentration of 0.05 mg/ml with (a) 45 min, (b) 60 min, (c) 75 min, (d) 90 min and (e) 120 min probe sonication

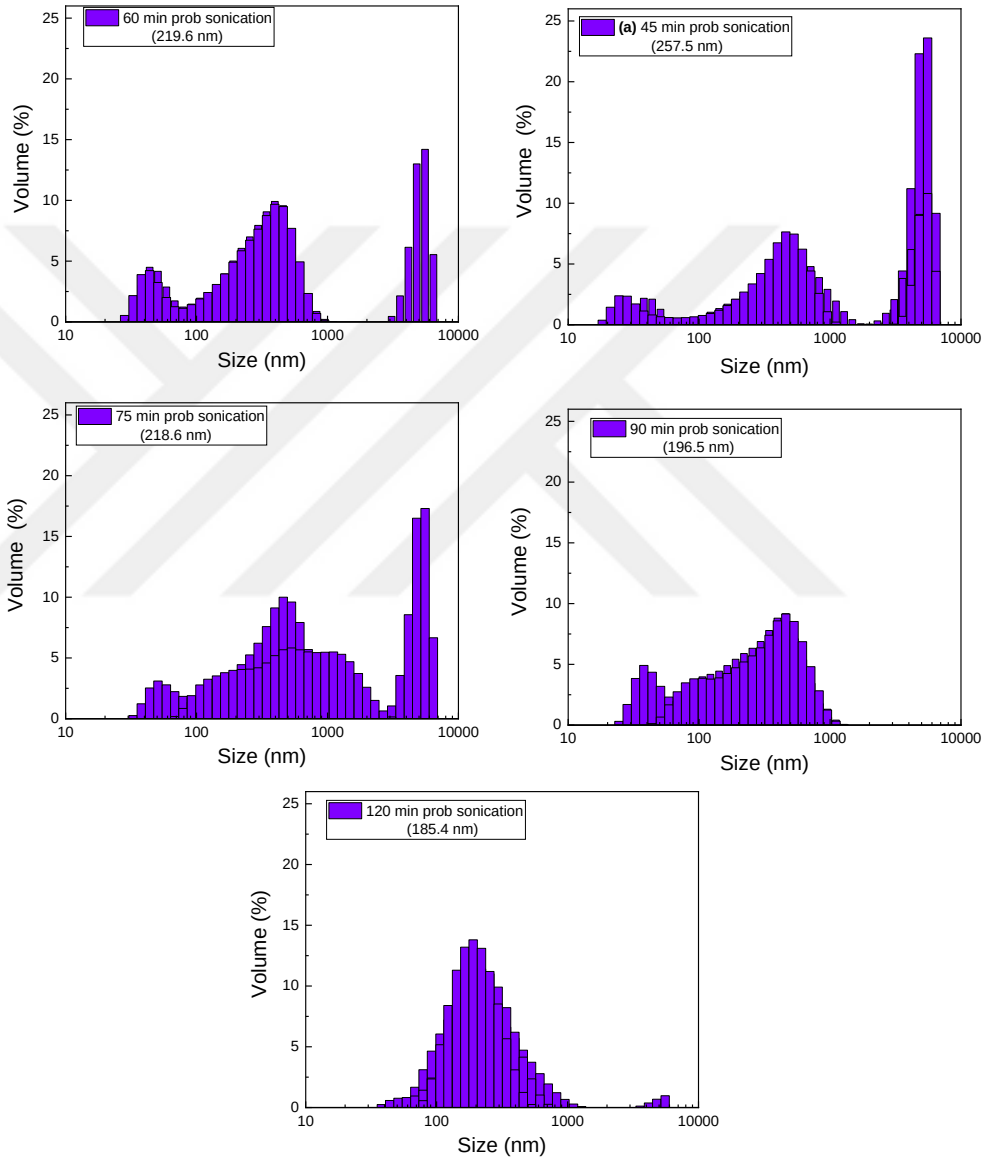

Figure D1. Particle size distribution of GO + water mixture at different sonication times using Probe B

E. Malvern Zeta-Sizer program graphs of GO2 in TFE at different times in sonication bath

(a) 15 min, (b) 20 min, (c) 25min, (d) 30 min, (e) 35 min and (f) 40 min

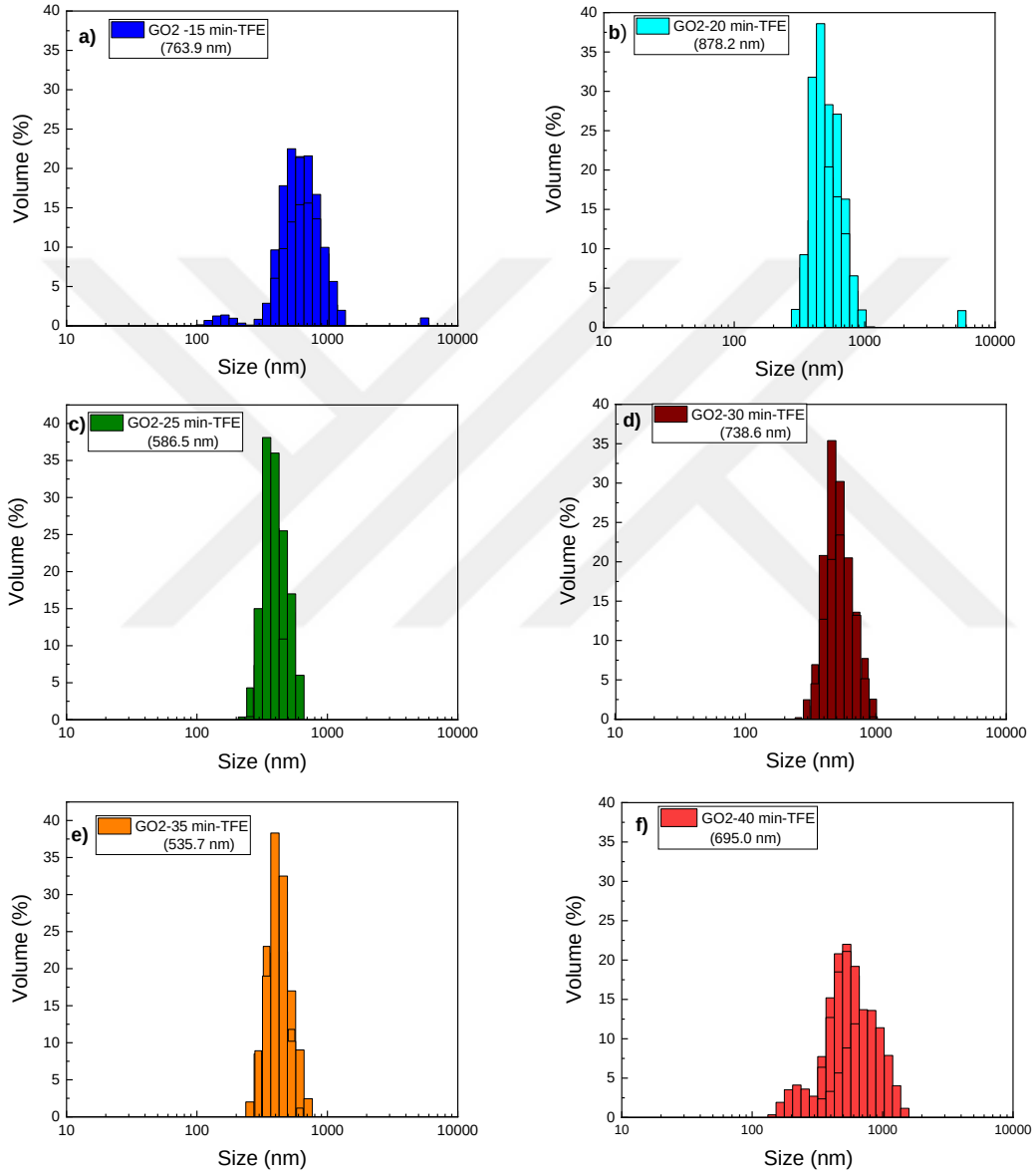

Figure E1. Particle size distribution of GO2 + TFE mixture at different sonication times